SANDIA REPORT

SAND94-1346 • UC-721
Unlimited Release
Printed May 1997

Evaluation of Methods for Measuring Relative Permeability of Anhydrite from the Salado Formation: Sensitivity Analysis and Data Reduction

Richard L. Christiansen, James S. Kalbus, Susan M. Howarth

Prepared by
Sandia National Laboratories
Albuquerque, New Mexico 87185 and Livermore, California 94550

Sandia is a multiprogram laboratory operated by Sandia Corporation, a Lockheed Martin Company, for the United States Department of Energy under Contract DE-AC04-94AL85000.

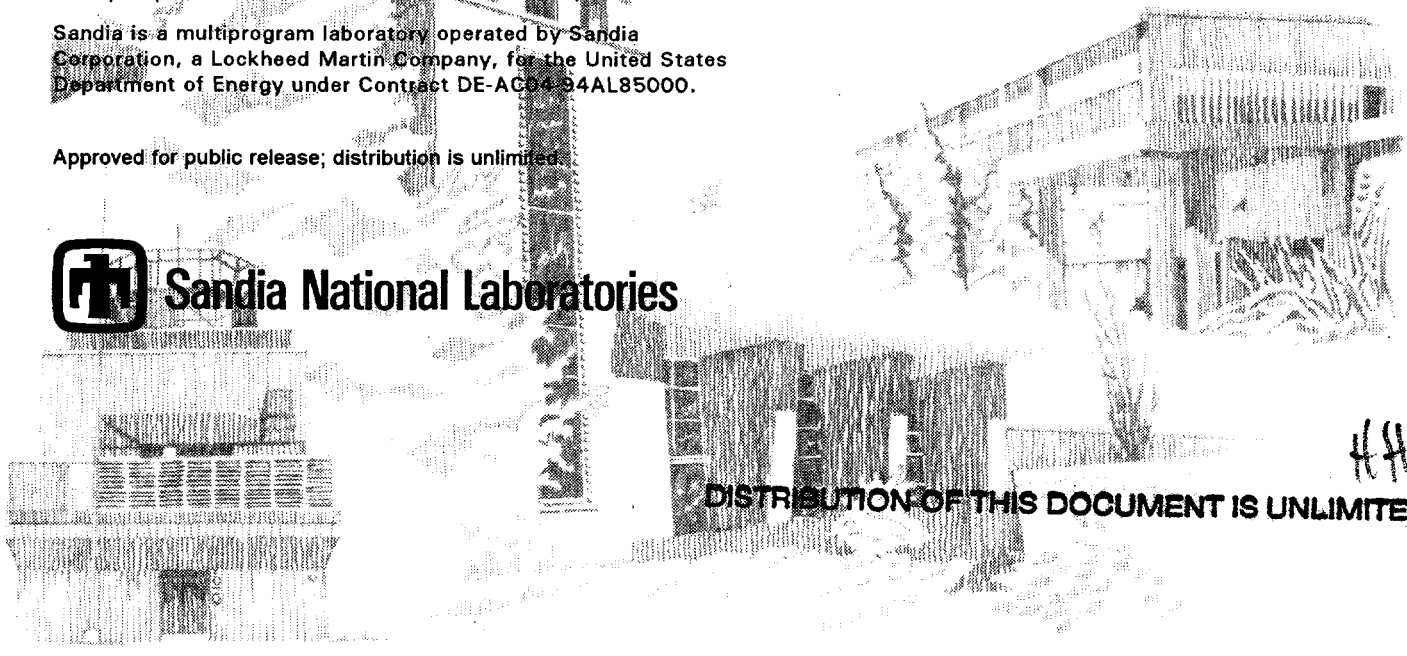

Sandia National Laboratories

Issued by Sandia National Laboratories, operated for the United States Department of Energy by Sandia Corporation.

Available to DOE and DOE contractors from
Office of Scientific and Technical Information
P.O. Box 62
Oak Ridge, TN 37831

Prices available from (615) 576-8401, FTS 626-8401

Available to the public from
National Technical Information Service
U.S. Department of Commerce
5285 Port Royal Rd
Springfield, VA 22161

NTIS price codes
Printed copy: A06
Microfiche copy: A01

SAND94-1346
Unlimited Release
Printed May 1997

Distribution
Category UC-721

Evaluation of Methods for Measuring Relative Permeability of Anhydrite from the Salado Formation: Sensitivity Analysis and Data Reduction

Richard L. Christiansen and James S. Kalbus
Petroleum Engineering Department
Colorado School of Mines
Golden, CO 80401

Susan M. Howarth
WIPP Deputy Project Management and
Technical Integration Department 6801
Sandia National Laboratories
P.O. Box 5800
Albuquerque, NM 87185-1335

ABSTRACT

This report documents, demonstrates, evaluates, and provides theoretical justification for methods used to convert experimental data into relative permeability relationships. The report facilitates accurate determination of relative permeabilities of anhydrite rock samples from the Salado Formation at the Waste Isolation Pilot Plant (WIPP). Relative permeability characteristic curves are necessary for WIPP Performance Assessment (PA) predictions of the potential for flow of waste-generated gas from the repository and brine flow into the repository. This report follows Christiansen and Howarth (1995), a comprehensive literature review of methods for measuring relative permeability. It focuses on unsteady-state experiments and describes five methods for obtaining relative permeability relationships from unsteady-state experiments. Unsteady-state experimental methods were recommended for relative permeability measurements of low-permeability anhydrite rock samples from the Salado Formation because these tests produce accurate relative permeability information and take significantly less time to complete than steady-state tests.

Five methods for obtaining relative permeability relationships from unsteady-state experiments are described: the Welge method, the Johnson-Bossler-Naumann method, the Jones-Roszelle method, the Ramakrishnan-Cappiello method, and the Hagoort method. A summary, an example of the calculations, and a theoretical justification are provided for each of the five methods. Displacements in porous media are numerically simulated for the calculation examples. The simulated production data were processed using the methods, and the relative permeabilities obtained were compared with those input to the numerical model. A variety of operating conditions were simulated to show sensitivity of production behavior to rock-fluid properties.

ACKNOWLEDGMENTS

The authors thank Louzolo Agostinho, Shabir Al-Lawati, Hugo Araujo, Stephen Ball, Albert Banahene, and Geraldine Oyebog for their suggestions for improving the readability and the accuracy of the manuscript. These graduate students in the Petroleum Engineering Department at the Colorado School of Mines also worked through the examples shown in Tables 2 through 8, making many suggestions for improvement. The authors also thank M. Kathy Knowles, Stephen Webb, and Peter Davies for their thorough review and helpful comments.

CONTENTS

CONTENTS (Continued)

DISCLAIMER

CONTENTS (Continued)

TABLES

FIGURES

FIGURES (Continued)

FIGURES (Continued)

NOMENCLATURE

Many of the symbols used in the text represent corresponding properties in or features of the brine and gas phases, such as S_b and S_g. In the list below, such symbols are written side by side. In the definitions of the symbols, the reader should choose "brine" or "gas" from the coupling "brine/gas" as appropriate. Some example equations that incorporate the symbols are listed in parentheses. At the end of each definition, SI units for the symbol are included in parentheses.

Roman Symbols

A = area perpendicular to the direction of flow (m^2) (Equations 1 and 2).

f_b, f_g = the volumetric fraction of the flow rate which is brine/gas (Equation 19).

f_b', f_g' = derivatives of brine/gas fractional flow with respect to brine/gas saturation (Equation 24).

f_{bL}', f_{gL}' = derivatives of brine/gas fractional flow with respect to brine/gas saturation evaluated at the outlet $x=L$ (Equation 26).

f_{bL}, f_{gL} = brine/gas fractional flow at the outlet $x=L$ (Equation 20).

g = acceleration of gravity (Equations 3 and 4) (m/s^2).

I_r = relative injectivity as defined in the text following Equation 39 and in Equation 46.

$J(S_b)$ = Leverett J function as defined by Equation 99.

J' = derivative with respect to brine saturation of the Leverett J function (Equation 102).

k = intrinsic or absolute permeability (Equations 1 and 2)(m^2).

k_{rb}, k_{rg} = brine/gas relative permeability (Equations 1, 2, 16, and 17).

k_{rb}', k_{rg}' = derivative with respect to brine/gas saturation of brine/gas relative permeability (Equation 104).

$k_{rb,\max}, k_{rg,\max}$ = brine/gas relative permeability at the maximum brine/gas saturation (Equations 16 and 17).

k_{rb0}, k_{rg0} = brine/gas relative permeability at the inlet, $x=0$ (Equation 75).

k_{rbL}, k_{rgL} = brine/gas relative permeability at the outlet, $x=L$ (Equation 20).

L = length of porous sample (Equations 1 and 2) (m).

M = mobility ratio as defined by Equation 13 and the text that follows Equation 13.

N_{cg} = capillary-gravity ratio as defined in text prior to Equation 106.

P = pressure (Equations 1 and 2) (Pa = N/m^2).

P_b, P_g = pressure in the brine/gas phase (Equations 3 and 4) (Pa = N/m^2).

P_c = capillary pressure as defined in the text after Equation 9 (Pa = N/m^2).

P_{c0} = capillary pressure at inlet $x=0$ (Equation 82) (Pa = N/m^2).

P_{th} = threshold capillary pressure as used in Equation 18 (Pa = N/m^2).

P_{sp} = "span" capillary pressure, a parameter in Equation 18 (Pa = N/m^2).

ΔP = pressure drop (Equations 1 and 2) (Pa = N/m^2).

ΔP_b, ΔP_g = brine/gas pressure drop (Equation 56) (Pa = N/m^2).

q = flow rate (Equation 56) (m^3/s).

q_b, q_g = brine/gas flow rate (Equations 1 and 2) (m^3/s).

Q_{bp} = cumulative pore volume of produced brine (Equation 19).

Q_{gi} = cumulative pore volume of injected gas (Equation 19).

$R(x)$ = radial distance from axis of spin of a centrifuge to position x in porous sample (Equations 14 and 15) (m).

R = radius of core on Figure 2.

s = seconds

S_b, S_g = brine/gas saturation.

S_{b0}, S_{g0} = brine/gas saturation at inlet, $x=0$ (Equation 76).

S_{bL}, S_{gL} = brine/gas saturation at outlet, $x=L$ (Equations 19, 65, and 66).

$\overline{S_b}$, $\overline{S_g}$ = average brine/gas saturation (Equation 19).

S_{br} = residual brine saturation (Equation 16, 17, and 18).

S_b^* = extrapolated value of brine saturation as defined by Equation 69.

S_{gc} = critical gas saturation (Equations 16, 17, and 18).

t^* = time (s).

= dimensionless time as defined in text after Equation 105.

v = velocity (m/s).

v_b,v_g = brine/gas Darcy velocity (m/s).

v_T = total Darcy velocity (Equation 5) (m/s).

x = position in porous sample (Equation 5) (m).

x = fractional distance (Equations 61 to 64).

z = position in porous sample (used in derivations for Hagoort method) (m).

z^* = dimensionless position as defined in text after Equation 105.

Greek Symbols

μ_b, μ_g = brine/gas viscosity (Equations 1 and 2) (Pa s = kg/m/s).

ρ_b, ρ_g = brine/gas density (Equations 3 and 4) (kg/m^3).

θ = angle from horizontal as defined in Figure 1 (Equation 3 and 4) (radians).

σ = interfacial tension between brine and gas (Equation 99) (N/m).

λ = relative mobility as described in text after Equation 71.

λ^{-1} = reciprocal relative mobility (Equation 71).

λ^{-1+} = extrapolated value of reciprocal relative mobility as used in Equation 60.

λ_L^{-1} = reciprocal relative mobility at outlet $x=L$ (Equation 56).

$\overline{\lambda^{-1}}$ = average reciprocal relative mobility (Equation 56).

ϕ = porosity (Equation 8).

Φ_b, Φ_g = brine/gas potential for flow (Equations 97 and 98) (Pa = N/m^2).

ω = centrifuge spin rate (Equations 14 and 15) (radians/s).

$\Delta\rho_{bg}$ = (ρ_b - ρ_b) density difference between brine and gas (Equation 13) (kg/m^3).

1.0 INTRODUCTION

The Waste Isolation Pilot Plant (WIPP) near Carlsbad, New Mexico, is a research and development project of the U.S. Department of Energy (DOE). The WIPP is designed as a mined geologic repository to demonstrate the safe management, storage, and disposal of transuranic radioactive wastes generated by DOE defense programs. Before permanently disposing of radioactive wastes at the WIPP, the DOE must evaluate the repository based on various regulatory criteria for disposal of all the waste components. This evaluation includes a performance assessment of the WIPP disposal system.

The WIPP repository horizon is located in the Salado Formation, a bedded salt formation approximately 660 m below ground surface. Salt has been identified as an excellent geologic material to host a nuclear waste repository because its high ductility alleviates fracturing and will aid in encapsulating the waste over the long repository storage times. The Salado salt must be characterized accurately for WIPP Performance Assessment (PA) calculations.

1.1 Objective

The objective of this report is to document, demonstrate, evaluate, and provide theoretical justification for methods that are used to convert experimental data into relative permeability relationships. This report will facilitate accurate determination of the relative permeabilities of anhydrite rock samples taken from the Salado Formation at the WIPP. Relative permeabilities are necessary for WIPP PA predictions of the potential for flow of brine and waste-generated gas between the repository and surrounding Salado Formation. This study was motivated by reports in the literature that low-rate unsteady-state experiments can simultaneously yield relative permeability and capillary pressure information. Because fluid movement through the Salado Formation anhydrite is expected to occur at low rates, low-rate methods for measuring relative permeability and capillary pressure are pertinent.

This report follows Christiansen and Howarth (1995), a comprehensive literature review of methods for measuring relative permeability. That report classified the methods for measuring relative permeability as either steady-state or unsteady-state. The present report focuses on unsteady-state experiments and describes five methods for obtaining relative permeability relationships from unsteady-state experiments. These experimental methods were recommended for relative permeability measurements of low permeability anhydrite rock

samples from the Salado Formation because they produce accurate information and take significantly less time to complete than steady-state tests. Steady-state experiments are only briefly discussed in Section 1.3.1 because data conversion processes for these experiments are comparatively straightforward, requiring little explanation.

Five methods for obtaining relative permeability relationships from unsteady-state experiments are described: the Welge method, the Johnson-Bossler-Naumann method, the Jones-Roszelle method, the Ramakrishnan-Cappiello method, and the Hagoort method. Each requires differentiation of pressure, volume, and/or time data. A summary is provided for each of the five methods. Brine displacements by gas in porous media were numerically simulated for the calculation examples. Simulated production data (i.e., pressures, injected volumes of gas, gas and brine flow rates, and produced volumes of gas and brine) were then processed using the data-reduction methods. The relative permeabilities obtained were compared with those input to the numerical model. A variety of operating conditions were simulated to determine the sensitivity of gas/brine flow and production behavior to rock-fluid properties.

1.2 Organization of the Report

Numerical models used to simulate unsteady-state experiments are described in Section 2. These models are one-dimensional, and the modeling techniques were taken from the literature on reservoir simulation. The results of a sensitivity study, essential to interpreting unsteady-state low-rate experiments with the numerical models, are also reported in Section 2. Finally, the literature about methods for obtaining relative permeabilities by matching observed production history with numerical models is described.

In Section 3, conversion techniques for unsteady-state methods that require differentiation of data are described. These are the most commonly reported techniques in the literature. For each method, a summary of the necessary calculations, an example of the calculations, and a theoretical justification are provided.

Conclusions and recommendations for determining the relative permeabilities of anhydrite from the Salado Formation are presented in Section 4.

1.3 Background

1.3.1 Steady-State Methods

Within the classification of steady-state methods, four subgroups were identified in Christiansen and Howarth (1995): the multiple-core methods (also called the Penn State method), the high-rate methods, the stationary-liquid methods, and the uniform capillary pressure methods (also called the Hassler method). Christiansen and Howarth note (1995) that of the four methods the high-rate method is used most often. It is discussed below to illustrate its simplicity and provide background information.

In the steady-state high-rate method, two fluids are displaced through a rock sample at constant rates that are sufficiently high to minimize the impact of capillary end effects on flow behavior. After pressure drop and saturation in the rock sample reach a constant value, the relative permeabilities for brine and gas are calculated using Equations 1 and 2:

$$k_{rb} = - \frac{\mu_b L q_b}{k A \Delta P} \quad (1)$$

$$k_{rg} = - \frac{\mu_g L q_g}{k A \Delta P} \quad (2)$$

Thus, using viscosities of both fluids, sample dimensions, and intrinsic (single-phase) permeability, relative permeabilities can be calculated from the flow rates and pressure drops. The saturation of fluids in the rock sample is determined by weighing the sample or by measuring x-ray absorption. By injecting fluids in different flow-rate ratios, relative permeability can be determined as a function of saturation.

Further discussion of steady-state experimental procedures and data reduction methods is found in Christiansen and Howarth (1995). Because of the simplicity of the data reduction process for steady-state experiments, the remainder of this report will describe the more complex process, data reduction methods for unsteady-state experiments.

1.3.2 Unsteady-State Methods

Within the classification of unsteady-state methods, three subgroups were identified in Christiansen and Howarth (1995): high-rate methods, low-rate methods, and centrifuge methods. Of these, unsteady-state high-rate methods are the most commonly cited in the past 20 years. The low-rate methods and the centrifuge methods are relatively new, appearing in the literature only within the past 10 years. To illustrate the differences in experimental process, data collection, and analysis between the steady-state and unsteady-state high-rate methods, the unsteady-state high-rate method is discussed below.

In the unsteady-state high-rate method, a fluid is injected into a rock sample that is saturated with another fluid. Using iterative, trial-and-error techniques, the injection rate is maintained sufficiently high to minimize the impact of capillary end effects on flow behavior. Fingering and channeling could occur during any experiment, but the complications of these effects have largely been ignored in the two-phase relative permeability literature. The cumulative volume of injected fluid, the cumulative volumes of the produced fluids, and the pressure drop across the core are measured throughout the experiment. To obtain relative permeability relationships, differentiation of the volume and pressure data is required. The data conversion process is substantially more complicated than that needed for steady-state experiments. Although it is more difficult to process the data, the unsteady-state high-rate experiment requires much less time to complete than the steady-state high-rate experiment. The amount of time saved depends on the intrinsic permeability of the individual core sample.

2.0 NUMERICAL MODELS, SENSITIVITY STUDY, AND HISTORY MATCHING

Two one-dimensional, finite-difference models are described for simulating unsteady-state experiments. The first is for modeling constant pressure drop, high- and low-flow rate experiments; the second is for modeling constant-spin-rate centrifuge experiments. Using these two models, sensitivity to rock properties is demonstrated. The sensitivity analyses are important for understanding the effects of operating conditions and rock-fluid properties on experimental results. In addition, these models provide simulated production information for testing the data reduction procedures described in Section 3. The results of the analyses may be useful for planning experiments, and may be used to demonstrate the ability to measure relative permeability and capillary pressure with specific experiments. The numerical models may also be used to obtain relative permeability and capillary pressure information by matching the production histories (i.e., pressures, injected volumes of gas, gas and brine flow rates, and produced volumes of gas and brine) of unsteady-state experiments.

2.1 Numerical Approach

Two numerical simulation models, CONSTDPCPOEFLOOD and CENTRIFUGE, were developed to replicate the flow of fluids in a core-flooding experiment during primary displacement and in a centrifuge experiment during primary drainage, respectively. The models represent one-dimensional, two-phase flow in rock to simulate two-phase flow-displacement experiments. The models account for the mobility of both brine and gas, capillary effects, and gravitational acceleration parallel to the direction of flow. Two-dimensional effects such as bypassing caused by rock heterogeneity, viscous fingering, and gravitationally induced segregation of fluids were not modeled.

A sequential numerical algorithm for solving the differential equations, referred to as "sequential solution with total velocity," was taken from the literature (Mattax and Dalton, 1990; Peaceman, 1977). The algorithm consists of two parts: solution of a differential pressure equation and solution of a differential saturation equation. Relative permeability and capillary pressure are evaluated in a semi-implicit manner for solution of the differential saturation equation as originally suggested by Spillette et al. (1986) and summarized by Mattax and Dalton (1990). The two models are described in Sections 2.1.1 and 2.1.2. Sections 2.1.3 through 2.1.7 contain details regarding the development and application of the two models.

2.1.1 Constant Pressure Drop Experiment Numerical Simulation Model

The constant pressure drop model, CONSTDPCPOEFLOOD, is a one-dimensional numerical simulation program that simulates a conventional core flooding experiment operated at a constant pressure drop for primary drainage given relative permeability and capillary pressure information, rock and fluid properties, and rock dimensions. At the beginning of simulation, a core is saturated with a fluid that will be displaced by another fluid, which is being injected into the core at a constant pressure drop. The experiment can continue up to a point where no more of the initial fluid can be produced at a particular injection rate.

The solution technique used is described as a sequential solution with total velocity and is described by Mattax and Dalton (1990). The pressure equations are solved first for the displacing phase; then the saturation equations are solved for the change in displacing phase saturation. Relative permeability is taken at the old time step in the saturation equations while the capillary pressure is estimated in a semi-implicit manner in the saturation equations. Relative permeability and capillary pressure for the pressure equations are calculated from the current fluid saturation level using a Brooks-Corey relative permeability relationship, which is valid for primary drainage at any fluid saturation level. For the saturation equations, capillary pressure is estimated in a semi-implicit manner for the upcoming saturation change while relative permeability is calculated from the previous fluid saturation level.

Relative permeability and capillary pressure are independent in this simulation and depend only on fluid saturations and the individual relationships built into the source code. Shape factors for the Brooks-Corey relationship are entered through an input data file, allowing calculation of relative permeability data at any fluid saturation level. The form of the relative permeability relationships is for primary drainage of a wetting phase fluid. Capillary pressure is modeled by Bentsen-Anli capillary pressure relationships built into the source code. The form of the capillary pressure relationship is also for primary drainage. Capillary pressure is calculated at all fluid saturation levels using shape factors for this relationship.

The following assumptions are built into the CONSTDPCPOEFLOOD source code: (1) capillary pressure is zero outside the core; (2) the relative permeability of the injected phase is at its maximum at the inlet face of the core when the core flood begins; (3) the relative permeability of the displaced phase is zero at the inlet face when the core flood begins; (4) the rock and fluid compressibilities are assumed to be zero; and (5) the rock sample may be oriented in any direction.

2.1.2 Centrifuge Experiment Numerical Simulation Model

The centrifuge experiment model, CENTRIFUGE, is a one-dimensional numerical simulation program that simulates a centrifuge experiment operated at a constant spin rate for primary drainage given relative permeability and capillary pressure information, rock and fluid properties, and rock and centrifuge dimensions. At the beginning of the simulation, a core is saturated with a fluid that will be displaced as centrifugal forces are applied at a specific spin rate. Another fluid, such as gas, will enter the core and replace the volume occupied by the displaced fluid. The experiment can continue up to a point where no more collection of an initial fluid can be achieved at a particular spin rate.

The solution technique used in CENTRIFUGE is a sequential solution with total velocity as described by Mattax and Dalton (1990). In the first step, the pressure equations are solved for invading (in this case, gas) phase pressure. Next the saturation equations are solved for the change in displaced phase saturation. Relative permeability and capillary pressure for the phase equations are calculated from the current fluid saturation level. For the saturation equations, capillary pressure is estimated in a semi-implicit manner for the upcoming saturation change; relative permeability is calculated from the previous fluid saturation level.

Relative permeability and capillary pressure are independent in this simulation. They depend only on fluid saturations and the individual relationships that are used to model their behavior. Relative permeability is modeled by Brooks-Corey relative permeability relationships, which are built into the source code. Shape factors for this relationship are entered through an input data file, allowing relative permeability data to be calculated at any fluid saturation level. The form of the relative permeability relationships is for primary drainage of a wetting phase fluid. Capillary pressure is modeled by Bentsen-Anli capillary pressure relationships, which are also built into the source code. The form of the capillary pressure relationship is also for primary drainage. Capillary pressure is calculated at all fluid saturation levels using shape factors for this relationship.

The following assumptions are built into the source code: (1) capillary pressure is zero outside the core; (2) the relative permeability of the injected phase is at its maximum at the inlet face of the core when the core flood begins; (3) the relative permeability of the displaced phase is zero at the inlet face when the core flood begins; (4) the rock and fluid compressibilities are assumed to be zero; and (5) the invading phase fluid can penetrate the core only to a distance that corresponds to the threshold pressure selected in the input file.

2.1.3 Derivation of Differential Pressure Equation

The differential equations are derived here to provide an outline of the solution technique. The differential equation for pressure in the gas phase, which describes Darcy flow of gas and brine, will be derived first.

$$v_g = - \frac{k\, k_{rg}}{\mu_g} \left(\frac{\partial P_g}{\partial x} + \rho_g\, g\, \sin\, \theta \right) \tag{3}$$

$$v_b = - \frac{k\, k_{rb}}{\mu_b} \left(\frac{\partial P_b}{\partial x} + \rho_b\, g\, \sin\, \theta \right) \tag{4}$$

where θ is measured counterclockwise from the horizontal, as shown in Figure 1.

The sum of v_g and v_b gives the total velocity v_T:

$$v_T = - \frac{k\, k_{rg}}{\mu_g} \left(\frac{\partial P_g}{\partial x} + \rho_g\, g\, \sin\, \theta \right) - \frac{k\, k_{rb}}{\mu_b} \left(\frac{\partial P_b}{\partial x} + \rho_b\, g\, \sin\, \theta \right) \tag{5}$$

For incompressible flow, the total flow rate does not depend on position at any one time, so:

$$0 = \frac{\partial v_T}{\partial x} \tag{6}$$

Usually gas flow is treated as compressible; however, if the pressure drop through a rock sample is small compared to the mean pressure, then the effect of expansion may be neglected (Johnson et al., 1959; Welge, 1952). For modeling centrifuge experiments, gas compressibility does not significantly affect the solution of the differential equations because

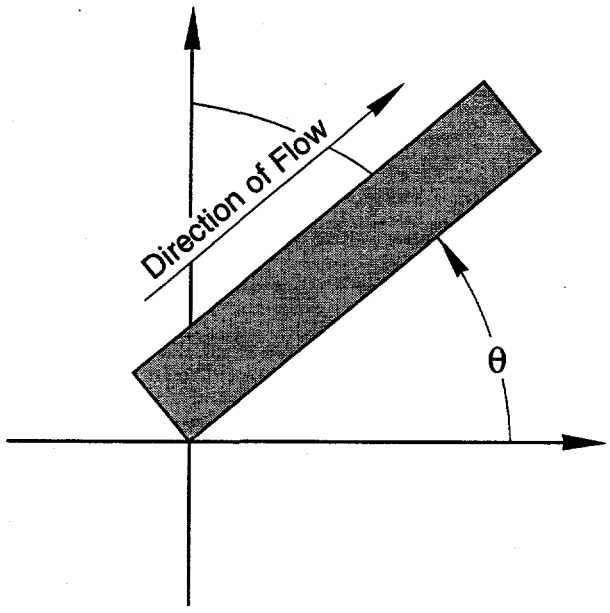

Figure 1. Definition of Angle θ relative to horizontal direction.

pressure variations in the gas are small compared to the mean pressure. When modeling constant pressure drop or constant flow rate experiments, gas compressibility could be important if the pressure drop is large compared to the mean pressure. However, the effect of gas expansion on laboratory-measured gas relative permeability is largely ignored in the oil and gas industry. Gas compressibility has mixed effects on the results of differential data reduction procedures, as discussed in Section 3. The differential equation for pressure in the gas phase is obtained by combining Equations 5 and 6 with the definition of capillary pressure, $P_c = P_g - P_b$.

$$0 = \frac{\partial}{\partial x}\left[\frac{k\, k_{rg}}{\mu_g}\left(\frac{\partial P_g}{\partial x} + \rho_g\, g\, \sin\theta\right) + \frac{k\, k_{rb}}{\mu_b}\left(\frac{\partial P_g}{\partial x} + \rho_b\, g\, \sin\theta - \frac{\partial P_c}{\partial x}\right)\right] \qquad (7)$$

The finite-difference formulation of this equation is not shown; however, it was developed according to the recommendations of Mattax and Dalton (1990): relative permeabilities are calculated with upstream weighting.

2.1.4 Derivation of Differential Saturation Equation

The differential equation for the saturation of the brine phase is derived by starting with the differential material balance on the brine phase.

$$\phi \frac{\partial S_b}{\partial t} + \frac{\partial v_b}{\partial x} = 0 \tag{8}$$

Substituting Darcy's expression for v_b from Equation 4, then yields

$$\phi \frac{\partial S_b}{\partial t} + \frac{\partial}{\partial x}\left[- \frac{k\, k_{rb}}{\mu_b}\left(\frac{\partial P_b}{\partial x} + \rho_b\, g\, \sin\theta \right)\right] = 0 \tag{9}$$

To obtain an expression for the pressure gradient in Equation 9, Equation 5 is combined with the definition of capillary pressure, $P_c = P_g - P_b$, to obtain

$$v_T = - \frac{k\, k_{rg}}{\mu_g}\left(\frac{\partial P_b}{\partial x} + \frac{\partial P_c}{\partial x} + \rho_g\, g\, \sin\theta \right) - \frac{k\, k_{rb}}{\mu_b}\left(\frac{\partial P_b}{\partial x} + \rho_b\, g\, \sin\theta \right) \tag{10}$$

Solving Equation 10 for pressure gradient in the brine phase yields Equation 11.

$$\frac{\partial P_b}{\partial x} = - \frac{v_T + \frac{k\, k_{rg}}{\mu_g}\left(\frac{\partial P_c}{\partial x} + \rho_g\, g\, \sin\theta \right) + \frac{k\, k_{rb}}{\mu_b}\rho_b\, g\, \sin\theta}{\frac{k\, k_{rg}}{\mu_g} + \frac{k\, k_{rb}}{\mu_b}} \tag{11}$$

Combining Equation 11 for the pressure gradient in the brine phase with Equation 9, yields Equation 12:

$$\frac{S_b}{t} + \frac{\partial}{\partial x}\left\{\frac{k\,k_{rb}}{\mu_b}\left[\frac{v_T + \frac{k\,k_{rg}}{\mu_g}\left(\frac{\partial P_c}{\partial x} + \rho_g\, g\, \sin\theta\right) + \frac{k\,k_{rb}}{\mu_b}\rho_b\, g\, \sin\theta}{\frac{k\,k_{rg}}{\mu_g} + \frac{k\,k_{rb}}{\mu_b}} - \rho_b\, g\, \sin\theta\right]\right\} \qquad (12)$$

or, combining terms, yields

$$\phi\frac{\partial S_b}{\partial t} + \frac{\partial}{\partial x}\left\{\frac{1}{(1+M)}\left[v_T + \frac{k\,k_{rg}}{\mu_g}\left(\frac{\partial P_c}{\partial x} - \Delta\rho_{bg}\, g\, \sin\theta\right)\right]\right\} = 0 \qquad (13)$$

where $M = \frac{\mu_b}{k_{rb}}\frac{k_{rg}}{\mu_g}$.

Again, the finite-difference formulation of this equation is not shown; however, it was developed according to the recommendations of Mattax and Dalton (1990). Relative permeabilities were calculated with upstream weighting.

2.1.5 Boundary Conditions

For simulated experiments at gravitational acceleration, the inlet boundary conditions consisted of setting both the capillary pressure and relative permeability of the displaced phase (brine in all cases) to zero. The outlet capillary pressure was also set to zero.

2.1.6 Size of Nodes and Time Steps

The number of nodes in the models was varied from 10 to 50 during initial testing. It was determined in this testing that 40 nodes provided sufficient resolution (i.e., with 40 or more nodes, identical results were obtained). The length of time steps was varied as necessary to obtain a stable solution and to provide the production information at convenient intervals to test the data reduction procedures.

2.1.7 Features of Models for Centrifuge Experiments

With minor changes, the above equations can be used for modeling displacements in a centrifuge experiment, shown schematically in Figure 2. Specifically, the acceleration terms in Darcy's law must be expressed in terms of spin rate, ω, and the radial distance $R(x)$ from the center of spin to the position x in the model:

$$v_g = - \frac{k\, k_{rg}}{\mu_g} \left[\frac{\partial P_g}{\partial x} - \rho_g\, \omega^2\, R(x) \right] \tag{14}$$

$$v_b = - \frac{k\, k_{rb}}{\mu_b} \left[\frac{\partial P_b}{\partial x} - \rho_b\, \omega^2\, R(x) \right] \tag{15}$$

Boundary conditions must also be adjusted for modeling centrifuge experiments. The capillary pressure at the outlet is set to zero, and the pressure gradient in the gas phase is set equal to $\rho_g\, \omega^2\, R$.

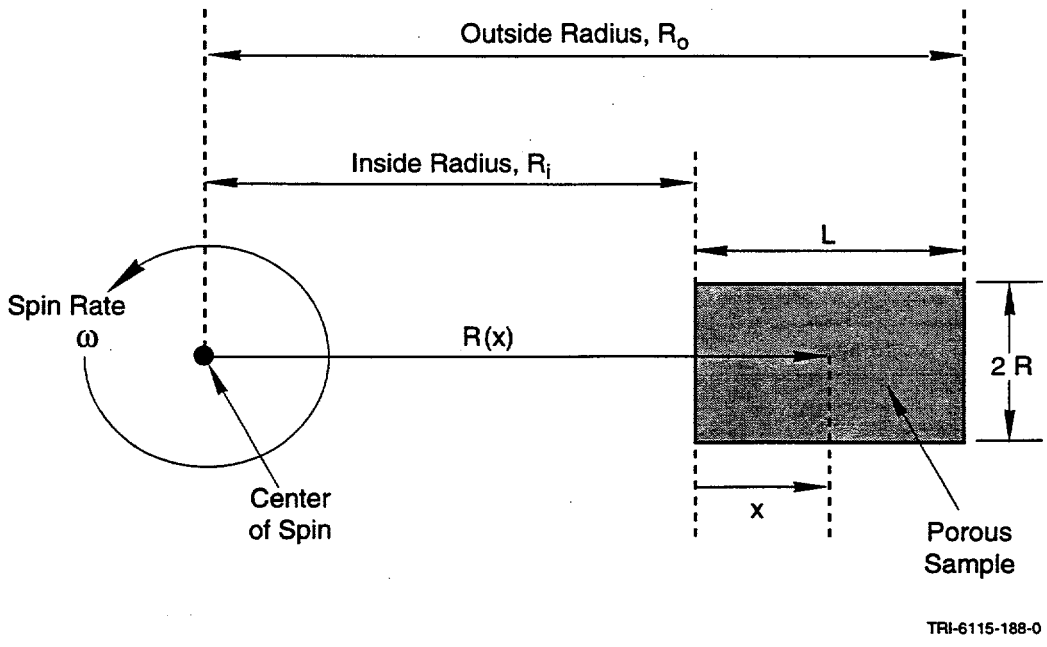

Figure 2. Critical dimensions for centrifuge experiment, where R = radius of core.

The gas phase pressure gradient corresponds to a rock sample that is surrounded by a stationary gas phase, as it is in a centrifuge experiment. This derivation assumes that the core is oriented horizontal to the direction of flow and that $\omega^2 R(x) >> g$. Descriptions of numerical models for centrifuge experiments are provided by O'Meara and Crump (1985), Firoozabadi and Aziz (1991), and Hirasaki et al. (1992).

2.2. Sensitivity Analysis

Sensitivity of the behavior of brine displaced by gas in a low-permeability rock is described in this section for constant pressure drop and centrifuge experiments. The constant pressure drop experiments were simulated at many different levels. Centrifuge experiments were simulated at different spin rates. In addition, intrinsic permeability, relative permeability, and capillary pressure were varied. The following representations of relative permeability and capillary pressure relationships (Brooks and Corey, 1966) were used:

$$k_{rb} = k_{rb,\max} \left[\frac{(S_b - S_{br})}{(1 - S_{br})} \right]^{nb} \tag{16}$$

$$k_{rg} = k_{rg,\max} \left[\frac{(S_g - S_{gc})}{(1 - S_{gc} - S_{br})} \right]^{ng} \tag{17}$$

$$P_c = P_{th} + P_{sp} \ln \left[\frac{(S_b - S_{br})}{(1 - S_{br})} \right] \tag{18}$$

With these representations, the effect of variations in relative permeability can be assessed by changing $k_{rb,\max}$ and $k_{rg,\max}$, the exponents nb and ng, or the end-point saturations, S_{gc} and S_{br}. Consequences of variations in the capillary pressure can be assessed by varying the threshold pressure P_{th}, the "span" pressure P_{sp}, and the residual brine saturation, S_{br}.

2.2.1 Constant Pressure Drop Experiments

Unsteady-state high-rate experiments used for determining relative permeability are often operated at constant pressure drop across the core, particularly when the displacing phase is a gas. As described in Christiansen and Howarth (1995), the gas is typically introduced to the upstream face of the rock sample from a pressure regulator, and it is withdrawn at the downstream face through a back-pressure regulator. Using iterative, trial-and-error techniques, the injection rate is maintained sufficiently high to minimize the impact of capillary end-effects on flow behavior. Fingering and channeling could occur during any experiment, but the complications of these effects have largely been ignored in the two-phase relative permeability literature. Although the pressure drop is constant, the gas flow rate varies throughout the experiment in response to the propagating saturation profiles and the associated rock-fluid properties. The flow rate of the gas can be measured by mass-flow meters, by gas accumulators, or other methods. The cumulative volume of injected fluid, the cumulative volumes of the produced fluids, and the pressure drop across the core are measured throughout the experiment.

Simulated production of brine displaced by gas from a low-permeability rock is shown in Figure 3a for five experiments operating at different pressure drops. For each simulated experiment, brine production approaches a plateau after many pore volumes of gas injection. For low pressure drop experiments, brine is retained in the rock sample by capillary end effects. As pressure drop increases, retention of brine by capillary end effects diminishes. Examples of simulated saturation profiles for a pressure drop of 20 atm are shown in Figure 3b. The profile for simulated time of 400,000 seconds (approximately 4.6 days) is almost constant at a brine saturation of 0.20 except near the outlet end of the sample. The small upward curve in the saturation profile near the outlet results from capillary end (boundary) effects.

Retention by capillary end effects is assumed to be negligible for data reduction procedures such as the Welge, Johnson-Bossler-Naumann (JBN) method, and Jones-Roszelle methods. Therefore, a sufficiently large pressure drop must be applied in experiments for which data will be processed using these methods. One can imagine doing a sequence of experiments at increasing pressure drop similar to those of Figure 3a to determine a pressure drop for which brine production is not influenced by capillary end effects. For the simulations of Figure 3a, capillary end effects are negligible for pressure drops greater than 5 atm.

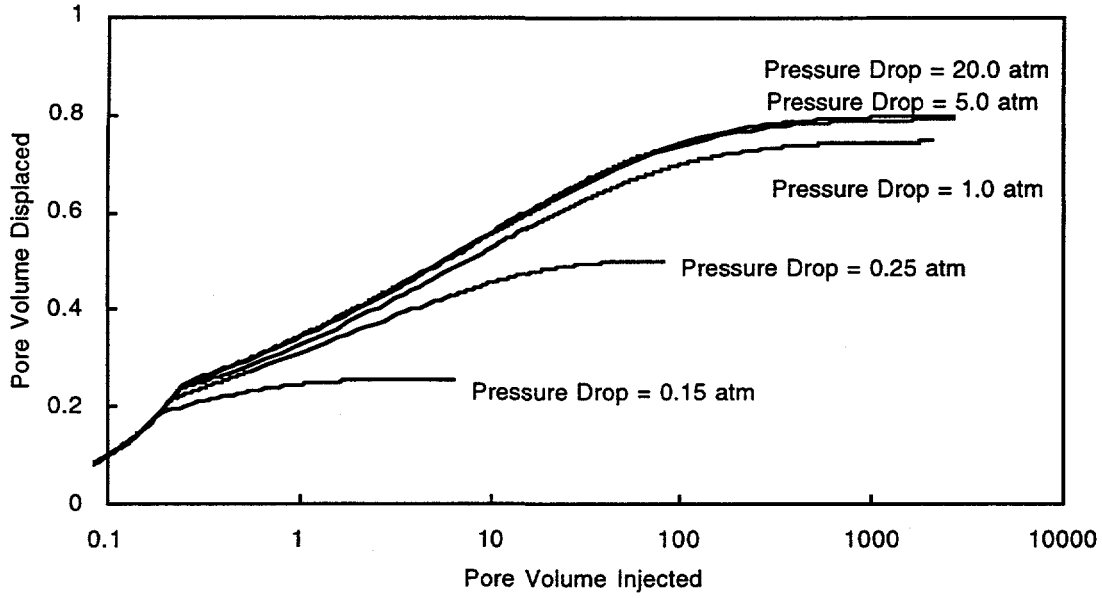

Figure 3a. Sensitivity of brine production to pressure drop. Simulations of constant pressure drop and horizontal displacements. Rock properties: k = 0.01 md, $k_{rb,\max}$ = $k_{rg,\max}$ = 1, nb = ng = 1.75, S_{br} = 0.2, S_{gc} = 0.1, and P_{th} = P_{sp} = 0.1 atm.

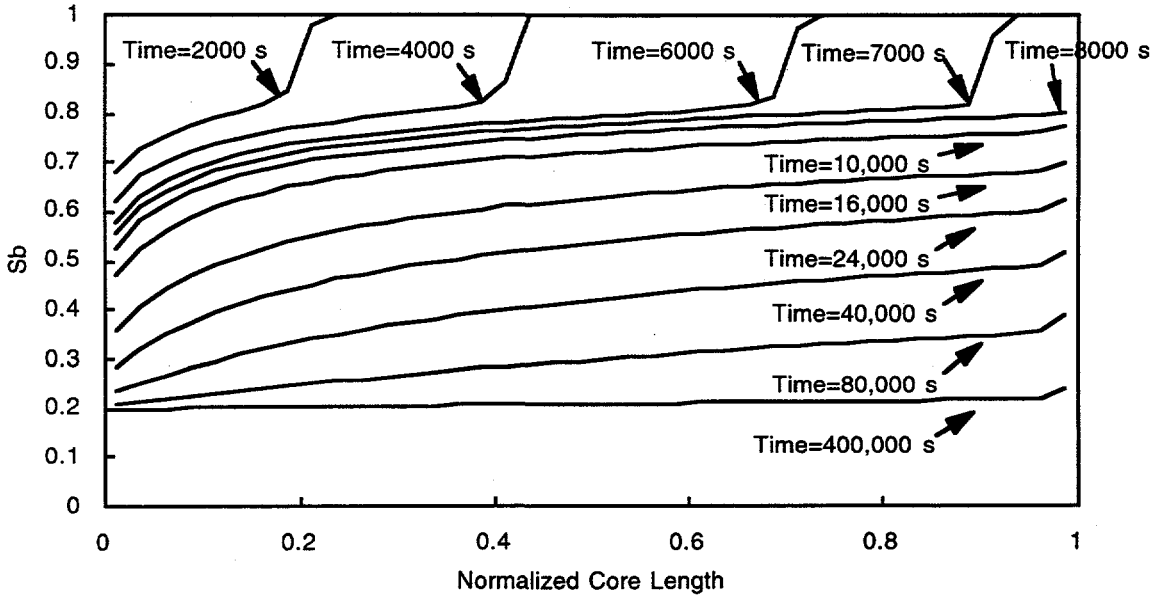

Figure 3b. Evolution of saturation profiles for pressure drop = 20 atm. Simulations of constant pressure drop and horizontal displacements. Rock properties: k = 0.01 md, $k_{rb,\max}$ = $k_{rg,\max}$ = 1, nb = ng = 1.75, S_{br} = 0.2, S_{gc} = 0.1, and P_{th} = P_{sp} = 0.1 atm.

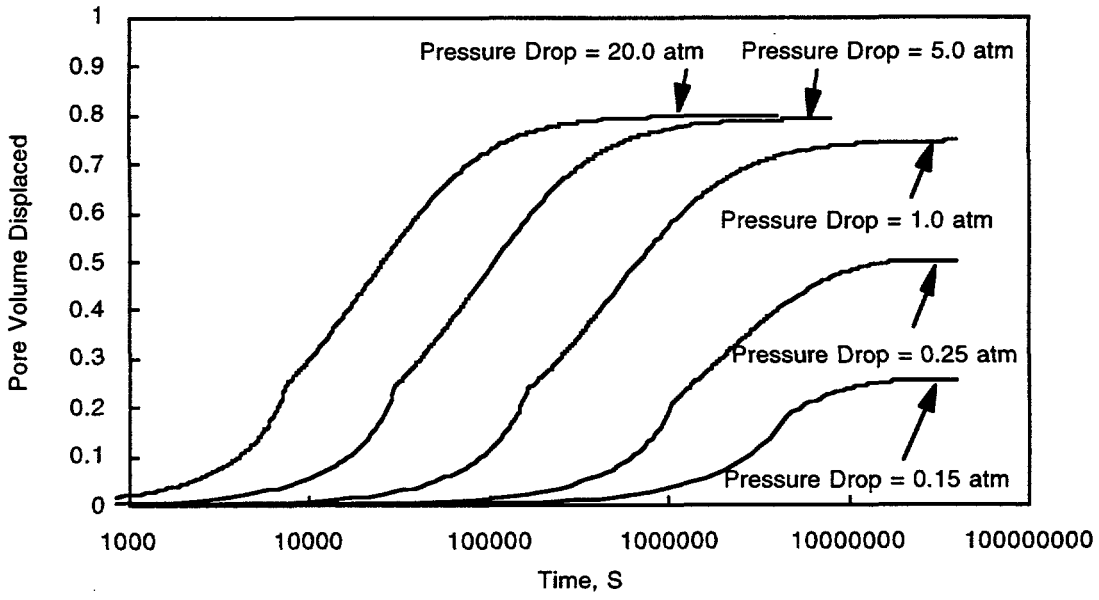

Figure 3c. Time dependence of brine production. Simulations of constant pressure drop and horizontal displacements. Rock properties: k = 0.01 md, $k_{rb,\max} = k_{rg,\max} = 1$, $nb = ng = 1.75$, $S_{br} = 0.2$, $S_{gc} = 0.1$, and $P_{th} = P_{sp} = 0.1$ atm.

The simulated brine production data of Figure 3a are replotted in Figure 3c as a function of time. For a pressure drop equal to 20 atm, the volume of brine produced reaches a plateau after an elapsed time of one million seconds, or about 12 days. For a 0.15-atm pressure drop, more than 120 days are required for the produced brine volume to reach a plateau. Operating at large pressure drops is essential for completing displacements in an acceptable length of time for low-permeability rock samples.

In Figures 4a to 4d, the effects of variations in the relative permeability relationships are shown for simulations in which capillary end effects were eliminated. These figures show that brine production is sensitive to all the parameters of the relative permeability relationships of Equations 16 and 17. The cumulative volume of displaced brine for infinite injection volume depends on the residual brine saturation S_{br}. In Figures 4a, 4b, and 4c, S_{br} is constant, and the cumulative brine production converges to the same value for large volumes of gas injection. In Figure 4d, production behavior for two values of S_{br} is contrasted.

For the low-pressure drop simulations in Figures 4e and 4f, capillary end effects were included. Variations in the threshold pressure P_{th} and "span" pressure P_{sp} in Equation 18 lead to divergence of the production behavior with increasing injection.

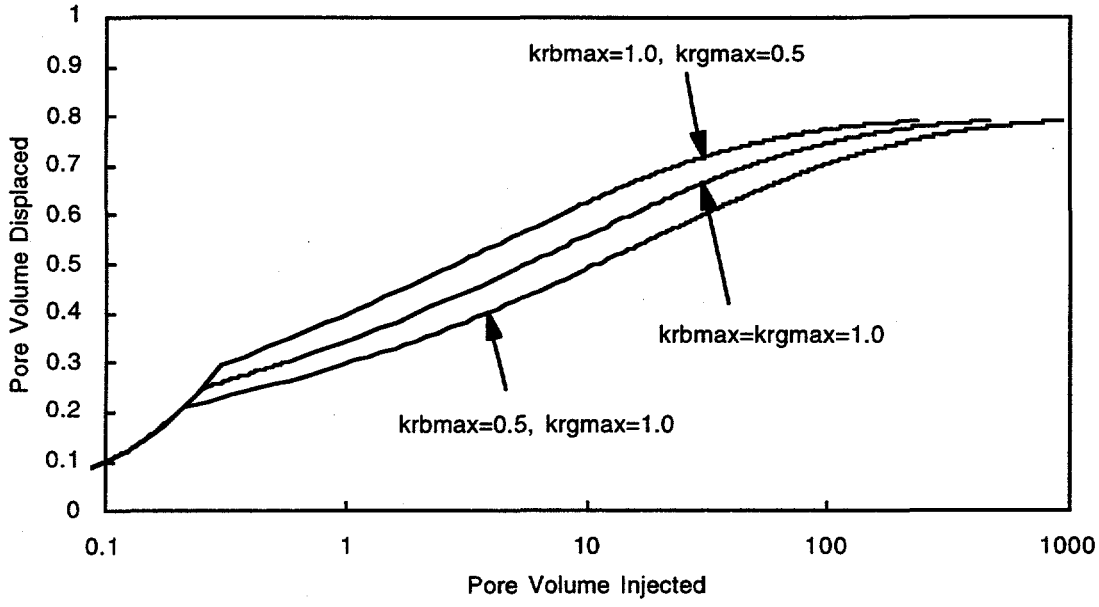

Figure 4a. Sensitivity of brine production to relative permeabilities parameters ($k_{rb,}$max) and ($k_{rg,}$max). Simulations of vertical displacements with constant pressure drop. Rock properties (except as noted): k = 0.01 md, $k_{rb,}$max = $k_{rg,}$max = 1, nb = ng = 1.75, S_{br} = 0.2, S_{gc} = 0.1, and P_{th} = P_{sp} = 0.0 atm.

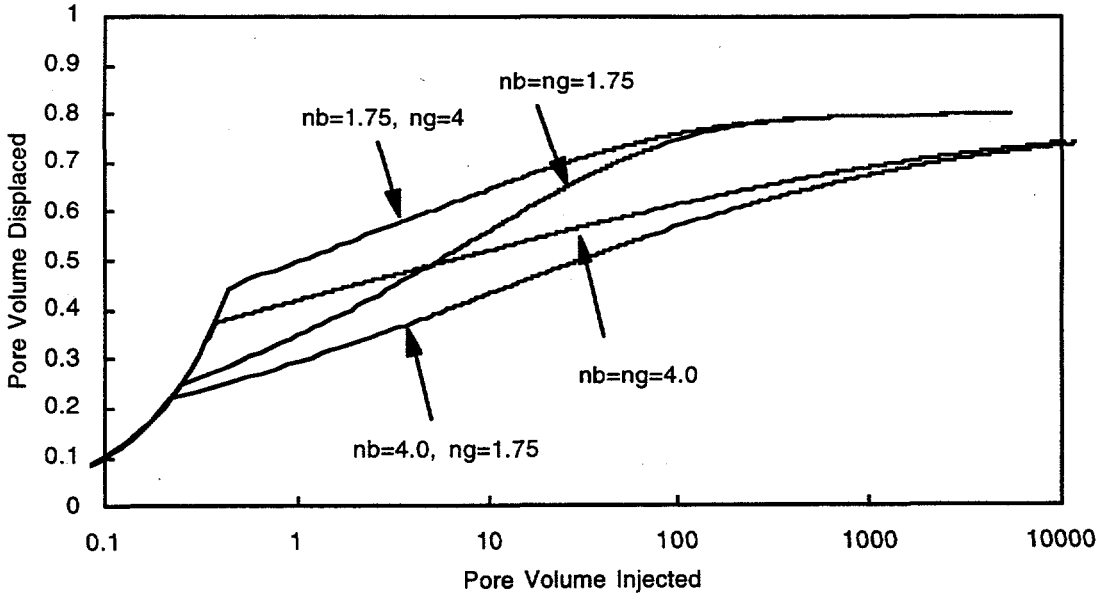

Figure 4b. Sensitivity of brine production to exponents nb and ng. Simulations of vertical displacements with constant pressure drop. Rock properties (except as noted): k = 0.01 md, $k_{rb,}$max = $k_{rg,}$max = 1, nb = ng = 1.75, S_{br} = 0.2, S_{gc} = 0.1, and P_{th} = P_{sp} = 0.0 atm.

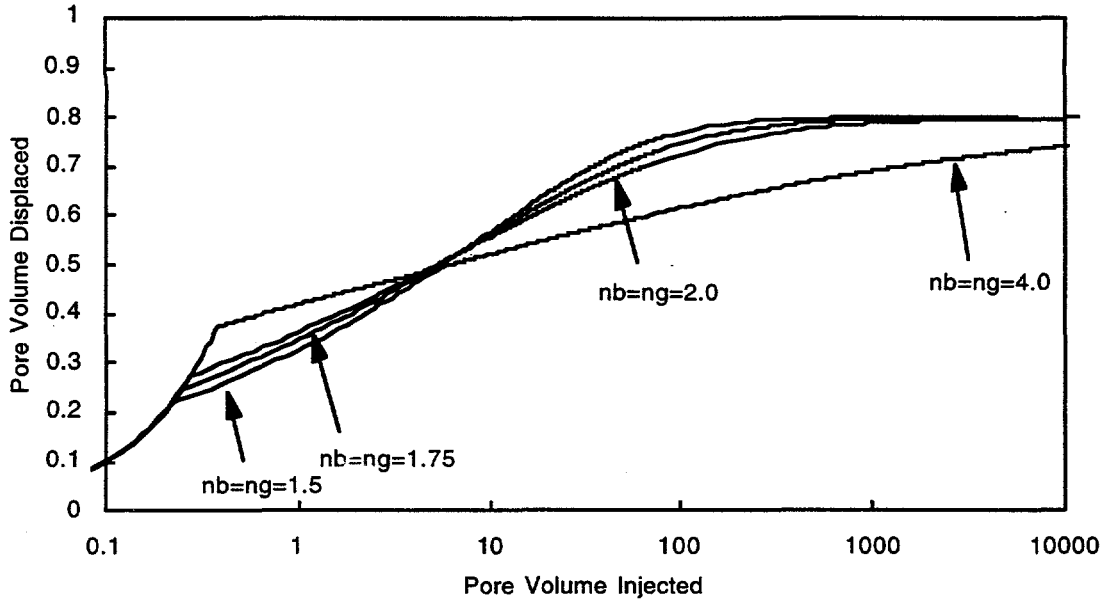

Figure 4c. More sensitivity of brine production to exponents *nb* and *ng*. Simulations of vertical displacements with constant pressure drop. Rock properties (except as noted): $k = 0.01$ md, $k_{rb,\max} = k_{rg,\max} = 1$, $nb = ng = 1.75$, $S_{br} = 0.2$, $S_{gc} = 0.1$, and $P_{th} = P_{sp} = 0.0$ atm.

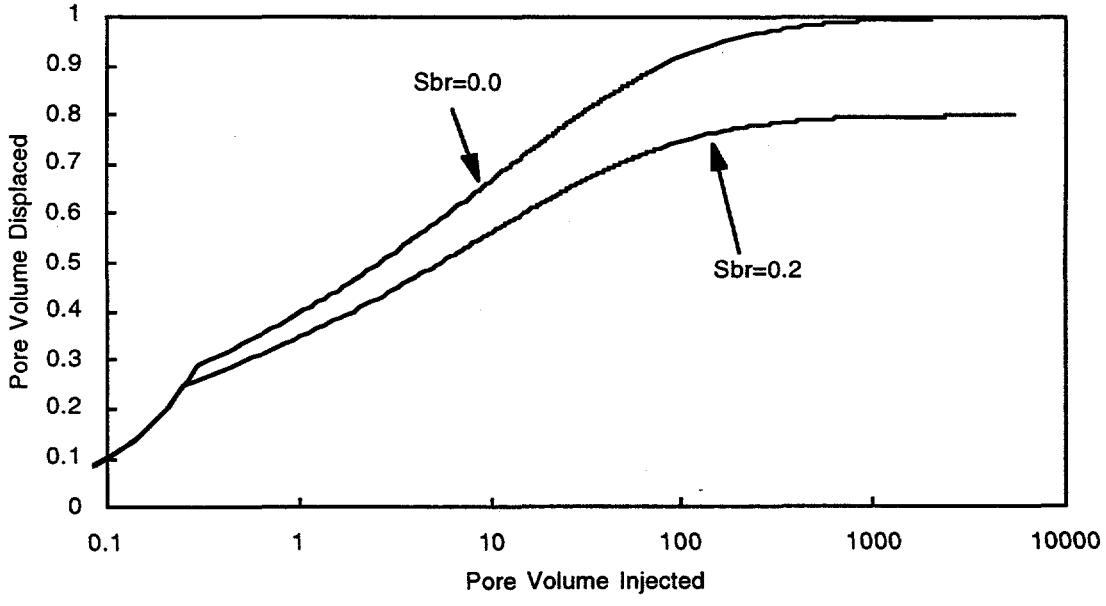

Figure 4d. Sensitivity of brine production to S_{br}. Simulations of vertical displacements with constant pressure drop. Rock properties (except as noted): $k = 0.01$ md, $k_{rb,\max} = k_{rg,\max} = 1$, $nb = ng = 1.75$, $S_{br} = 0.2$, $S_{gc} = 0.1$, and $P_{th} = P_{sp} = 0.0$ atm.

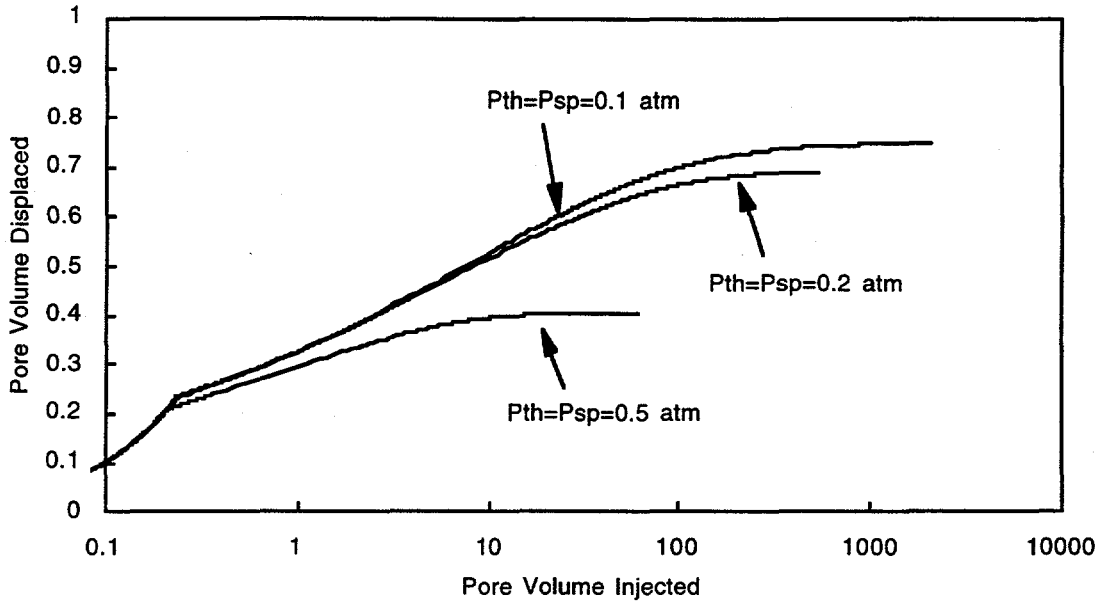

Figure 4e. Sensitivity of brine production to P_{th} and P_{sp}. Simulations of vertical displacements with constant pressure drop. Rock properties (except as noted): k = 0.01 md, $k_{rb,max} = k_{rg,max} = 1$, $nb = ng = 1.75$, $S_{br} = 0.2$, $S_{gc} = 0.1$, and $P_{th} = P_{sp} = 0.0$ atm.

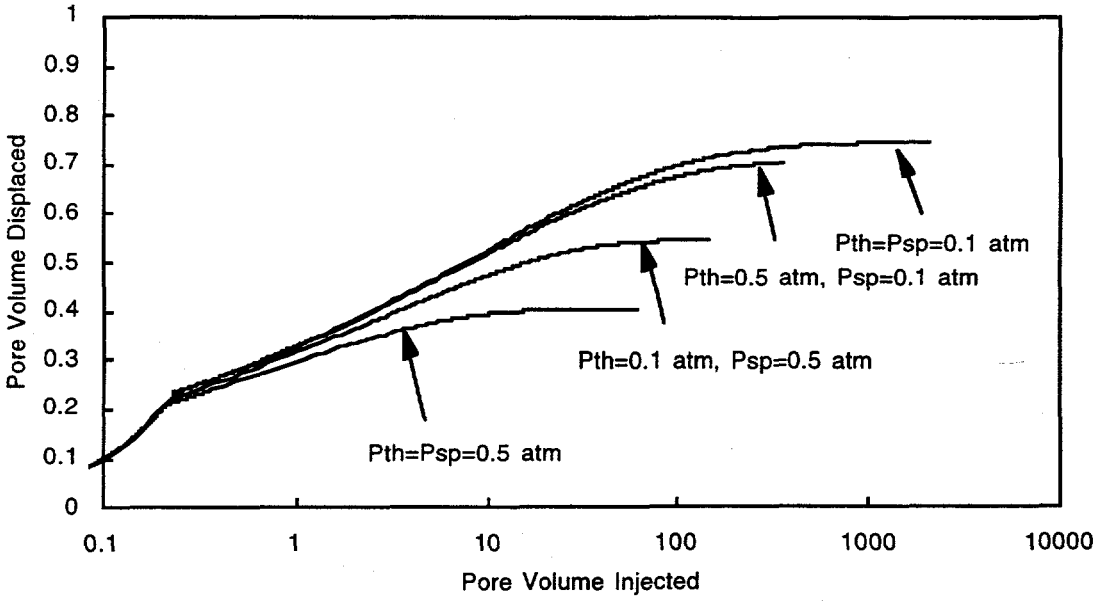

Figure 4f. More sensitivity of brine production to P_{th} and P_{sp}. Simulations of vertical displacements with constant pressure drop. Rock properties (except as noted): k = 0.01 md, $k_{rb,max} = k_{rg,max} = 1$, $nb = ng = 1.75$, $S_{br} = 0.2$, $S_{gc} = 0.1$, and $P_{th} = P_{sp} = 0.0$ atm.

2.2.2 Centrifuge Experiments

In the literature of the past 10 years, increasing use of centrifuge methods for measuring relative permeability relationships was observed by Christiansen and Howarth (1995). Centrifuge methods can provide results quickly, and the centrifuge displacement is a gravity-stable displacement, free from effects of viscous fingering. In unsteady-state high-rate or low-rate methods, viscous fingering may occur. Although an often ignored phenomenon, viscous fingering is undesirable because it complicates the interpretation of experiments.

The production behavior of simulated centrifuge experiments shows many similarities to the simulated constant-pressure-drop experiments discussed in Section 2.2.1. In constant-pressure-drop experiments, the capillary end effects can be reduced by increasing the pressure drop as shown in Figure 3a. In a centrifuge experiment, capillary end-effects can be reduced by increasing the spin rate as shown in Figure 5a. At 1000 rpm the average residual brine saturation is about 0.36, while at 3000 rpm it is about 0.22. In Figure 5b, the evolution of brine saturation profiles for the 3000 rpm example in Figure 5a is shown. After 10,000 seconds of simulation, the brine saturation profile changes very little. At this elapsed time, equilibrium between centrifugal forces and capillary forces is established.

Figures 6a to 6e show the dependence of produced brine volume on changes in rock-fluid properties for simulated centrifuge experiments at 3000 rpm. Figure 6a shows that the time needed to complete a centrifuge experiment depends on the permeability of the rock sample: for a constant spin rate, as permeability decreases, the time required to complete a centrifuge experiment increases. The longest time needed for the experiments of Figures 6a to 6e is about 100,000 seconds, or about 28 hours. To decrease the required time, the centrifuge spin rate may be increased. By doubling the spin rate, the required time decreases by a factor of four, as demonstrated qualitatively by the three examples in Figure 5a. Figures 6b, 6c, and 6d show that the brine production history is sensitive to the parameters of brine relative permeability but not to gas relative permeability because the pressure difference in the gas phase cannot be measured, a result of its low viscosity. Therefore, centrifuge experiments operated according to current practice cannot produce gas relative permeability relationships. If a means for injecting gas at a measurable flow rate and pressure drop were added to a centrifuge, then gas relative permeability could be measured. In some test laboratories, the gas relative permeability of high permeability cores is measured at the completion of each spin rate by removing the core from the centrifuge and measuring permeability in a separate apparatus using the steady-state method.

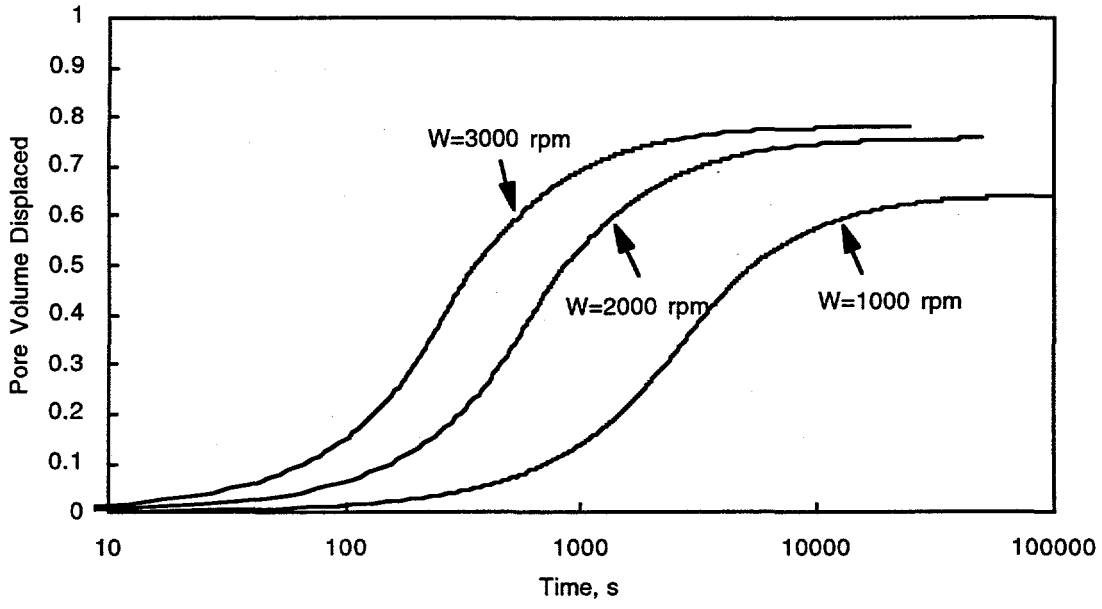

Figure 5a. Sensitivity of brine production to reduction of capillary end effects by increasing the spin rate. Simulations of constant spin rate centrifuge displacements. Rock properties: $k = 0.1$ md, $k_{rb,\max} = k_{rg,\max} = 1$, $nb = ng = 1.75$, $S_{br} = 0.2$, $S_{gc} = 0.1$, and $P_{th} = P_{sp} = 0.2$ atm. Geometric dimensions of centrifuge experiment: radius to inlet face of rock = 10.16 cm, length of rock = 10.16 cm.

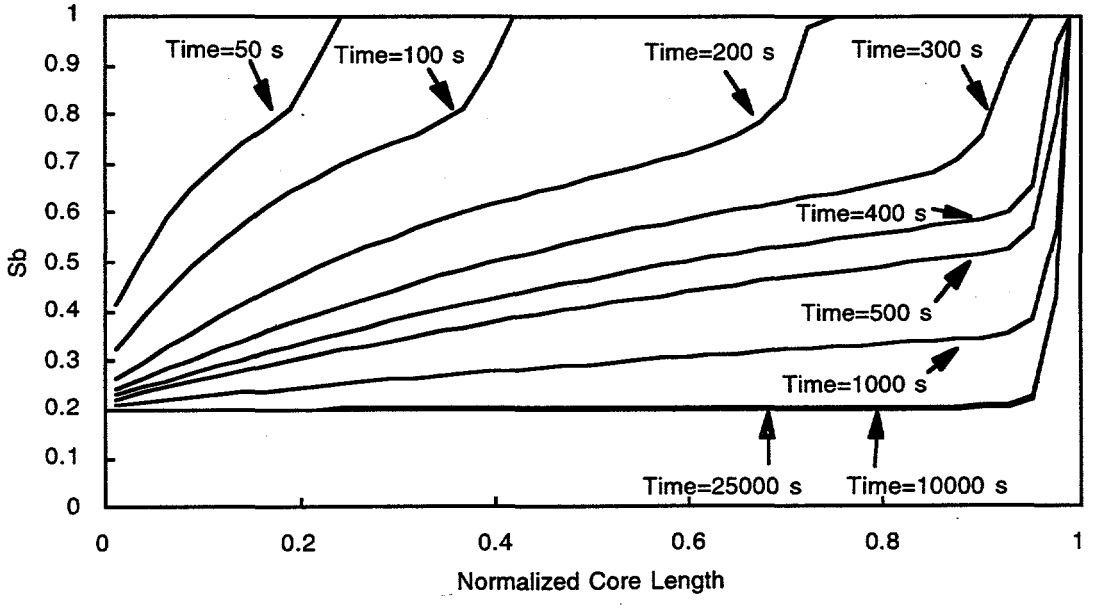

Figure 5b. Evolution of saturation profiles for spin rate of 3000 rpm. Simulations of constant spin rate centrifuge displacements. Rock properties: $k = 0.1$ md, $k_{rb,max} = k_{rg,max} = 1$, $nb = ng = 1.75$, $S_{br} = 0.2$, $S_{gc} = 0.1$, and $P_{th} = P_{sp} = 0.2$ atm. Geometric dimensions of centrifuge experiment: radius to inlet face of rock = 10.16 cm, length of rock = 10.16 cm.

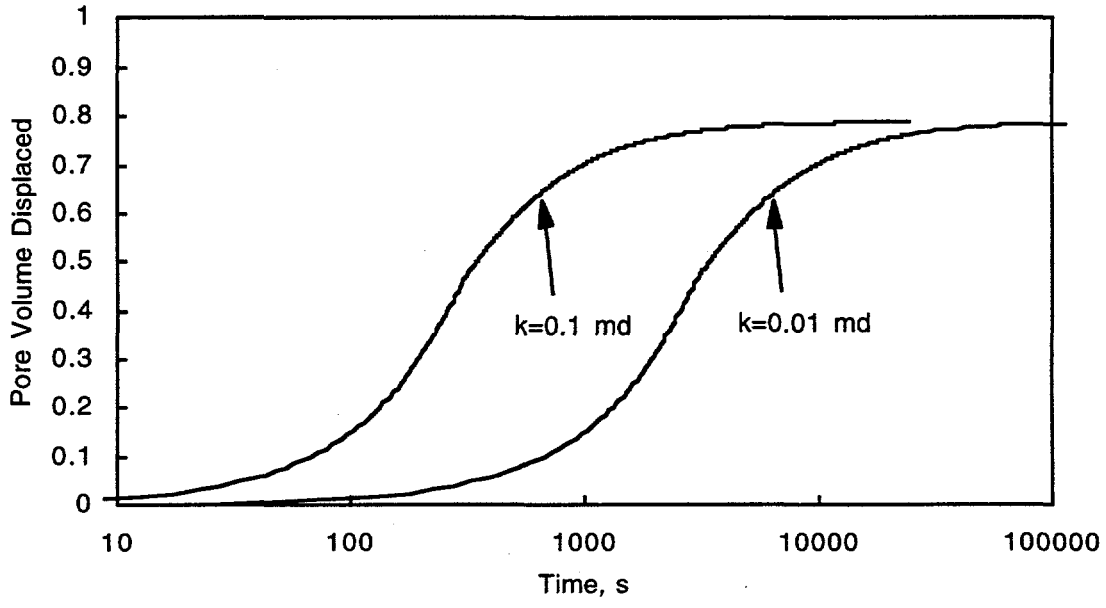

Figure 6a. Sensitivity of brine production to absolute permeability of sample (k). Simulations of centrifuge displacements with constant spin rate of 3000 rpm. Rock properties (except as noted): k = 0.1 md, k_{rb},max = k_{rg},max = 1, nb = ng = 1.75, S_{br} = 0.2, S_{gc} = 0.1, and P_{th} = P_{sp} = 0.1 atm. Geometric dimensions of centrifuge experiment: radius to inlet face of rock = 10.16 cm, length of rock = 10.16 cm.

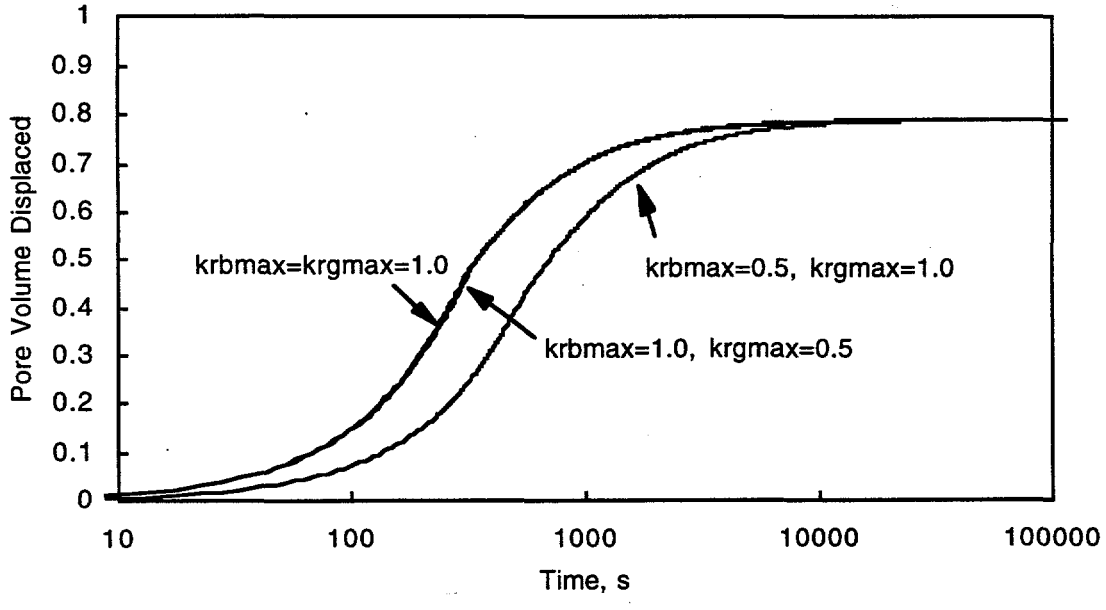

Figure 6b. Sensitivity of brine production to relative permeability parameters (k_{rb},max) and (k_{rg},max). Simulations of centrifuge displacements with constant spin rate of 3000 rpm. Rock properties (except as noted): k = 0.1 md, k_{rb},max = k_{rg},max = 1, nb = ng = 1.75, S_{br} = 0.2, S_{gc} = 0.1, and P_{th} = P_{sp} = 0.1 atm. Geometric dimensions of centrifuge experiment: radius to inlet face of rock = 10.16 cm, length of rock = 10.16 cm.

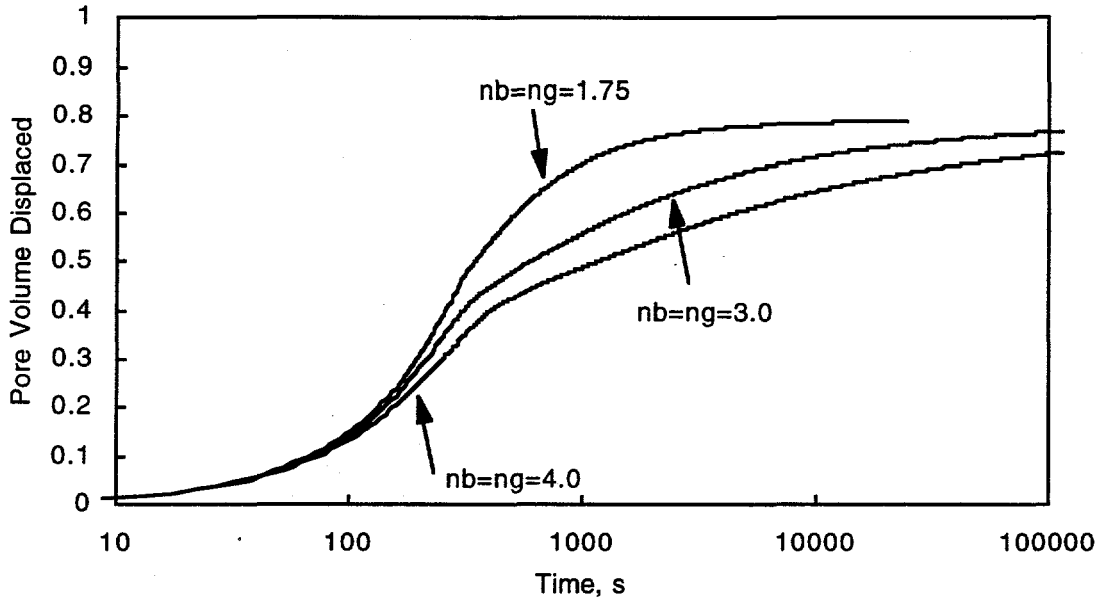

Figure 6c. Sensitivity of brine production to exponents *nb* and *ng*. Simulations of centrifuge displacements with constant spin rate of 3000 rpm. Rock properties (except as noted): $k = 0.1$ md, $k_{rb,\max} = k_{rg,\max} = 1$, $nb = ng = 1.75$, $S_{br} = 0.2$, $S_{gc} = 0.1$, and $P_{th} = P_{sp} = 0.1$ atm. Geometric dimensions of centrifuge experiment: radius to inlet face of rock = 10.16 cm, length of rock = 10.16 cm.

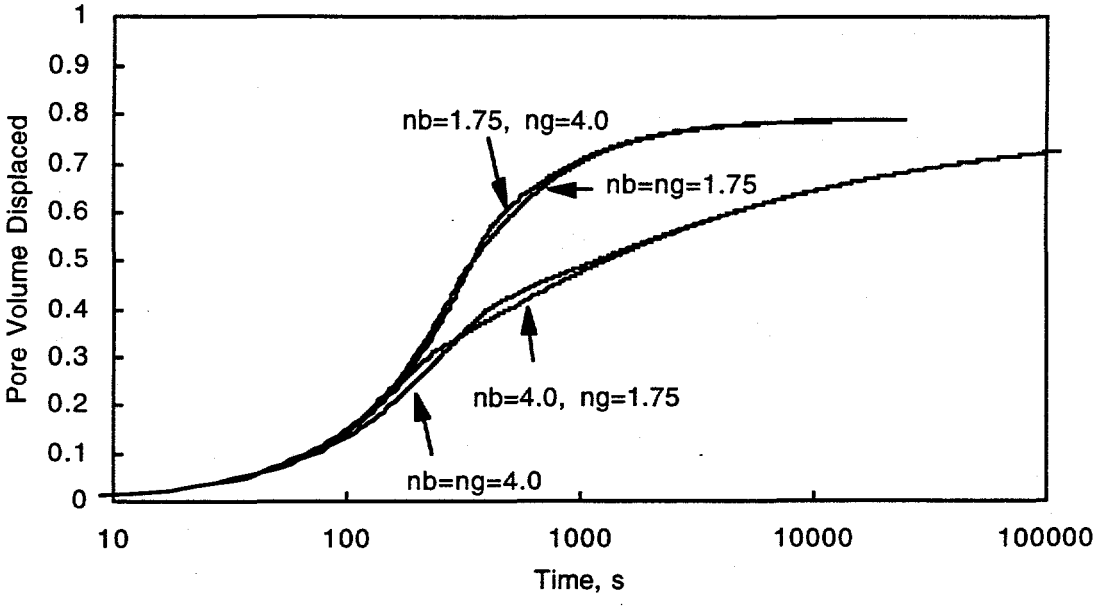

Figure 6d. More sensitivity of brine production to exponents *nb* and *ng* . Simulations of centrifuge displacements with constant spin rate of 3000 rpm. Rock properties (except as noted): $k = 0.1$ md, $k_{rb,\max} = k_{rg,\max} = 1$, $nb = ng = 1.75$, $S_{br} = 0.2$, $S_{gc} = 0.1$, and $P_{th} = P_{sp} = 0.1$ atm. Geometric dimensions of centrifuge experiment: radius to inlet face of rock = 10.16 cm, length of rock = 10.16 cm

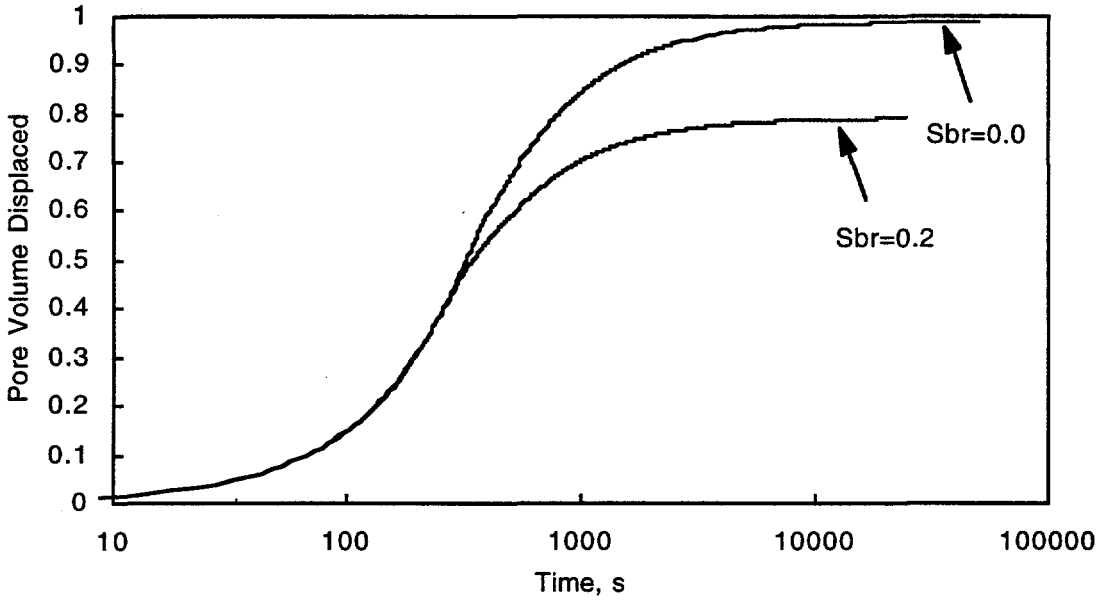

Figure 6e. Sensitivity of brine production to S_{br}. Simulations of centrifuge displacements with constant spin rate of 3000 rpm. Rock properties (except as noted): k = 0.1 md, $k_{rb,\max} = k_{rg,\max} = 1$, $nb = ng = 1.75$, $S_{br} = 0.2$, $S_{gc} = 0.1$, and $P_{th} = P_{sp} = 0.1$ atm. Geometric dimensions of centrifuge experiment: radius to inlet face of rock = 10.16 cm, length of rock = 10.16 cm.

To understand the four production histories shown in Figure 6d, consider the series of brine saturation profiles shown in Figures 7a to 7d. The brine saturation profile for the longest elapsed time approximates the profile that would be observed at infinite elapsed time and reflects a balance of the capillary forces and the centrifugal forces. The profile development for each simulation is unique. However, because the capillary pressure relationship is the same for the four simulations, the longest elapsed time saturation profiles are the same. The profile development in Figure 7a is quite different from that in Figure 7b, but the differences in corresponding brine production histories in Figure 6d are negligible. Saturation profiles for the four simulations are compared at equal elapsed times in Figures 8a and 8b, which show that the profiles are not sensitive to ng or kg, especially at longer elapsed times (Figure 8b). In Figure 8b, the curves for nb=4.0, ng =1.75 and nb=4.0, ng=4.0 overlie each other. Similarly, the curves for nb=1.75, ng =1.75 and nb=1.75, ng=4.0 overlie each other.

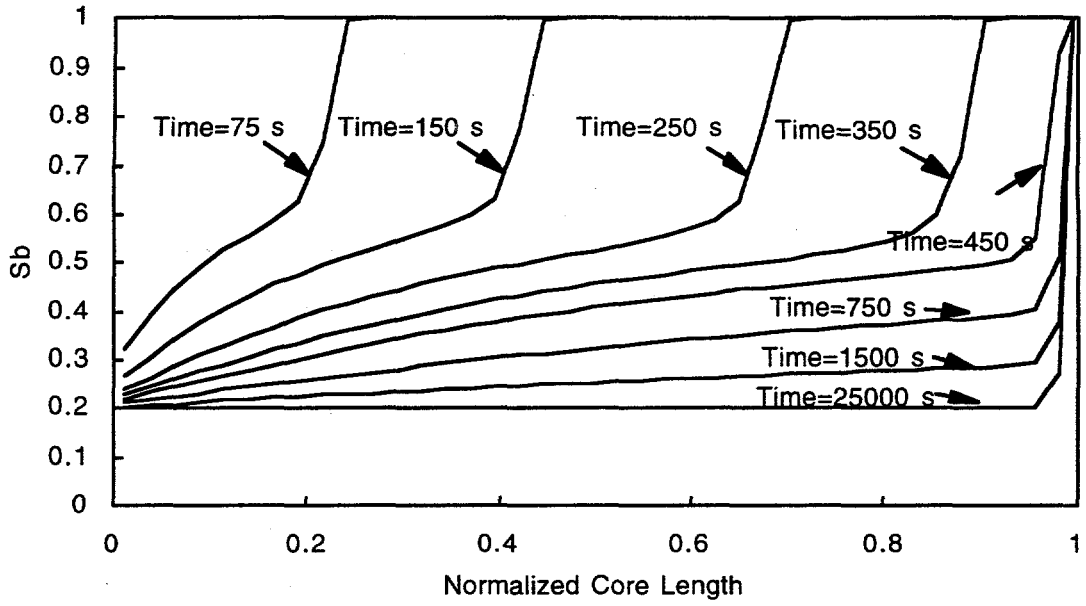

Figure 7a. Evolution of saturation profiles for simulations of centrifuge displacements with constant spin rate of 3000 rpm for $nb = 1.75$ and $ng = 4.00$. Rock properties: $k =$ 0.1 md, $k_{rb,\max} = k_{rg,\max} = 1$, $S_{br} = 0.2$, $S_{gc} = 0.1$, and $P_{th} = P_{sp} = 0.1$ atm. Geometric dimensions of centrifuge experiment: radius to inlet face of rock = 10.16 cm, length of rock = 10.16 cm.

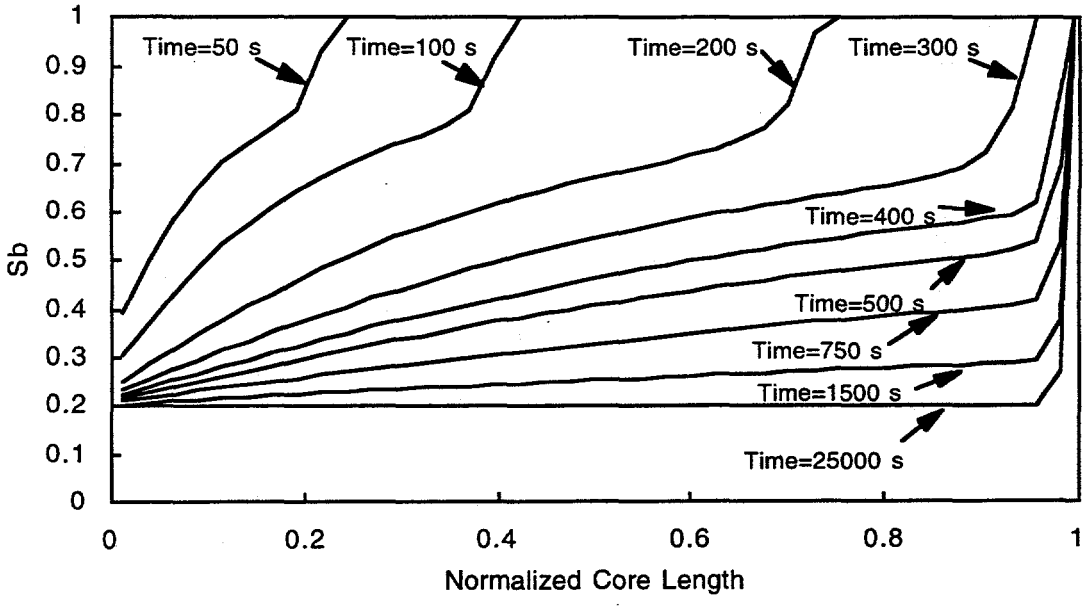

Figure 7b. Evolution of saturation profiles for simulations of centrifuge displacements with constant spin rate of 3000 rpm for $nb = 1.75$ and $ng = 1.75$. Rock properties: $k =$ 0.1 md, $k_{rb,\max} = k_{rg,\max} = 1$, $S_{br} = 0.2$, $S_{gc} = 0.1$, and $P_{th} = P_{sp} = 0.1$ atm. Geometric dimensions of centrifuge experiment: radius to inlet face of rock = 10.16 cm, length of rock = 10.16 cm.

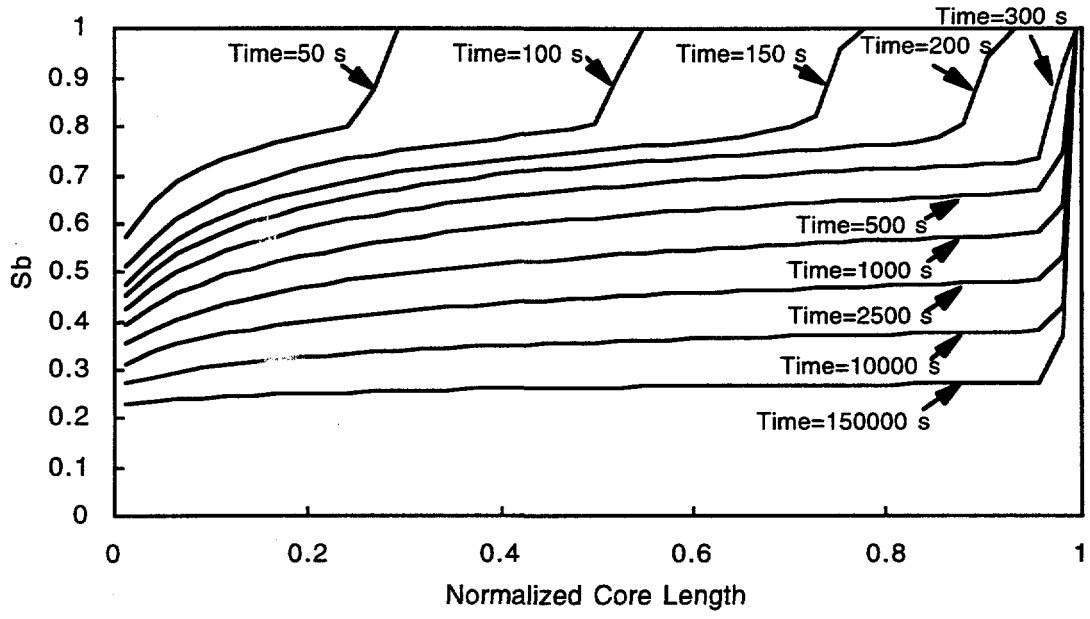

Figure 7c. Evolution of saturation profiles for simulations of centrifuge displacements with constant spin rate of 3000 rpm for $nb = 4.00$ and $ng = 1.75$. Rock properties: $k =$ 0.1 md, $k_{rb},\max = k_{rg},\max = 1$, $S_{br} = 0.2$, $S_{gc} = 0.1$, and $P_{th} = P_{sp} = 0.1$ atm. Geometric dimensions of centrifuge experiment: radius to inlet face of rock = 10.16 cm, length of rock = 10.16 cm.

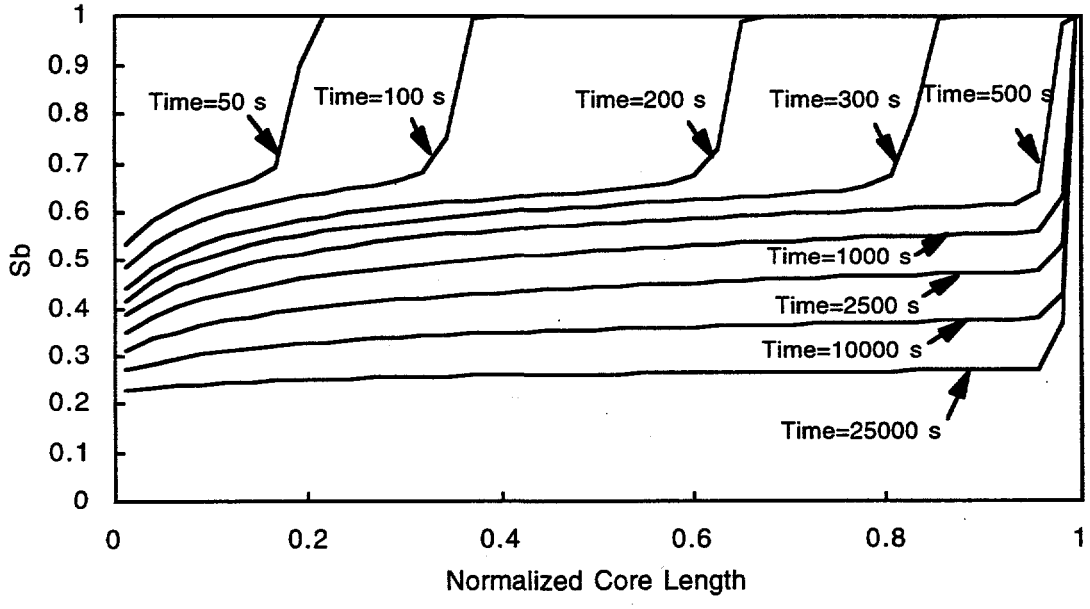

Figure 7d. Evolution of saturation profiles for simulations of centrifuge displacements with constant spin rate of 3000 rpm for $nb = 4.00$ and $ng = 4.00$. Rock properties: $k =$ 0.1 md, $k_{rb},\max = k_{rg},\max = 1$, $S_{br} = 0.2$, $S_{gc} = 0.1$, and $P_{th} = P_{sp} = 0.1$ atm. Geometric dimensions of centrifuge experiment: radius to inlet face of rock = 10.16 cm, length of rock = 10.16 cm.

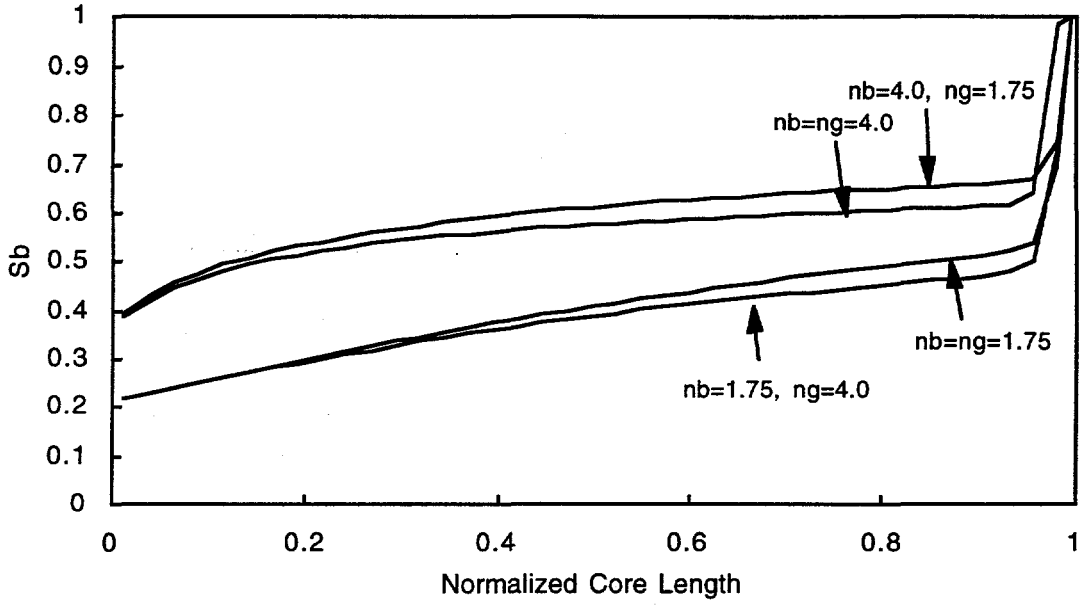

Figure 8a. Comparison of saturation profiles for simulations of centrifuge displacements with constant spin rate of 3000 rpm and elapsed time of 500 seconds. Rock properties: k = 0.1 md, k_{rb},max = k_{rg},max = 1, S_{br} = 0.2, S_{gc} = 0.1, and P_{th} = P_{sp} = 0.1 atm. Geometric dimensions of centrifuge experiment: radius to inlet face of rock = 10.16 cm, length of rock = 10.16 cm.

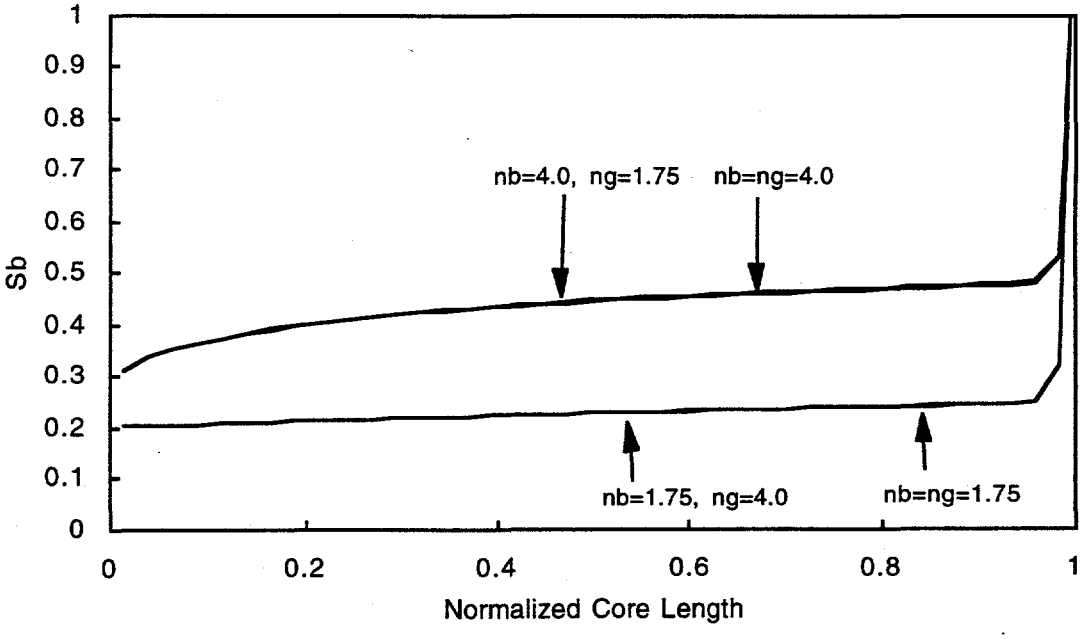

Figure 8b. Comparison of saturation profiles for simulations of centrifuge displacements with constant spin rate of 3000 rpm and elapsed time of 2500 seconds. Rock properties: k = 0.1 md, k_{rb},max = k_{rg},max = 1, S_{br} = 0.2, S_{gc} = 0.1, and P_{th} = P_{sp} = 0.1 atm. Geometric dimensions of centrifuge experiment: radius to inlet face of rock = 10.16 cm, length of rock = 10.16 cm

Figures 9 and 10a show brine production histories for simulated centrifuge experiments at 1000 and 2000 rpm. In these two figures, the parameters of the capillary pressure relationship are varied from low to high values. As P_{th} and P_{sp} increase, the cumulative volume of produced brine decreases. With increasing P_{sp}, the final saturation profiles of Figure 10b show greater brine retention.

2.3 Relative Permeability by History Matching

The history-match phase of the simulation entails a sequence of model runs in which input description parameters are altered to improve the agreement between model results and observed behavior (i.e., production data such as volumes, rates, and cumulative volumes). History matching is a trial-and-error procedure that requires considerable engineering judgment and experience (Coats, 1987). A thorough literature review of the use of history matching to estimate relative permeability was not included in Christiansen and Howarth (1995); therefore it is included in this report for completeness.

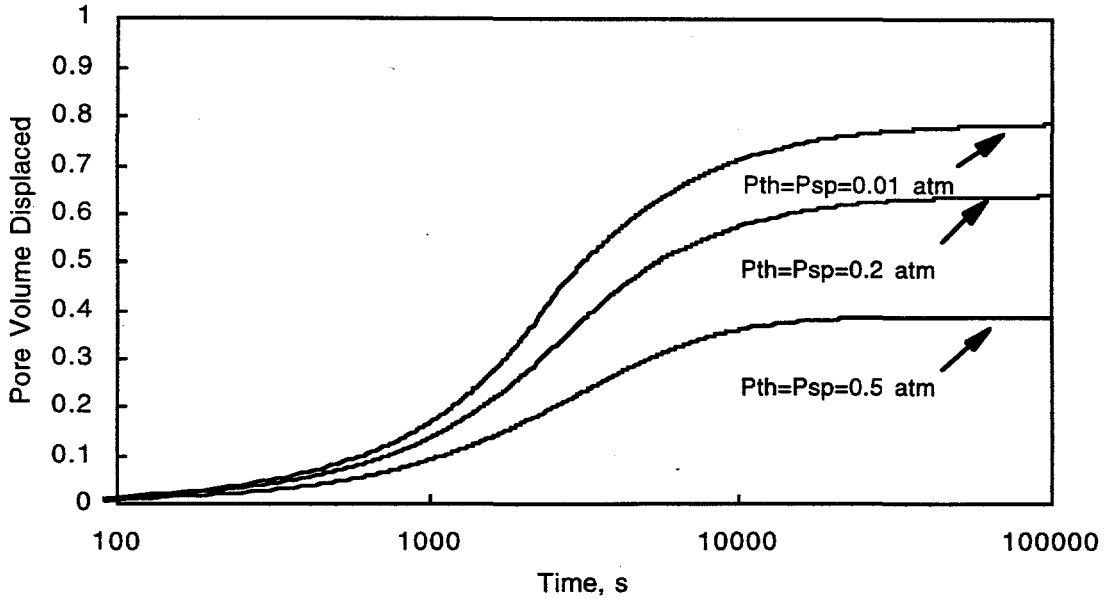

Figure 9. Sensitivity to P_{th} and P_{sp} for simulations of centrifuge displacements with constant spin rate of 1000 rpm. Rock properties: k = 0.1 md, $k_{rb,max} = k_{rg,max} = 1$, $nb = ng = 1.75$, $S_{br} = 0.2$, $S_{gc} = 0$. Geometric dimensions of centrifuge experiment: radius to inlet face of rock = 10.16 cm, length of rock = 10.16 cm.

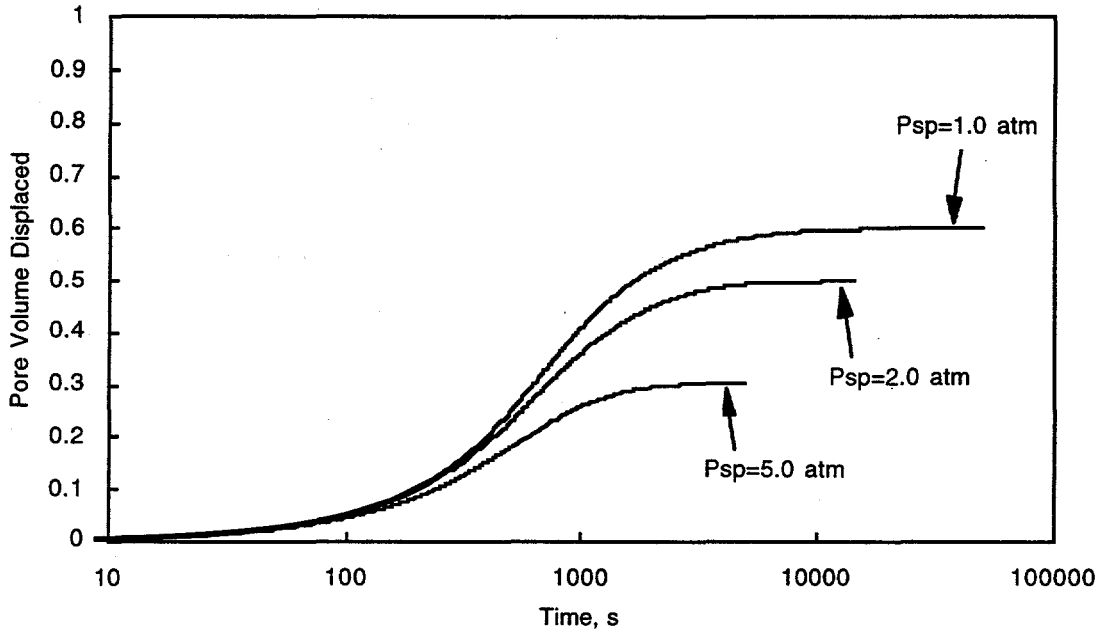

Figure 10a. Production histories for different P_{sp}. Sensitivity to P_{sp} for simulations of centrifuge displacements with constant spin rate of 2000 rpm. Rock properties: k = 0.1 md, k_{rb},max = k_{rg},max = 1, $nb = ng = 1.75$, $S_{br} = 0.2$, $S_{gc} = 0.1$, $P_{th} = 1.0$ atm. Geometric dimensions of centrifuge experiment: radius to inlet face of rock = 10.16 cm, length of rock = 10.16 cm

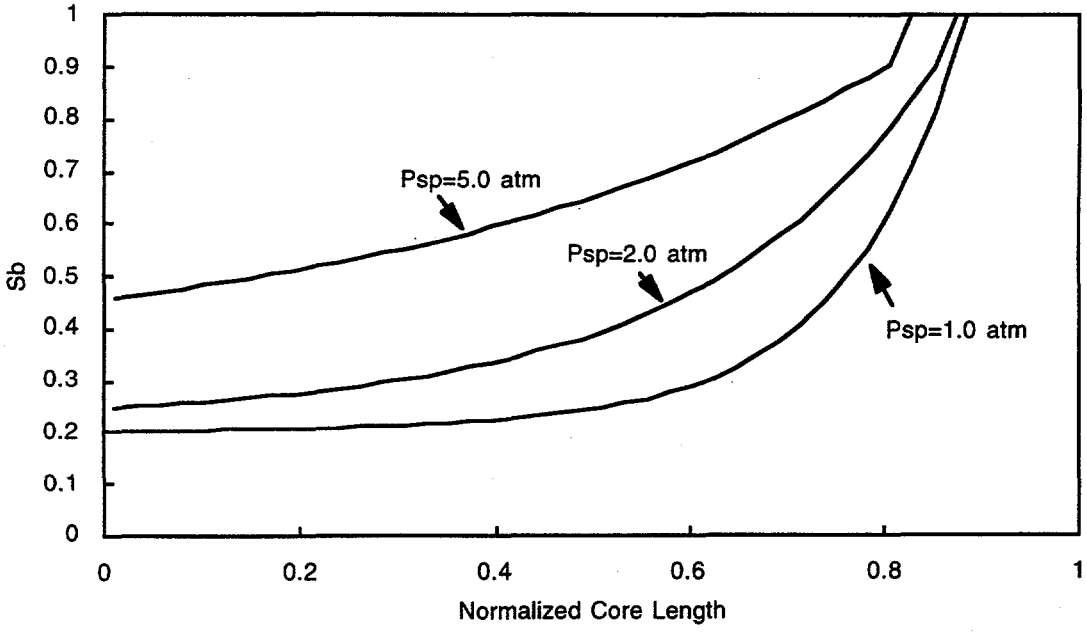

Figure 10b. Final saturation profiles for different P_{sp}. Sensitivity to P_{sp} for simulations of centrifuge displacements with constant spin rate of 2000 rpm. Rock properties: k = 0.1 md, k_{rb},max = k_{rg},max = 1, $nb = ng = 1.75$, $S_{br} = 0.2$, $S_{gc} = 0.1$, $P_{th} = 1.0$ atm. Geometric dimensions of centrifuge experiment: radius to inlet face of rock = 10.16 cm, length of rock = 10.16 cm.

2.3.1 Background

Archer and Wong (1973) were first to document history matching with a numerical simulator for measurement of relative permeability. Capillary effects were not included in their simulator. To obtain a match to the production behavior of an experiment, they manually adjusted the relative permeability relationships. For heterogeneous samples, Archer and Wong concluded that the history-matching approach was more accurate than the Johnson-Bossler-Naumann (JBN) approach, which is described in Section 3.1.2.

Sigmund and McCaffery (1979) and Batycky et al. (1981) reported success using numerical models that included capillary effects for determining relative permeabilities from unsteady-state low-rate displacements. In their simulators, relative permeabilities were represented by expressions qualitatively similar to Equations 16 and 17. The parameters of the relative permeability expressions were adjusted by a nonlinear least-squares routine to obtain a match with experimental data. Qadeer et al. (1988), Jennings et al. (1988), and Fassihi (1989) used similar approaches.

Rather than using expressions like Equations 16, 17, and 18, Kerig and Watson (1986; 1987), and Watson et al. (1988) chose to represent relative permeabilities with spline functions. With spline functions, the shapes of the relative permeability relationships obtained by nonlinear regression are not constrained to a single arbitrarily chosen function and therefore a higher quality of fit is obtained.

Capillary pressure information is most strongly represented by the asymptotic production behavior that occurs after many pore volumes are injected. To reduce the required experimental time without losing essential asymptotic information, Hyman et al. (1991a and b; 1992) and Ohen et al. (1991) proposed a procedure for extrapolating data from shortened experiments. They used a simulator to match the observed data and the extrapolated behavior by varying the parameters of capillary pressure and relative permeability expressions of the form suggested by Brooks and Corey (1966).

Other researchers have explored interesting variations on the approaches described above. MacMillan (1987) used nonlinear programming methods to match just the volumetric production data with a numerical simulator. Lai and Brandt (1988) matched only the pressure history. Civan and Donaldson (1989) described a semianalytic approach to determining relative permeability by history matching. The method used by Udegbunam (1991) is similar to that of Civan and Donaldson (1989).

History matching can be accomplished by either manual or automated adjustment of the relative permeability and capillary pressure relationships. Firoozabadi and Aziz (1991) matched production behavior using nonlinear regression on the parameters of relationships similar to those of Equations 16, 17, and 18 that were incorporated into a numerical model of the centrifuge process. Nordtvedt et al. (1993) used the Marquardt-Levenberg algorithm to adjust B-spline representations of relative permeability and capillary pressure.

2.3.2 Unsteady-State Low-Rate Experiments

The volumetric, pressure drop, and flow rate performance of unsteady-state low-rate experiments can be matched by adjusting the relationships for relative permeability and capillary pressure in a numerical simulator that properly accounts for capillary end-effects. The accuracy of this history matching approach depends on the sensitivity of production behavior to both relationships. As shown in Figures 4a through 4f, changes in relative permeability shift the production behavior horizontally along the "Pore Volume Injected" axis. Changes in the capillary pressure relationship also shift the production behavior horizontally, but more strongly shift production vertically along the "Pore Volume Displaced" axis. The vertical shift is most evident in the asymptotic behavior for large volumes of injected fluid. These simulations indicate that produced volumes, pressure drop, and flow rate data for large injected volumes are needed to obtain relative permeability and capillary pressure information from the same low-rate experiment.

2.3.3 Centrifuge Experiments

The production behavior of centrifuge experiments can be matched by adjusting the relative permeability and capillary pressure relationships of a numerical model. The success of centrifuge methods depends on the sensitivity of production behavior to both relationships. As shown in Figures 6b through 6e, changes in relative permeability cause a shift in the production behavior to the left or right along the time axis. Changes in the capillary pressure relationship shift the production behavior vertically along the Pore Volume Displaced axis, as shown in Figures 9, 10a, and 10b. The vertical shift, which reflects increased production or increased production rate, is most evident in the asymptotic behavior at late time. O'Meara and Crump (1985) concluded that centrifuge experiments that measure both early transient behavior and late asymptotic behavior are needed to obtain relative permeability and capillary pressure information. Firoozabadi and Aziz (1991) concluded that relative permeability and

capillary pressure relationships cannot be uniquely determined when asymptotic production behavior at long centrifuge times is not available.

3.0 DIFFERENTIAL DATA REDUCTION METHODS

In the oil and gas literature, unsteady-state methods, particularly those at high flow rate, are the most often reported methods for measuring relative permeability (Christiansen and Howarth, 1995). Although high-rate unsteady-state experiments take less time to complete than the steady-state experiments, conversion of the experimental data to relative permeability relationships is more complicated. In the following discussion, the data reduction methods for unsteady-state experiments are described in detail; all require differentiation of experimental data. First the methods for reducing data from unsteady-state high-rate experiments are described, including the Welge, Johnson-Bossler-Naumann, and Jones-Roszelle methods. Next the Ramakrishnan-Cappiello method for low-rate experiments is described. Finally the Hagoort method and a new modification of the Hagoort method for conversion of unsteady-state data from a centrifuge are described.

As shown in Table 1, the relationship resulting from data processing depends on the method used. For example, the Welge method gives a gas-brine relative permeability ratio, whereas the Ramakrishnan-Cappiello method gives relationships for gas relative permeability and capillary pressure. Each of the methods in Table 1 is described in this section, including a brief summary of the method, application of the method with an example, and derivation of the theoretical basis. The numerical models described in Section 2 provided the raw data for the example calculations. The rock properties used in the models were selected to approximate those of Salado anhydrite.

Table 1. Differential Data Reduction Methods for Unsteady-State Experiments

Method	Date	Results of Method
For High-Rate Experiments:		
Welge	1952	$k_{rg}(S_b) \,/\, k_{rb}(S_b)$
Johnson-Bossler-Naumann	1959	$k_{rg}(S_b)$, $k_{rb}(S_b)$
Jones-Roszelle	1978	$k_{rg}(S_b)$, $k_{rb}(S_b)$
For Low-Rate Experiments:		
Ramakrishnan-Cappiello	1991	$k_{rg}(S_b)$, $P_c(S_b)$
For Centrifuge Experiments:		
Hagoort	1980	$k_{rb}(S_b)$

3.1 High-Rate Experiments

3.1.1 Welge Method

Welge derived a procedure for obtaining relative permeability ratio k_{rg}/k_{rb} as a function of saturation from unsteady-state high-rate displacement data. The method requires differentiation of fluid production data to estimate the permeability ratio and fluid saturation at the outlet face of a porous medium.

To use the Welge method, the volumes of fluids produced as a function of the volume of injected fluid are required. For example, consider gas injection into an initially brine-saturated porous medium. The gas may be injected at either constant pressure drop or constant rate as long as the rate of flow is sufficient to overwhelm capillary end effects. By running several experiments at increasing pressure drops or flow rates, one can determine if capillary end effects are negligible by plotting all the production data versus pore volume injected on a single graph. If capillary end effects can be neglected, the data for the separate tests will be superimposed.

After satisfactory production data are obtained, the ratio k_{rg}/k_{rb} and brine saturation can be calculated by differentiation of the data. In the following discussion, the calculations for the method are summarized, followed by an example calculation and a detailed derivation.

3.1.1.1 Summary of the Method

The Welge method consists of two main steps. First the saturation at the outlet end of the rock sample is calculated:

$$S_{gL} = \overline{S_g} - Q_{gi} f_{bL} \tag{19}$$

where $f_{bL} = \dfrac{dQ_{bp}}{dQ_{gi}}$.

Average gas saturation, $\overline{S_g}$, is equal to the fractional pore volume of produced brine Q_{bp}.

Preferably, pressure drop is small compared to the mean operating pressure for experiments intended for gas relative permeability measurement. If pressure drop is small compared to the

mean operating pressure, Q_{gi} may be estimated by converting the injected volume to the mean operating pressure drop in a rock sample (Welge, 1952). However, for experiments operated with a constant pressure drop, gas expansion will not affect the outcome of Equation 19 because Q_{gi} appears implicitly in the numerator and denominator of the product $Q_{gi}f_{bL}$. For constant pressure-drop experiments, the uncertainty in Q_{gi} could be represented by a proportionality constant, which would cancel out the same constant in the denominator.

Second the relative permeability ratio, k_{rg}/k_{rb}, at the outlet of the rock sample is calculated using Equation 20:

$$\frac{k_{rgL}}{k_{rbL}} = \frac{\mu_g}{\mu_b}\left(\frac{1 - f_{bL}}{f_{bL}}\right) \tag{20}$$

Unlike Equation 19, Equation 20 is sensitive to the uncertainty in the volume of injected gas as it expands from the injection pressure to the production pressure. Therefore experiments should be designed and run with a slightly lower pressure than the mean operating pressure in order to obtain satisfactory results with Equation 20. In the oil and gas industry, the consequences of gas expansion are generally ignored; other uncertainties, such as heterogeneity and fingering effects, are considered more important.

3.1.1.2 Example

As noted in Table 1, application of the Welge method results in the relative permeability ratio, which is sufficient for modeling flow through porous media when capillary effects and gravitational segregation of fluids are neglected. For many other applications, the relative permeability ratio does not provide sufficient information for accurate modeling.

To clarify the use of this data-reduction method and demonstrate its viability, gas-brine displacements were simulated numerically for a variety of conditions using the models described in Section 2. An example of simulated production data required for Welge's method is shown in Figure 11. In addition to these data, gas and brine viscosity are also required.

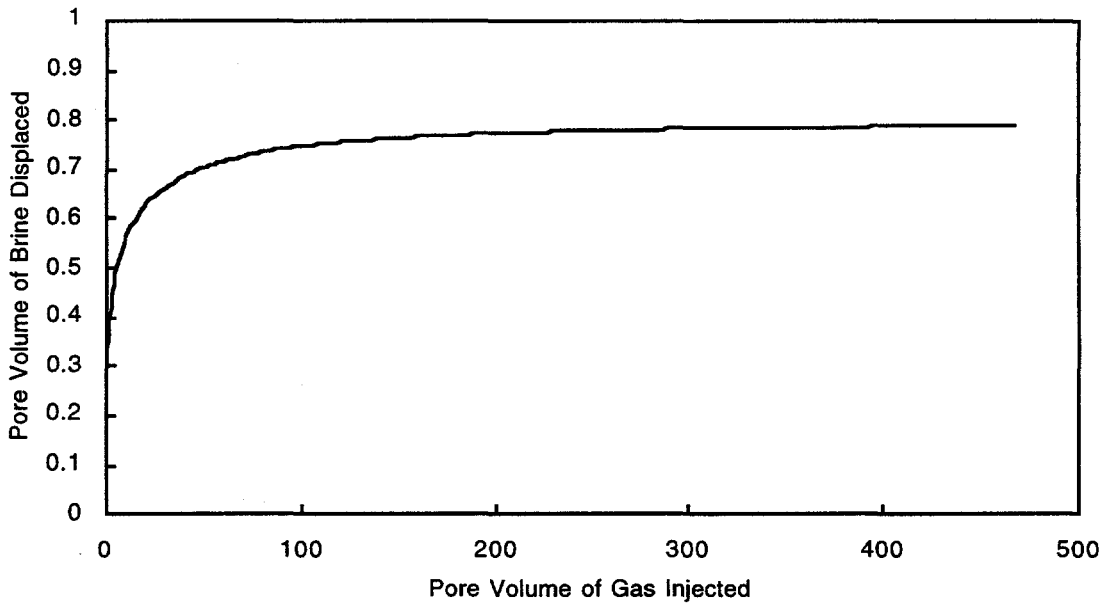

Figure 11. Simulated production data needed for Welge method of data reduction. Brine production for vertical displacement with constant pressure drop = 20 atm. Rock properties: k = 0.01 md, $k_{rb,\max} = k_{rg,\max} = 1$, $nb = ng = 1.75$, $S_{br} = 0.2$, $S_{gc} = 0.1$, and $P_{th} = P_{sp} = 0.0$ atm.

Using production and injection data as shown in Figure 11, the saturation at the outlet face and the relative permeability ratio can be calculated using Equations 19 and 20. Because data must be differentiated, experimental error is magnified in applying Equations 19 and 20. Many researchers fit a smooth curve to the production data (Collins, 1961), then differentiate the curve. Although this approach smooths the data, the resulting saturations and relative permeability ratios will depend on the choice of the smoothing function. For simulated production data like that shown in Table 2, smoothing is not an important issue. The data in the table are numerically differentiated using an expression for nonequally spaced data (Chapra and Canale, 1988; Wylie, 1975).

$$\left.\frac{dg(x)}{dx}\right|_{x=xi} \cong g(x_{i-1})\frac{x_i - x_{i+1}}{(x_{i-1}-x_i)(x_{i-1}-x_{i+1})} + g(x_i)\frac{2\,x_i - x_{i-1} - x_{i+1}}{(x_i - x_{i-1})(x_i - x_{i+1})}$$

$$+ g(x_{i+1})\frac{x_i - x_{i-1}}{(x_{i+1}-x_{i-1})(x_{i+1}-x_i)} \qquad (21)$$

Equation 21 is obtained by differentiating a second-order Lagrange interpolating polynomial for the three points x_{i-1}, x_i, and x_{i+1}.

The results from applying the Welge method to the numerically generated data are compared in Figure 12 with the ratio of relative permeabilities that were input for the numerical model. The agreement between the input and the estimated values is good.

Table 2. Example of Welge Data Reduction Method

Simulator Input Data

Pressure Drop: 20 atm

Rock Dimensions

L = 30.48 cm

R = 5.08 cm

Rock Properties

k = 0.01 md

ϕ = 0.01

$nb = ng = 1.75$

$S_{br} = 0.2$, $S_{gc} = 0.1$

$P_{th} = P_{sp} = 0$

Fluid Properties

ρ_b = 1.0 g/cm^3

ρ_g = 0.001 g/cm^3

μ_b = 1.0 cp

μ_g = 0.015 cp

Definitions of Table Headings

Q_{gi} = Pore volumes of gas injected

Q_{bp} = Pore volumes of brine produced

f_{bL} = Fractional flow of brine at outlet

S_{gL} = Saturation of gas at outlet

S_{bL} = Saturation of brine at outlet

k_{rgL}/k_{rbL} = Relative permeability ratio at outlet

Q_{gi}	Q_{bp}	f_{bL}	S_{bL}	S_{gL}	k_{rgL}/k_{rbL}
0.2697	0.2534				
0.3182	0.2642	0.2068	0.8016	0.1984	0.0575
0.3721	0.2744	0.1785	0.7920	0.2080	0.0690
0.4315	0.2843	0.1577	0.7838	0.2162	0.0801
0.4964	0.2939	0.1402	0.7757	0.2243	0.0920
0.5669	0.3032	0.1260	0.7682	0.2318	0.1041
0.6430	0.3123	0.1137	0.7608	0.2392	0.1169
0.7249	0.3211	0.1030	0.7535	0.2465	0.1307
0.8125	0.3297	0.0941	0.7468	0.2532	0.1443
0.9060	0.3381				

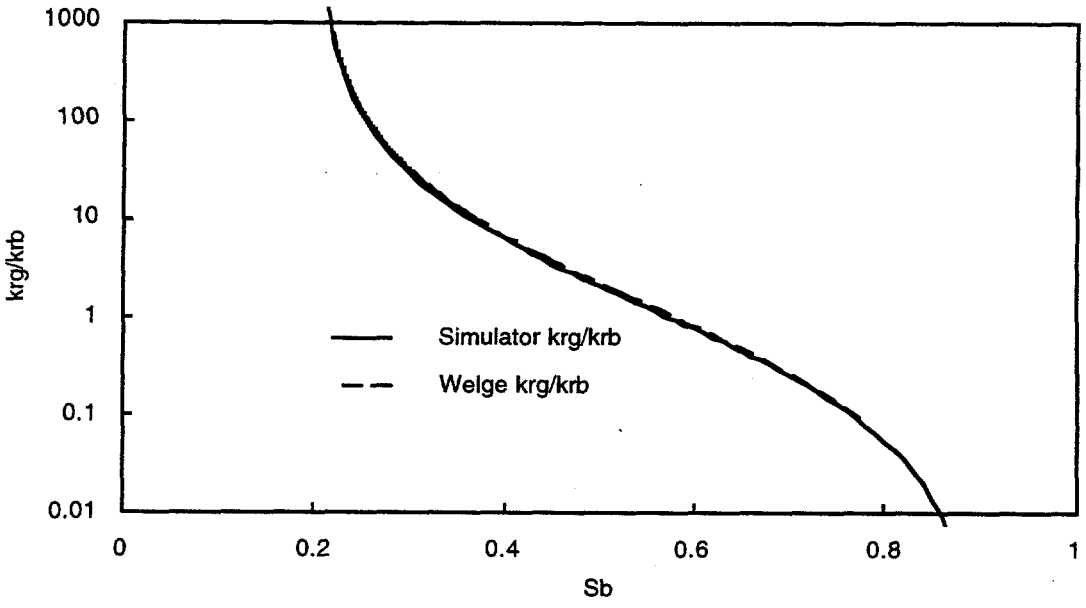

Figure 12. Comparison of results of Welge method and relative permeabilities input to numerical model.

3.1.1.3 Derivation

The derivation of this method consists of three steps. First, the Buckley-Leverett expression (Dake, 1978; Willhite, 1986; and Collins, 1961) is derived from a differential mass balance. Second, the Buckley-Leverett expression is used to develop Equation 19 for average saturation. Third, Equation 20 for the relative permeability ratio k_{rg}/k_{rb} is obtained.

BUCKLEY-LEVERETT EXPRESSION

The starting point for deriving the Buckley-Leverett expression is a differential gas balance for a one-dimensional volume element in a porous medium:

$$\left(\frac{\partial S_g}{\partial t}\right)_x + u\left(\frac{\partial f_g}{\partial x}\right)_t = 0 \qquad (22)$$

where the interstitial velocity, u, is equal to the Darcy velocity, v, divided by porosity, ϕ. Equation 22 can be modified by recognizing that

$$\left(\frac{\partial f_g}{\partial x}\right)_t = \frac{df_g}{dS_g}\left(\frac{\partial S_g}{\partial x}\right)_t \tag{23}$$

Then Equation 22 can be rearranged to yield Equation 24, which gives the velocity at which a gas saturation propagates through the porous medium.

$$\left(\frac{\partial x}{\partial t}\right)_{Sg} = -\frac{\left(\frac{\partial S_g}{\partial t}\right)_x}{\left(\frac{\partial S_g}{\partial x}\right)_t} = u\,\frac{df_g}{dS_g} \equiv u\,f_g' \tag{24}$$

Equation 24 can be integrated to obtain the Buckley-Leverett expression:

$$x_{Sg} = u\,f_g'\,t \tag{25}$$

Equation 25 describes the position, x_{Sg}, at which a saturation, S_g, is found after elapsed time, t. The derivative of the fractional flow relationship is evaluated at S_g. By replacing x_{Sg} with the length of the porous medium, a relation between time, t_{SgL}, and saturation, $S_{gL,}$ at the outlet of the sample is obtained:

$$L = u\left[f_g'\right]_{x=L} t_{SgL} = u\,f_{gL}'\,t_{SgL} \tag{26}$$

AVERAGE SATURATION

In the second step of the derivation of the Welge method, the average saturation is calculated by integrating the saturation profile over the length of the porous medium with the assumption that flow is one-dimensional:

$$\overline{S_g} = \frac{1}{L}\int_0^L S_g\,dx \tag{27}$$

Next, the variable of integration is changed from x to f_g' using the differential of the Buckley-Leverett expression of Equation 25 at constant time t:

$$\begin{aligned} dx &= \lim_{\Delta Sg \to 0} \left(x_{Sg+\Delta Sg} - x_{Sg} \right) \\ &= u \left[\lim_{\Delta Sg \to 0} \left(f_g'\Big|_{Sg+\Delta Sg} - f_g'\Big|_{Sg} \right) \right] t \\ &= u \, df_g' \, t \end{aligned} \tag{28}$$

Then changing the variable of integration from x to f_g, and substituting for L using Equation 26,

$$\overline{S_g} = \frac{1}{L} \int_0^L S_g \, dx = \frac{1}{u \, f_{gL}' \, t} \int_0^L S_g \, u \, df_g' \, t = \frac{1}{f_{gL}'} \int_0^L S_g \, df_g' \tag{29}$$

Integrating by parts,

$$\overline{S_g} = \frac{\left[S_g f_g' \right]_0^L - \int_0^L f_g' \, dS_g}{f_{gL}'} = \frac{S_{gL} f_{gL}' - \int_0^L \left(\frac{df_g}{dS_g} \right) dS_g}{f_{gL}'} = S_{gL} - \frac{\int_0^L df_g}{f_{gL}'} \tag{30}$$

Then, by evaluating the right-most integral of Equation 30,

$$\overline{S_g} = S_{gL} - \frac{f_{gL} - 1}{f_{gL}'} \tag{31}$$

Equation 31 can be simplified by first rearranging Equation 26,

$$\frac{1}{f'_{gL}} = \frac{u\,t}{L} = Q_{gi} \tag{32}$$

and recognizing that ut/L equals the pore volumes of gas injected, Q_{gi}. Substituting Equation 32 into Equation 31 yields

$$\overline{S_g} = S_{gL} - Q_{gi}\left(f_{gL} - 1\right) = S_{gL} + Q_{gi} f_{bL} \tag{33}$$

or

$$S_{gL} = \overline{S_g} - Q_{gi} f_{bL} \tag{34}$$

The fractional flow of brine, f_{bL} ,at the outlet can be expressed as a derivative of the pore volume of produced brine, Q_{bp}, with respect to the pore volume of gas injected, Q_{gi}:

$$f_{bL} = \frac{dQ_{bp}}{dQ_{gi}} \tag{35}$$

Equations 34 and 35 are the desired results for this step of the derivation. With Equation 34, the saturation of gas at the outlet of the porous medium can be calculated from experimentally observed production and injection volumes.

RELATIVE PERMEABILITY RATIO

The objective of the third step in the derivation of the Welge method is to obtain an expression for the relative permeability ratio k_{rgL}/k_{rbL}. This objective is easily obtained because the fractional flow of brine, f_{bL}, at the outlet of the porous medium can be written in terms of the viscosity ratio and the relative permeability ratio, provided that capillary effects and gravity effects are negligible. At sufficiently high flow rates or pressure drop across the porous medium, capillary effects and gravity effects become negligible. Then at the outlet,

$$f_{bL} = \frac{1}{1 + \dfrac{\mu_b\, k_{rgL}}{k_{rbL}\, \mu_g}} \tag{36}$$

By rearranging this equation, the desired expression for the relative permeability ratio k_{rg}/k_{rb} is obtained:

$$\frac{k_{rgL}}{k_{rbL}} = \frac{\mu_g}{\mu_b}\left(\frac{1 - f_{bL}}{f_{bL}}\right) \tag{37}$$

3.1.2 Johnson-Bossler-Naumann Method

The method developed by Johnson, Bossler, and Naumann (1959) is the most commonly used data reduction method for obtaining relative permeability relationships from unsteady-state data. This method (referred to throughout the literature as the JBN method) is used to calculate relative permeabilities for each phase. Similar to the Welge method, differentiation of data is required and negligible capillary end effects are assumed when using the JBN method.

To apply the JBN method, information on pore volumes of fluids injected and produced, the pressure drop across the porous medium, and fluid viscosities is needed. Gas may be injected into an initially brine-saturated porous medium either at constant pressure drop or constant rate as long as the flow rate is sufficient to overcome capillary end effects. As discussed for the Welge method, displacements for a series of experiments at increasing flow rates or pressure drops should be compared to ensure that capillary end effects are not affecting the production data.

After satisfactory production and pressure drop data are obtained, the relative permeabilities, k_{rg} and k_{rb}, and brine saturation can be calculated by differentiation of the data. In the following discussion, the calculations for the method will be summarized, followed by an example calculation and a detailed derivation.

3.1.2.1 Summary of the Method

The JBN method can be summarized in three steps. First the gas saturation at the outlet face of the rock sample is obtained by Equation 19 of the Welge method:

$$S_{gL} = \overline{S_g} - Q_{gi} f_{bL} \tag{38}$$

where $f_{bL} = \dfrac{dQ_{bp}}{dQ_{gi}}$.

Second the relative permeability at the outlet of the rock sample is obtained by a differentiation involving the relative injectivity I_r:

$$k_{rbL} = k_{rb,\max} f_{bL} \frac{d\left(\dfrac{1}{Q_{gi}}\right)}{d\left(\dfrac{1}{Q_{gi} I_r}\right)} \tag{39}$$

In this case, $k_{rb,\max}$ is the relative permeability of the displaced phase at its initial saturation, measured relative to the intrinsic or total permeability of the rock. If the rock sample is initially 100% saturated with brine, then $k_{rb,\max}$ is equal to one. The relative injectivity, I_r, is defined as the ratio of $v/\Delta P$ at the current time to $(v/\Delta P)_b$ just before the start of injection of the gas phase when the rock is completely saturated with brine:

$$I_r = \frac{(v/\Delta P)}{(v/\Delta P)_b} \tag{40}$$

In the final step, the relative permeability of the gas at the outlet face of the rock sample is calculated:

$$k_{rgL} = k_{rbL} \frac{\mu_g}{\mu_b} \left(\frac{1 - f_{bL}}{f_{bL}} \right) \tag{41}$$

Equation 39 for k_{rbL} can be simplified using the definition of f_{bL}:

$$k_{rbL} = k_{rb,\max} I_r^2 \frac{dQ_{bp}}{d(Q_{gi} I_r)} \tag{42}$$

As indicated in the example calculation below, Equation 42 provides results equivalent to Equation 39 suggested by Johnson et al. (1959). To implement Equation 39, data must be differentiated twice: once to compute f_{bL}, and once to compute the derivative.

Tao and Watson (1984a; 1984b) investigated the accuracy of the JBN method with respect to propagation of experimental errors and to the numerical algorithm for calculating derivatives of the data. As noted in the summary of the Welge method, pressure drop should be small compared to the mean operating pressure for experiments intended for gas relative permeability measurement (Johnson et al., 1959). The value of Q_{gi} is estimated by converting the injected volume to the mean operating pressure in a rock sample. Although gas expansion does not affect Equation 38, Equations 39, 41 and 42 are sensitive to gas expansion effects.

3.1.2.2 Example

If, in addition to the production data shown in Figure 11, velocity data at constant pressure drop, as shown in Figure 13, are also available, relative injectivity can be calculated. The relative permeabilities can then be estimated using the viscosities of the gas and brine, as outlined above. Application of the JBN method is demonstrated in this section by applying it to production and velocity data from numerical simulation of a displacement experiment.

In Table 3, a portion of the production and velocity data from Figures 11 and 13 is listed. The data are processed using Equations 38 through 41 of the JBN method. The data are differentiated with Equation 21. In Figure 14, the results of the method compare well with the relative permeability relationships used in the numerical simulations.

In Table 4, the same portion of the data is processed using a modified JBN method in which Equation 39 is replaced by Equation 42. The results of both methods are equivalent.

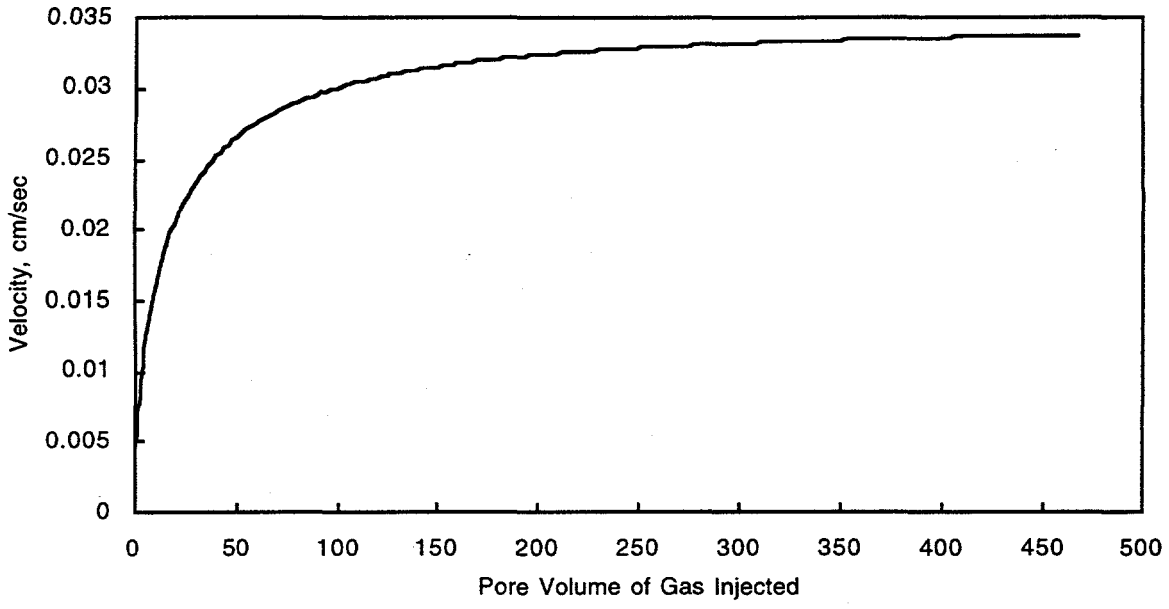

Figure 13. Simulated velocity data needed for JBN method of data reduction. Total velocity for vertical displacement with constant pressure drop = 20 atm. Rock properties: k = 0.01 md, $k_{rb,\max} = k_{rg,\max} = 1$, $nb = ng = 1.75$, $S_{br} = 0.2$, $S_{gc} = 0.1$, and $P_{th} = P_{sp} = 0.0$ atm.

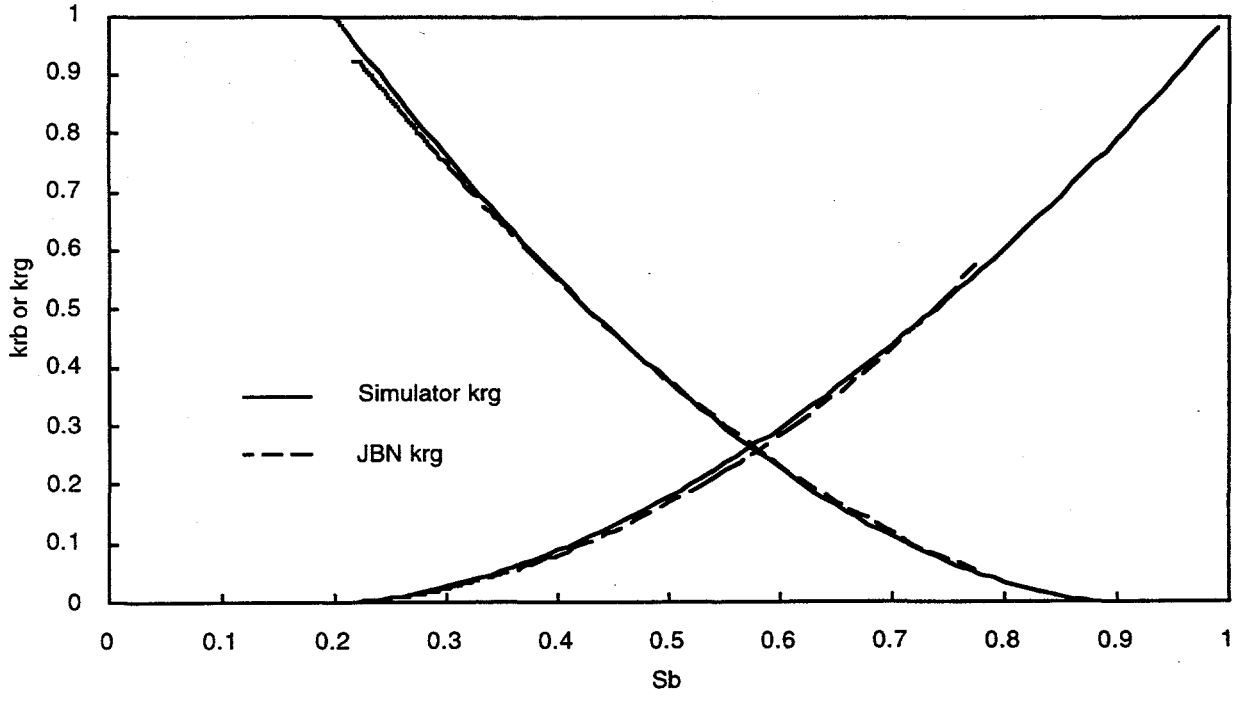

Figure 14. Comparison of relative permeabilities obtained from JBN method with input to numerical model.

Table 3. Example of JBN Data Reduction Method

Simulator Input Data

Pressure Drop: 20 atm

Rock Dimensions

L = 30.48 cm

R = 5.08 cm

Rock Properties

k = 0.01 md

ϕ = 0.01

$nb = ng = 1.75$

$S_{br} = 0.2$, $S_{gc} = 0.1$

$P_{th} = P_{sp} = 0$

Fluid Properties

$\rho_b = 1.0$ g/cm^3

$\rho_g = 0.001$ g/cm^3

$\mu_b = 1.0$ cp

$\mu_g = 0.015$ cp

Definitions of Table Headings

Q_{gi} = Pore volume of gas injected

Q_{bp} = Pore volume of brine produced

v = Total velocity, cm/s

I_r = Relative injectivity

f_{bL} = Fractional flow of brine at outlet

$\frac{d(1/Q_{gi})}{d(1/Q_{gi}I_r)}$ = From Eq. 34.

S_{bL} = Saturation of brine at outlet

S_{gL} = Saturation of gas at outlet

k_{rgL}, k_{rbL} = Relative permeabilies of brine and gas at outlet

Q_{gi}	Q_{bp}	v (cm/s)	I_r	f_{bL}	$\frac{d(1/Q_{gi})}{d(1/Q_{gi}I_r)}$	S_{bL}	S_{gL}	k_{rbL}	k_{rgL}
0.0000	0.0000	0.000533	1.0000						
0.2697	0.2534	0.002250	4.2214						
0.3182	0.2642	0.002520	4.7280	0.2068	2.8582	0.8016	0.1984	0.5912	0.0340
0.3721	0.2744	0.002790	5.2345	0.1785	3.2189	0.7920	0.2080	0.5746	0.0397
0.4315	0.2843	0.003060	5.7411	0.1577	3.5775	0.7838	0.2162	0.5642	0.0452
0.4964	0.2939	0.003330	6.2477	0.1402	3.9064	0.7757	0.2243	0.5479	0.0504
0.5669	0.3032	0.003610	6.7730	0.1260	4.2495	0.7682	0.2318	0.5354	0.0557
0.6430	0.3123	0.003890	7.2983	0.1137	4.6172	0.7608	0.2392	0.5251	0.0614
0.7249	0.3211	0.004170	7.8236	0.1030	4.9504	0.7535	0.2465	0.5097	0.0666
0.8125	0.3297	0.004460	8.3677	0.0941	5.2987	0.7468	0.2532	0.4988	0.0720
0.9060	0.3381	0.004750	8.9118						

Table 4. Example of Modified JBN Data Reduction Method

Simulator Input Data

Pressure Drop: 20 atm

Rock Dimensions

L = 30.48 cm

R = 5.08 cm

Rock Properties

k = 0.01 md

ϕ = 0.01

$nb = ng = 1.75$

$S_{br} = 0.2$, $S_{gc} = 0.1$

$P_{th} = P_{sp} = 0$

Fluid Properties

$\rho_b = 1.0$ g/cm^3

$\rho_g = 0.001$ g/cm^3

$\mu_b = 1.0$ cp

$\mu_g = 0.015$ cp

Definitions of Table Headings

Q_{gi} = Pore volume of gas injected

Q_{bp} = Pore volume of brine produced

v = Velocity, cm/s

I_r = Relative injectivity

f_{bL} = Fractional flow of brine at outlet

$\frac{dQ_{bp}}{d(Q_{gi}I_{ri})}$ = From Eq. 37

S_{bL} = Saturation of brine at outlet

S_{gL} = Saturation of gas at outlet

k_{rgL}, k_{rbL} = Relative permeabilies of brine and gas at outlet

Q_{gi}	Q_{bp}	v (cm/s)	I_r	f_{bL}	$\frac{dQ_{bp}}{d(Q_{gi}I_{ri})}$	S_{bL}	S_{gL}	k_{rbL}	k_{rgL}
0.0000	0.0000	0.000533	1.0000						
0.2697	0.2534	0.002250	4.2214						
0.3182	0.2642	0.002520	4.7280	0.2068	0.0266	0.8016	0.1984	0.5940	0.0342
0.3721	0.2744	0.002790	5.2345	0.1785	0.0210	0.7920	0.2080	0.5766	0.0398
0.4315	0.2843	0.003060	5.7411	0.1577	0.0172	0.7838	0.2162	0.5661	0.0454
0.4964	0.2939	0.003330	6.2477	0.1402	0.0141	0.7757	0.2243	0.5506	0.0506
0.5669	0.3032	0.003610	6.7730	0.1260	0.0117	0.7682	0.2318	0.5368	0.0559
0.6430	0.3123	0.003890	7.2983	0.1137	0.0099	0.7608	0.2392	0.5266	0.0616
0.7249	0.3211	0.004170	7.8236	0.1030	0.0084	0.7535	0.2465	0.5116	0.0669
0.8125	0.3297	0.004460	8.3677	0.0941	0.0071	0.7468	0.2532	0.4999	0.0722
0.9060	0.3381	0.004750	8.9118						

3.1.2.3 Derivation

The derivation of the JBN method begins by integrating the pressure gradient from the inlet to outlet end of a porous sample:

$$\Delta P = \int_0^L \frac{\partial P}{\partial x}\, dx \tag{43}$$

From Darcy's law, the pressure gradient is $\frac{\partial P}{\partial x} = - \frac{\mu_b f_b v}{k\, k_{rb}}$.

Substituting the Buckley-Leverett expressions of Equations 25, 26 and 28, dx equals $L \frac{df_g'}{f_{gL}'}$.

Then, substituting for $\frac{\partial P}{\partial x}$ and dx, the integral of Equation 43 becomes

$$\Delta P = \int_0^L \frac{\partial P}{\partial x}\, dx = - \frac{v\, \mu_b\, L}{k\, f_{gL}'} \int_0^{f_{gL}'} \frac{f_b}{k_{rb}}\, df_g' \tag{44}$$

Solving for the integral on the extreme right of Equation 44, and using a form of Darcy's law, $\frac{k\, k_{rb,\max}}{\mu_b\, L} = \left(\frac{v}{\Delta P} \right)_b$, to represent the relationship between flow velocity, pressure drop, and rock-fluid properties at the start of gas injection (i.e., the rock sample is saturated with brine) Equation 45 is obtained:

$$\int_0^{f_{gL}'} \frac{f_b}{k_{rb}}\, df_g' = - \frac{k\, f_{gL}'\, \Delta P}{v\, \mu_b\, L} = \frac{f_{gL}'}{k_{rb,\max}} \frac{(v\ /\ \Delta P)_b}{(v\ /\ \Delta P)} \tag{45}$$

The relative permeability to brine at the start of gas injection, $k_{rb,\max}$, can be defined as one. But that simplification is avoided here to broaden the application of the derivation. Next, Equation 45 is revised by defining a new quantity, the relative injectivity I_r:

$$\int_0^{f'_{gL}} \frac{f_b}{k_{rb}}\, df'_g = \frac{f'_{gL}}{k_{rb,\max}\, I_r} \tag{46}$$

where $\frac{1}{I} = \frac{(v/\Delta P)_b}{(v/\Delta P)}$.

As in the Welge derivation, Equation 46 is differentiated with respect to f'_{gL} to obtain:

$$\frac{f_{bL}}{k_{rbL}} = \left[\frac{1}{k_{rb,\max}}\right]\left[\frac{d\left(f'_{gL} / I_r\right)}{df'_{gL}}\right] \tag{47}$$

or

$$\frac{f_{bL}}{k_{rbL}} = \left[\frac{1}{k_{rb,\max}}\right]\left[\frac{d\left(\frac{1}{Q_{gi}\, I_r}\right)}{d\left(\frac{1}{Q_{gi}}\right)}\right] \tag{48}$$

With $k_{rb,\max} = 1$, Equation 48 is the same as Equation 8a of Johnson et al. (1959). They define relative permeability equal to one at the start of a displacement, regardless of the saturation of fluids in the rock. Here, relative permeability is defined with respect to the permeability of rock saturated with a single fluid. This difference was also noted in Appendix B of Jones and Roszelle (1978).

An alternative expression of Equation 48 is obtained by incorporating the expression for fractional flow from Equation 35,

$$f_{bL} = \frac{dQ_{bp}}{dQ_{gi}} \tag{49}$$

into Equation 48 to yield:

$$k_{rbL} = k_{rb,\max} \frac{\left[\frac{dQ_{bp}}{dQ_{gi}}\right]}{\left[\frac{d\left(1/Q_{gi}I_r\right)}{d\left(1/Q_{gi}\right)}\right]}$$

$$= k_{rb,\max} \left[\frac{dQ_{bp}}{dQ_{gi}}\right]\left[\frac{d\left(1/Q_{gi}\right)}{d\left(1/Q_{gi}I_r\right)}\right]$$

$$= k_{rb,\max} I_r^{\,2}\left[\frac{dQ_{bp}}{dQ_{gi}}\right]\left[\frac{dQ_{gi}}{d\left(Q_{gi}I_r\right)}\right] \qquad (50)$$

With further rearranging of the derivatives in the last line of Equation 50, a simplified expression for the brine relative permeability at the outlet of the porous medium is obtained:

$$k_{rbL} = k_{rb,\max} I_r^{\,2} \frac{dQ_{bp}}{d\left(Q_{gi}I_r\right)} \qquad (51)$$

Although this simplification does not alter the performance of the method in principle, it may propagate less error by differentiation than Equation 48.

An expression for gas relative permeability is obtained by rearranging Equation 20 of the Welge method,

$$k_{rgL} = k_{rbL} \frac{\mu_g}{\mu_b}\left(\frac{1 - f_{bL}}{f_{bL}}\right) \qquad (52)$$

with k_{rbL} calculated from either Equation 48 or Equation 51. The saturation at the outlet face is calculated using Equation 19 of the Welge method:

$$S_{gL} = \overline{S_g} - Q_{gi} f_{bL} \qquad (53)$$

3.1.3 Jones-Roszelle Method

The method of Jones and Roszelle (1978) is similar to the JBN method in that it combines the Welge method with differentiation of pressure drop and flow rate data. However, the Jones-Roszelle method treats data reduction differently. This method uses graphical data processing, a technique described in detail in Section 3.1.3.2, which is useful for consistent interpretation of the data. Another unique feature of the Jones and Roszelle contribution is the derivation of the method, which is simpler than that outlined for the Welge and the JBN methods.

A modification of the Jones-Roszelle method was proposed by Odeh and Dotson (1985) to account for capillary end effects. The approach proposed by Odeh and Dotson is empirical.

3.1.3.1 Summary of the Method

The Jones-Roszelle method consists of four main steps, the first and third of which can be obtained by graphical constructions. First, the gas saturation at the outlet face of the rock sample is obtained by the Welge expression of Equation 19:

$$S_{gL} = \overline{S_g} - Q_{gi} \frac{d\overline{S_g}}{d\, Q_{gi}} \tag{54}$$

where $\overline{S_g} = Q_{bp}$.

Second, the gas and brine fractional flow at the outlet face of the rock sample must be calculated:

$$1 - f_{gL} = f_{bL} = \left(\overline{S_g} - S_{gL}\right)/Q_{gi} \tag{55}$$

Third, the effective viscosity, λ_L^{-1} , at the outlet face of the rock sample must be calculated:

$$\lambda_L^{-1} = \overline{\lambda^{-1}} - Q_{gi} \frac{d\overline{\lambda^{-1}}}{dQ_{gi}} \tag{56}$$

where $\overline{\lambda^{-1}} = \mu_b \frac{(\Delta P/q)}{(\Delta P/q)_b}$.

In Equation 56, λ^{-1} is the average effective viscosity. The quantity $(\Delta P/q)$ is the ratio of current pressure drop to current total flow rate, and $(\Delta P/q)_b$ is the ratio of pressure drop to total flow rate for the rock sample when it was completely saturated with brine.

Finally, the relative permeabilities of the gas and brine at the outlet face of the rock sample are obtained:

$$k_{rgL} = \frac{\mu_g f_{gL}}{\lambda_L^{-1}} \tag{57}$$

$$k_{rbL} = \frac{\mu_b f_{bL}}{\lambda_L^{-1}} \tag{58}$$

As noted in the summary of the Welge and JBN methods, pressure drop should be small compared to the mean operating pressure for experiments intended for gas relative permeability measurement. The value of Q_{gi} is estimated by converting the injected volume to the mean operating pressure in a rock sample. Although gas expansion does not affect the outcome of Equation 54, the results of Equations 55, 57, and 58 are sensitive to gas expansion effects.

For large volumes of injected fluid, Jones and Roszelle (1978) suggested alternatives to the first and third steps. For the first step,

$$S_{gL} = 2\,\overline{S_g} - S_g^+ \tag{59}$$

in which S_g^+ is obtained from a plot of $\overline{S_g}$ versus $1/Q_{gi}$. For a tangent to the $\overline{S_g}$ curve, S_g^+ is the intercept with the $\overline{S_g}$ axis where $1/Q_{gi}$ equals zero. Similarly, for the third step,

$$\lambda_L^{-1} = 2\,\overline{\lambda^{-1}} - \lambda^{-1+} \qquad (60)$$

in which λ^{-1+} is obtained from a plot of $\overline{\lambda^{-1}}$ versus $1/Q_{gi}$. For a tangent to the $\overline{\lambda^{-1}}$ curve, λ^{-1+} is the intercept with the $\overline{\lambda^{-1}}$ axis where $1/Q_{gi}$ equals zero.

3.1.3.2 Example

To use the Jones-Roszelle method, production data such as that shown in Figure 11 and either velocity data at constant pressure drop (Figure 13) or pressure drop data for constant injection rate are required. The gas saturation and the fractional flow at the outlet face of the rock sample can be calculated from production data of Figure 11. The effective viscosity λ_L^{-1} at the outlet face of the rock sample can be calculated from the velocity data of Figure 13. The relative permeabilities are then calculated using Equations 57 and 58.

To demonstrate use of their method, Jones and Roszelle (1978) graphically interpreted the terms in Equations 54, 55, 56, 59, and 60. For example, the terms in Equations 54 and 55 can be identified with features in Figure 15, and the terms in Equation 56 can be identified with the features in Figure 16. At any selected pore volumes of injected gas, Q_{gi}, the average gas saturation, $\overline{S_g}$, equals the fractional pore volume of produced brine, Q_{bp}, and the tangent to the Q_{pb} versus Q_{gi} relationship is $d\overline{S_g}/dQ_{gi}$. The gas saturation at the outlet end, S_{bL}, is obtained by extrapolating the tangent to $Q_{gi} = 0$. Extrapolating the tangent to $Q_{gi} = 0$ exemplifies the meaning of Equation 54.

Graphical interpretation of the Jones-Roszelle method is not essential to its use. In the example calculation shown in Table 5 with data from Figures 11 and 13, the data are differentiated numerically using Equation 21. The data are processed according to Equations 54 through 58. The results of the Jones-Roszelle method are indistinguishable from the results of the JBN method shown in Figure 14.

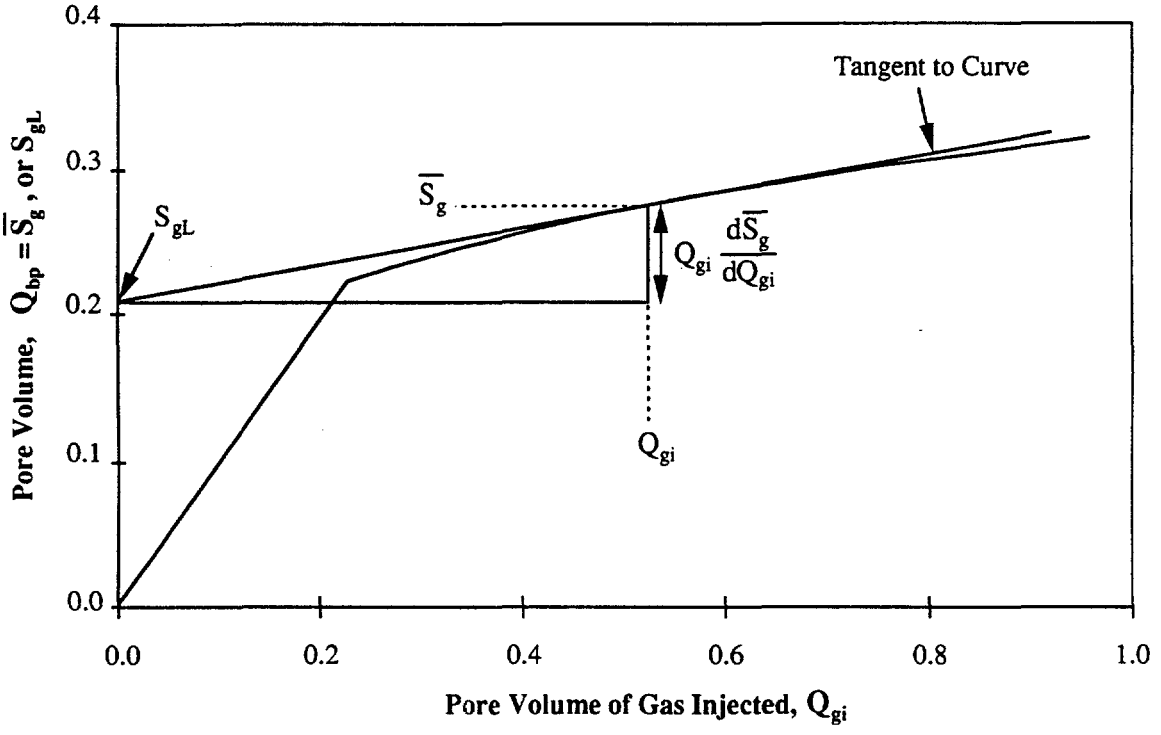

Figure 15. Graphical demonstration of Jones-Roszelle method using Equations 54 and 55.

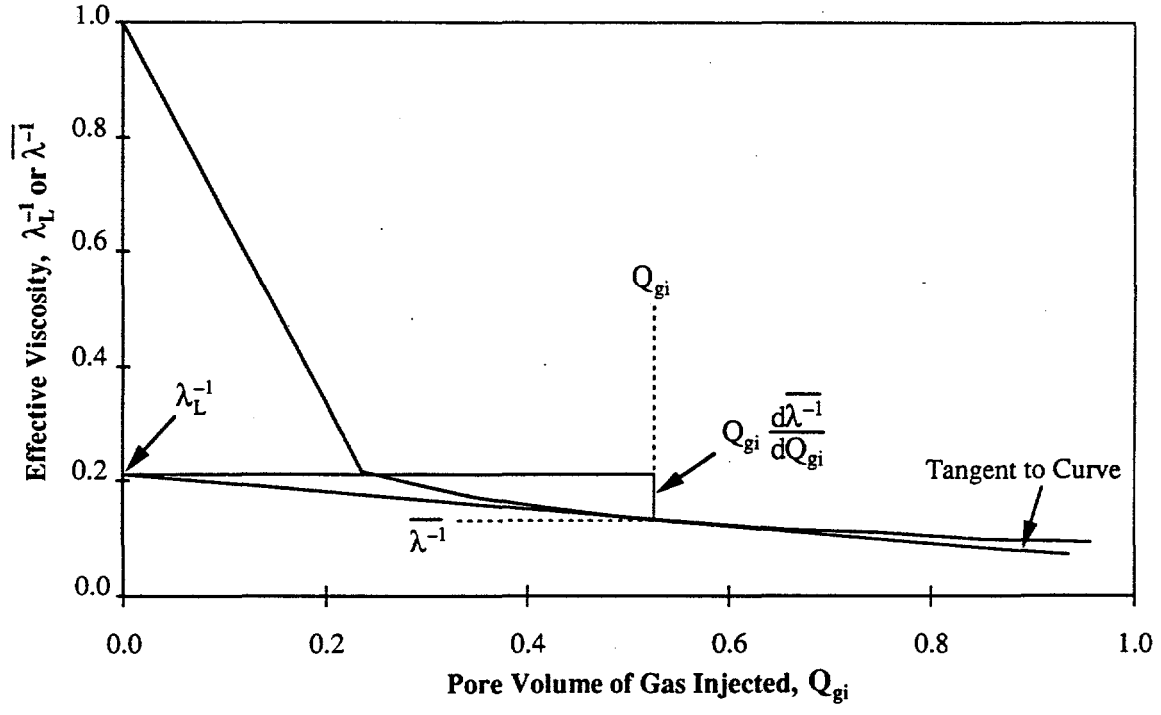

Figure 16. Graphical demonstration of Jones-Roszelle method using Equation 56.

Table 5. Example of Jones-Roszelle Data Reduction Method

Simulator Input Data

Pressure Drop: 20 atm	**Rock Properties**	**Fluid Properties**
	k = 0.01 md	ρ_b = 1.0 g/cm^3
Rock Dimensions	ϕ = 0.01	ρ_g = 0.001 g/cm^3
L = 30.48 cm	$nb = ng = 1.75$	μ_b = 1.0 cp
R = 5.08 cm	$S_{br} = 0.2$, $S_{gc} = 0.1$	μ_g = 0.015 cp
	$P_{th} = P_{sp} = 0$	

Definitions of Table Headings

Q_{gi}	= Pore volume of gas injected	$\overline{\lambda^{-1}}$	= Average reciprocal relative mobility, cp
$\overline{S_g}$	= Average gas saturation	λ_L^{-1}	= Reciprocal relative mobility at outlet, cp
S_{gL}	= Saturation of gas at outlet	k_{rgL}, k_{rbL}	= Relative permeabilies of brine and gas at outlet
v	= Velocity, cm/s		
f_{bL},f_{gL}	= Fractional flow of brine and gas at outlet		

Q_{gi}	$\overline{S_g}$	v (cm/s)	S_{gL}	f_{bL}	f_{gL}	$\overline{\lambda^{-1}}$ (cp)	λ_L^{-1} (cp)	k_{rbL}	k_{rgL}
0.0000	0.0000	0.000533				1.0000			
0.2697	0.2534	0.002250				0.2369			
0.3182	0.2642	0.002520	0.1984	0.2068	0.7932	0.2115	0.3564	0.5804	0.0334
0.3721	0.2744	0.002790	0.2080	0.1785	0.8215	0.1910	0.3154	0.5660	0.0391
0.4315	0.2843	0.003060	0.2162	0.1577	0.8423	0.1742	0.2830	0.5573	0.0446
0.4964	0.2939	0.003330	0.2243	0.1402	0.8598	0.1601	0.2582	0.5432	0.0499
0.5669	0.3032	0.003610	0.2318	0.1260	0.8740	0.1476	0.2375	0.5304	0.0552
0.6430	0.3123	0.003890	0.2392	0.1137	0.8863	0.1370	0.2184	0.5209	0.0609
0.7249	0.3211	0.004170	0.2465	0.1030	0.8970	0.1278	0.2031	0.5069	0.0662
0.8125	0.3297	0.004460	0.2532	0.0941	0.9059	0.1195	0.1900	0.4956	0.0715
0.9060	0.3381	0.004750							

3.1.3.3 Derivation

The derivations of key expressions in Appendices A and B of Jones and Roszelle (1978) provide a unique perspective on production behavior for fluid displacement in porous media. Their derivations of Equations 54 and 59 for outlet saturation, and the derivations of Equations

56 and 60 for outlet effective viscosity, are almost identical. The derivations for Equations 54 (the Welge equation) and 59 are shown in this section, followed by an explanation of effective viscosity.

OUTLET BRINE SATURATION

The derivation starts with a definition of the saturation at any fractional distance x into the rock sample from the inlet end:

$$S_b(Q_{gi}, x) = \lim_{\Delta x \to 0} \frac{\int_x^{x+\Delta x} S_b \, dx}{\Delta x}$$

$$= \lim_{\Delta x \to 0} \frac{\int_0^{x+\Delta x} S_b \, dx - \int_0^x S_b \, dx}{\Delta x} \tag{61}$$

Substituting average brine saturations for the two integrals of the second line in Equation 61, then

$$S_b(Q_{gi}, x) = \lim_{\Delta x \to 0} \frac{(x+\Delta x)\,\overline{S_b(Q_{gi}, x+\Delta x)} - x\,\overline{S_b(Q_{gi}, x)}}{\Delta x}$$

$$= \lim_{\Delta x \to 0} \left\{ \overline{S_b(Q_{gi}, x+\Delta x)} + \frac{x\left[\overline{S_b(Q_{gi}, x+\Delta x)} - \overline{S_b(Q_{gi}, x)}\right]}{\Delta x} \right\}$$

$$= \overline{S_b(Q_{gi}, x)} + x\left[\frac{\partial \overline{S_b(Q_{gi}, x)}}{\partial x}\right] \tag{62}$$

At this point in the derivation, Jones and Roszelle recognized that if capillary effects are negligible then the average saturation in a linear rock sample is a function of only the pore volumes of fluids that have been injected. More specifically, the average fluid saturation in a rock sample between fractional distance zero and x is only a function of Q_{gi} / x , in which Q_{gi}

is the cumulative pore volumes of gas injected into the sample. Using the chain rule on the derivative in Equation 62,

$$\frac{\partial \overline{S_b(Q_{gi},x)}}{\partial x} = \frac{\partial \overline{S_b(Q_{gi}/x)}}{\partial x} = \left[\frac{\partial \overline{S_b(Q_{gi}/x)}}{\partial (Q_{gi}/x)}\right]\left[\frac{\partial (Q_{gi}/x)}{\partial x}\right] = \frac{\partial \overline{S_b(Q_{gi}/x)}}{\partial (Q_{gi}/x)}\left(-Q_{gi}/x^2\right) \tag{63}$$

and the last line of Equation 62 becomes

$$S_b(Q_{gi}/x) = \overline{S_b(Q_{gi}/x)} - \left[\frac{Q_{gi}}{x}\right]\left[\frac{\partial \overline{S_b(Q_{gi}/x)}}{\partial (Q_{gi}/x)}\right] \tag{64}$$

At the outlet of the rock sample, $x = 1$, so

$$S_{bL}(Q_{gi}) = \overline{S_b(Q_{gi})} - Q_{gi}\left[\frac{\partial \overline{S_b(Q_{gi})}}{\partial Q_{gi}}\right] \tag{65}$$

Because $S_{gL} = 1 - S_{bL}$, Equation 65 can also be expressed for gas saturation, and is equivalent to Welge's expression (Equation 54):

$$S_{gL}(Q_{gi}) = \overline{S_g(Q_{gi})} - Q_{gi}\left[\frac{\partial \overline{S_g(Q_{gi})}}{\partial Q_{gi}}\right] \tag{66}$$

SATURATION FOR LARGE THROUGHPUT

For large amounts of injected fluid, Jones and Roszelle (1978) recognized that average saturation can be written as a function of x/Q_{gi} rather than Q_{gi}/x as shown in Equation 67.

$$S_b(x/Q_{gi}) = \overline{S_b(x/Q_{gi})} + x\left[\frac{\partial \overline{S_b(x/Q_{gi})}}{\partial Q_{gi}}\right] \tag{67}$$

Using the chain rule again, the brine saturation at the outlet face of the rock sample is expanded as shown in Equation 68.

$$S_{bL}\left(1/Q_{gi}\right) = \overline{S_b\left(1/Q_{gi}\right)} + \left[\frac{1}{Q_{gi}}\right]\left[\frac{d\overline{S_b\left(1/Q_{gi}\right)}}{d\left(1/Q_{gi}\right)}\right] \tag{68}$$

From a plot of the average saturation $\overline{S_b}$ versus $1/Q_{gi}$, it can be shown that

$$S^{+}_{bL}\left(1/Q_{gi}\right) = \overline{S_b\left(1/Q_{gi}\right)} - \left[\frac{1}{Q_{gi}}\right]\left[\frac{d\overline{S_b\left(1/Q_{gi}\right)}}{d\left(1/Q_{gi}\right)}\right] \tag{69}$$

in which $S^{+}_{b}\left(1/Q_{gi}\right)$ is defined as the intercept of the tangent to the curve with the $\overline{S_b}$ axis.

Using this expression for the intercept and omitting the functional dependence on $1/Q_{gi}$, Equation 68 becomes

$$S_{bL} = 2\,\overline{S_b} - S^{+}_{b} \tag{70}$$

This expression for calculating the outlet face saturation for large volumes of injected fluid is a unique feature of the Jones and Roszelle method (1978). For large volumes of injected fluid, the graphical procedure exemplified in Equation 70 will provide more accurate estimates of outlet face saturation than those for Equation 66.

EXPLANATION OF EFFECTIVE VISCOSITY

Equations 56 and 60 for the effective viscosity at the outlet face of the rock sample are derived in Appendix B of Jones and Roszelle (1978). The effective viscosity is defined as follows: Consider the flow of two phases in a linear rock sample; then the sum q of the flow rates of the two fluids can be written as

$$q = \frac{k\,A}{\lambda^{-1}\,L}\left(-\frac{\partial P}{\partial x}\right) \tag{71}$$

where x is the fractional distance along the sample of length L and λ^{-1} is an effective viscosity for the two flowing phases. The rather cumbersome notation for effective viscosity, λ^{-1}, was used by Jones and Roszelle because the effective viscosity is equivalent to the reciprocal of relative mobility, often denoted in the literature as λ.

Now consider the flow of one phase through a rock sample fully saturated with that phase. If that phase were brine, the flow rate q_b would be expressed as shown in Equation 72.

$$q_b = \frac{k\,A}{\mu_b\,L}\left(-\Delta P_b\right) \tag{72}$$

Combining Equations 71 and 72, the effective viscosity becomes

$$\lambda^{-1} = \left(\frac{q_b\,\mu_b}{\Delta P_b}\right)\,\frac{1}{q}\left(\frac{\partial P}{\partial x}\right) \tag{73}$$

Similarly, the average effective viscosity from fractional distance 0 to x in the rock sample is

$$\overline{\lambda^{-1}} = \left(\frac{q_b\,\mu_b}{\Delta P_b}\right)\left(\frac{\Delta P_x}{q\,x}\right) \tag{74}$$

The derivations in Appendix B of Jones and Roszelle (1978) for the effective viscosity at the outlet of the rock sample are the same as the derivations of Equations 54 and 59 with saturation $S_b\left(Q_{gi}, x\right)$ replaced by effective viscosity $\lambda^{-1}\left(Q_{gi}, x\right)$.

3.2 Low-Rate Experiments

3.2.1 Ramakrishnan-Cappiello Method

Capillary pressure and relative permeability of the displacing phase can be obtained from low-rate displacement experiments using the data reduction method devised by Ramakrishnan and Cappiello (1991). The method is designed for using pressure drop, flow rate, and average saturation data, all measured after many pore volumes of injection in unsteady-state displacements.

Specifically, consider gas injection at a constant pressure into an initially brine-saturated porous medium. The outlet flow is also controlled at constant pressure, so the pressure drop

across the medium is constant throughout the test. The pressure drop must exceed the threshold capillary pressure for gas to penetrate the porous medium.

After many pore volumes of gas injection, brine production will essentially cease, and gas flow rate through the medium will reach a constant value. Even if production does not cease entirely, or if flow rate is still increasing, it may be possible to extrapolate the data to final values. After final values are obtained at one pressure drop, the pressure drop is increased to a new level and the procedure is repeated. Continuing in this manner, a set of pressure drops and the associated final values of saturations and flow rates will have been collected at the end of a series of experiments.

The set of pressure drops, final saturations, and final gas inflow rates is required input for the Ramakrishnan-Cappiello method. Because the experimental data are differentiated, data quality is an important concern. In the following discussion, the method is summarized and derived, and an example of its application to numerically generated displacement data is given.

3.2.1.1 Summary of the Method

The Ramakrishnan-Cappiello method consists of two steps. First the relative permeability of gas at the inlet of the rock sample is calculated by differentiating the steady-state gas velocity with respect to the applied capillary pressure at the inlet, P_{c0} :

$$\left[k_{rg}\right]_{x=0} = k_{rg0} = \left(\frac{\mu_g L}{k}\right)\left(\frac{dv_g}{dP_{c0}}\right) \tag{75}$$

P_{c0} equals the applied pressure drop: $P_{c0} = P_{g0} - P_{gL}$. Second, brine saturation at the inlet is calculated by differentiating the product of steady-state gas velocity and average brine saturation:

$$\left[S_b\right]_{x=0} = S_{b0} = \left|\frac{\mu_g L}{k\, k_{rg0}}\right|\left|\frac{d\left(v_g \overline{S_b}\right)}{dP_{c0}}\right| \tag{76}$$

An alternative but equivalent form of Equation 76 is reminiscent of the Welge equation (19):

$$S_{b0} = \overline{S_b} + v_g \left(d\overline{S_b} / dv_g \right) \tag{77}$$

As noted in the summary of the Welge, JBN, and Jones-Roszelle methods, the pressure drop should be small compared to the mean operating pressure for experiments intended for gas relative permeability measurement. It is recommended that the value of v_g be estimated by converting the injected volumetric flow rate to the mean operating pressure in a rock sample.

3.2.1.2 Example

Some examples of production data are shown in Figure 17a. Brine production essentially ceases after five pore volumes of gas injection for a pressure drop of 0.15 atm. However, with a pressure drop of 20 atm, the production continues for more than a thousand pore volumes. This trend is expected because brine saturation remains high at a low pressure drop; therefore brine relative permeability is also high. With high brine relative permeability, the brine saturation can reach a stable value after just a few pore volumes of gas injection. However, at high pressure drop, the brine saturation held by capillary forces is small, and brine relative permeability is also small. Therefore at high pressure drop, many pore volumes of gas must be injected before the brine saturation stabilizes.

Figure 17b shows the production data of Figure 17a as a function of elapsed time. For very low pressure drops, the time needed to complete an experiment may be prohibitive. To obtain the final values of gas velocity and saturation, extrapolation of the data to infinite pore volume throughput is often helpful, as demonstrated in Figure 17c.

The final values of gas velocity and brine saturation can be plotted against pressure drop as shown in Figures 18a and 18b. Then by differentiating the data using Equation 21 as demonstrated in Table 6, the relationships for relative permeability and capillary pressure are obtained.

When the Ramakrishnan-Cappiello method is applied to the data of Figures 18a and 18b, the results shown in Figures 19a and 19b are obtained. Note that some of the resulting relative permeability and capillary pressure results are quite accurate. The less accurate results indicate poor extrapolations of the data to final velocities and saturations.

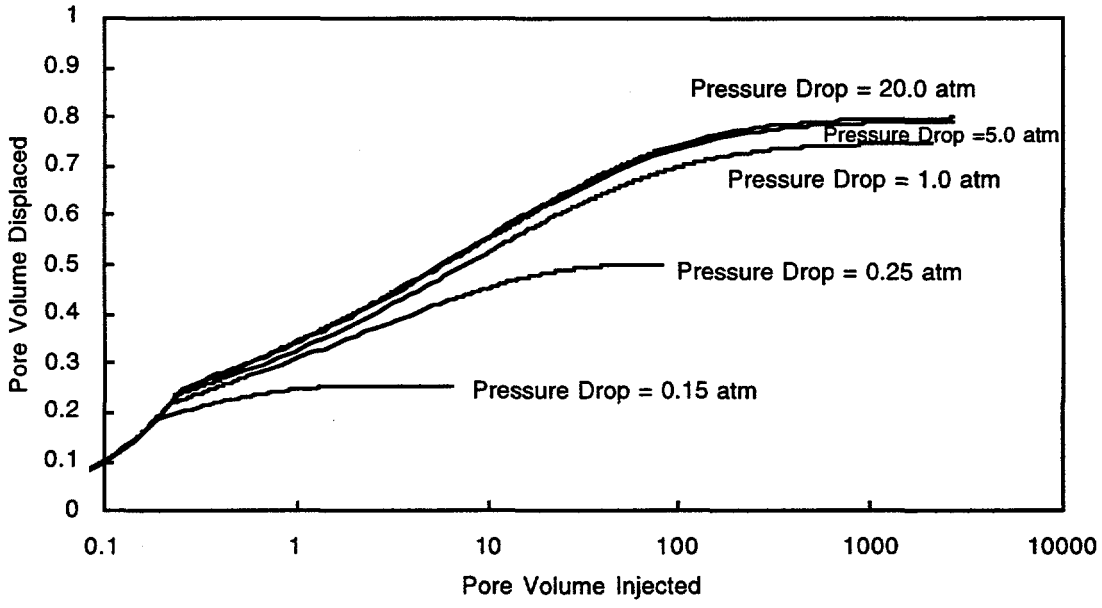

Figure 17a. Sensitivity of brine production to pressure drop. Simulations of constant pressure drop and horizontal displacements. Rock properties: $k = 0.01$ md, $k_{rb,\max} = k_{rg,\max} = 1$, $nb = ng = 1.75$, $S_{br} = 0.2$, $S_{gc} = 0.1$, and $P_{th} = P_{sp} = 0.1$ atm.

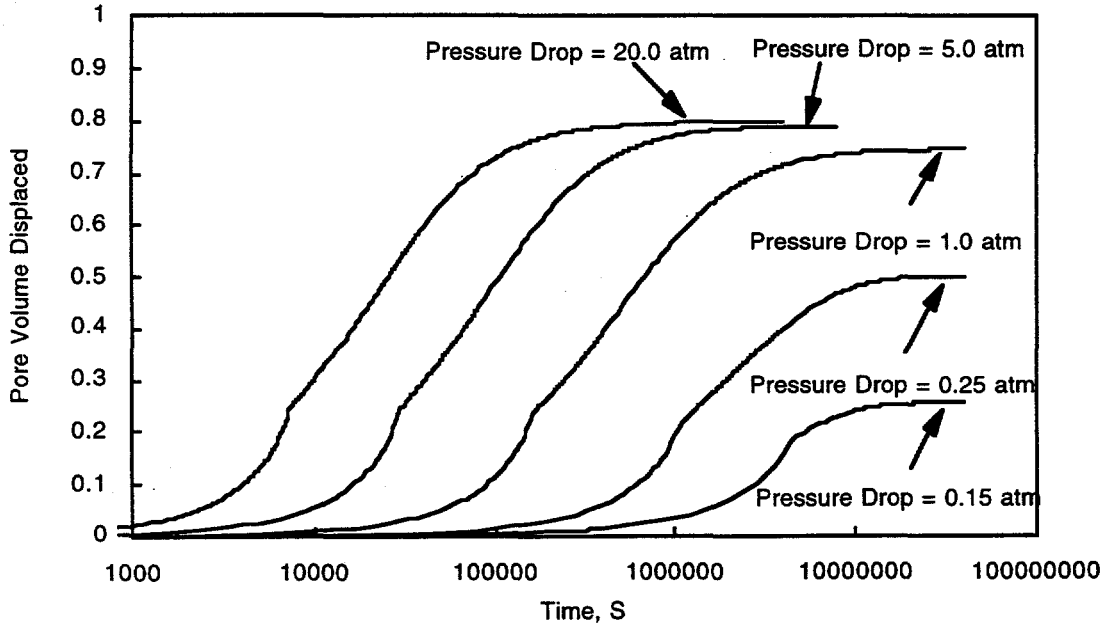

Figure 17b. Time dependence of brine production. Simulations of constant pressure drop and horizontal displacements. Rock properties: $k = 0.01$ md, $k_{rb,\max} = k_{rg,\max} = 1$, $nb = ng = 1.75$, $S_{br} = 0.2$, $S_{gc} = 0.1$, and $P_{th} = P_{sp} = 0.1$ atm.

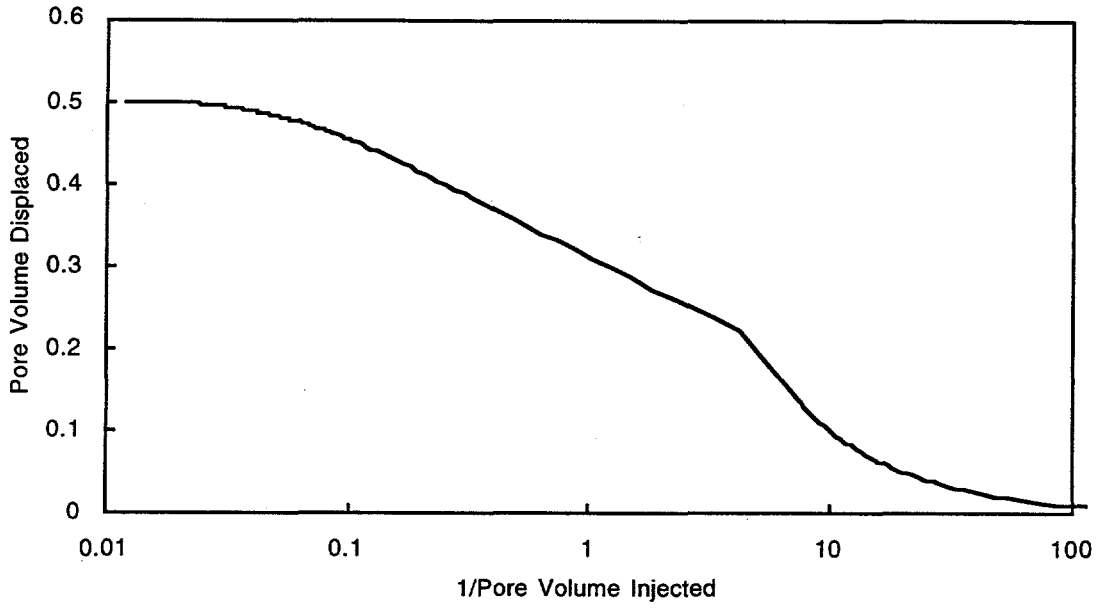

Figure 17c. Inverse pore volume dependence of brine production. Simulations of constant pressure drop and horizontal displacements. Rock properties: k = 0.01 md, $k_{rb,\max} = k_{rg,\max} = 1$, $nb = ng = 1.75$, $S_{br} = 0.2$, $S_{gc} = 0.1$, and $P_{th} = P_{sp} = 0.1$ atm.

3.2.1.3 Derivation

INLET CAPILLARY PRESSURE

After injecting many pore volumes of gas at low rate into an initially brine-saturated porous medium, production of brine will cease. The brine remaining in the medium is held by capillary forces. The saturation of brine varies from a low value at the injection face to a maximum value at the production face. The saturation distribution can be described in terms of capillary end effects.

Because brine production has ceased brine pressure is uniform; therefore the pressure gradient in the brine phase is zero. As a result, the pressure gradient in the gas phase is equal to the gradient of capillary pressure, as shown in Equations 78 through 80.

$$P_c = P_g - P_b \tag{78}$$

so

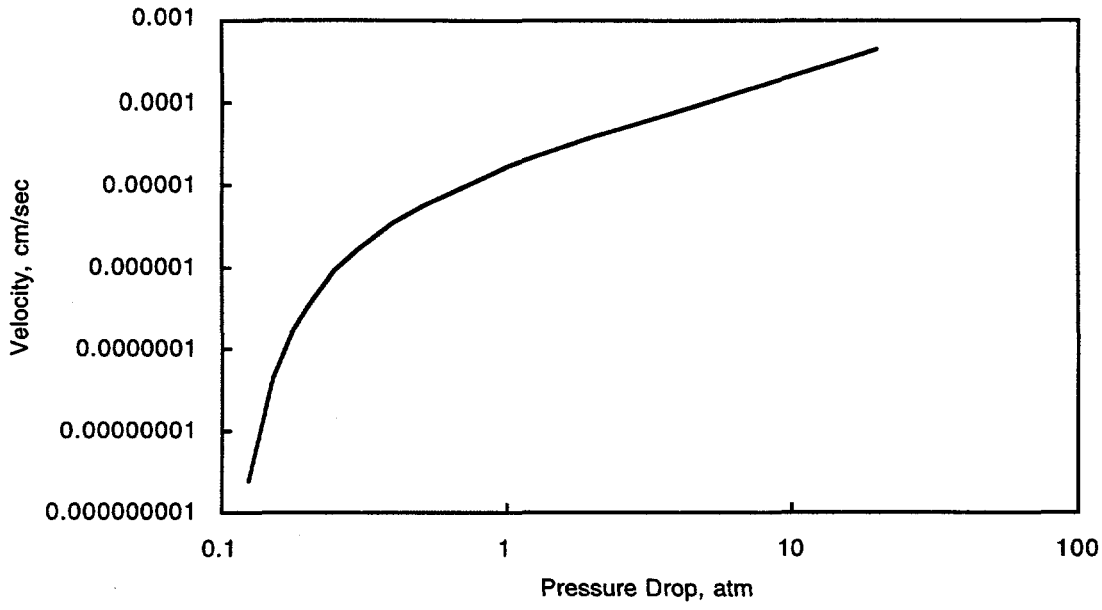

Figure 18a. Relationships between steady-state gas velocity and pressure drop for Ramakrishnan-Cappiello method.

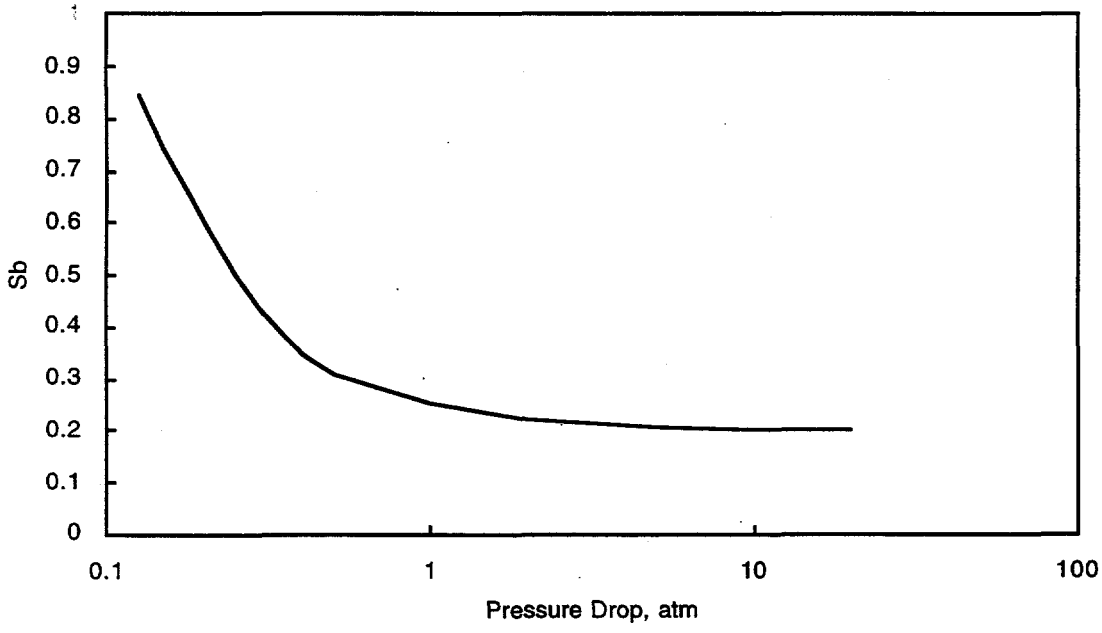

Figure 18b. Relationships between average steady-state brine saturation and pressure drop for Ramakrishnan-Cappiello method.

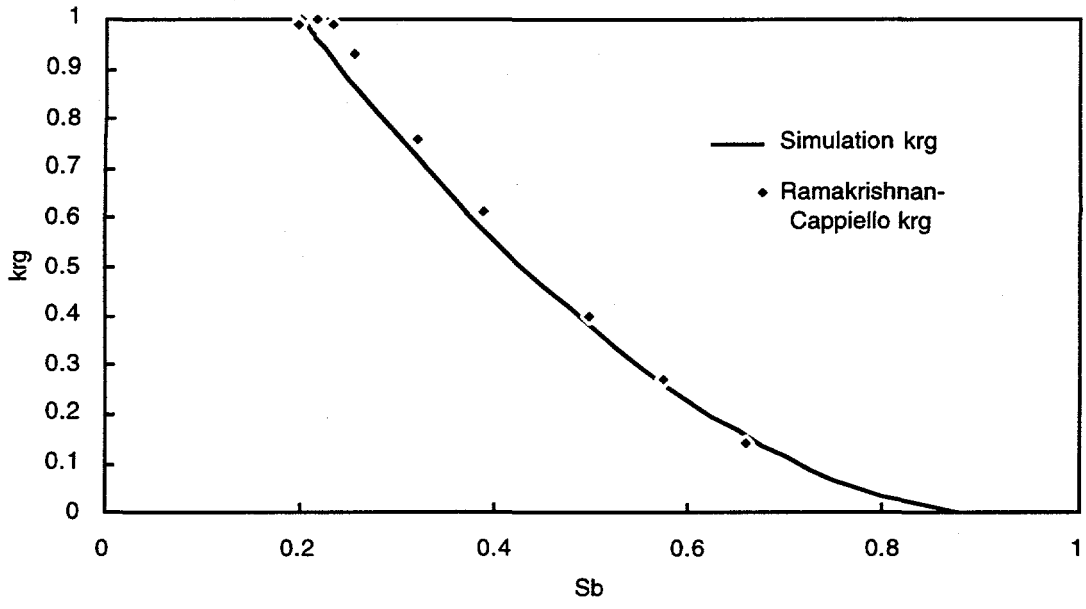

Figure 19a. Gas relative permeability obtained with the Ramakrishnan-Cappiello method using simulated data from Figures 18a and b.

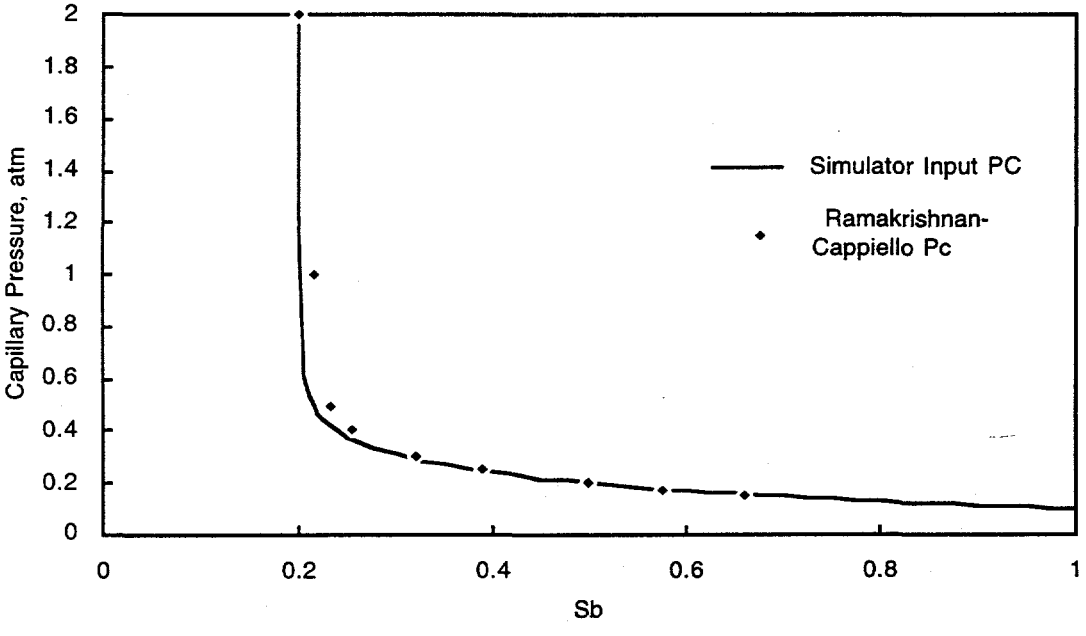

Figure 19b. Capillary pressure obtained with the Ramakrishnan-Cappiello method using simulated data from Figures 18a and b.

Table 6. Example of Ramakrishnan-Cappiello Data Reduction Method

Simulator Input Data

Rock Dimensions	**Rock Properties**	**Fluid Properties**
L = 30.48 cm	k = 0.01 md	ρ_b = 1.0 g/cm^3
R = 5.08 cm	ϕ = 0.01	ρ_g = 0.001 g/cm^3
$P_{th} = P_{sp}$ = 0.1 atm	nb = ng = 1.75	μ_b = 1.0 cp
	S_{br} = 0.2, S_{gc} = 0.1	μ_g = 0.015 cp

Definitions of Table Headings

ΔP	= Pressure drop across porous sample	k_{rg0}	= Relative permeabilies of gas at inlet
v_g	= Velocity of gas	$\overline{S_b}$	= Average brine saturation
P_{c0}	= Capillary pressure at inlet = ΔP	S_{g0}	= Saturation of gas at outlet

$\Delta P = P_{c0}$, atm	v_g (cm/s)	$dv_g/d\Delta P$ (cm/s/atm)	k_{rg0}	$\overline{S_b}$	$d(v_g\ \overline{S_b})/d\Delta P$ (cm/s/atm)	S_{b0}
0.125	2.480E-09			0.8451		
0.150	4.415E-08	3.078E-06	0.1408	0.7440	2.032E-06	0.6602
0.175	1.564E-07	5.907E-06	0.2701	0.6631	3.393E-06	0.5743
0.200	3.395E-07	8.693E-06	0.3975	0.5964	4.335E-06	0.4987
0.250	9.110E-07	1.339E-05	0.6125	0.5023	5.207E-06	0.3887
0.300	1.679E-06	1.655E-05	0.7569	0.4307	5.299E-06	0.3201
0.400	3.573E-06	2.029E-05	0.9278	0.3500	5.185E-06	0.2555
0.500	5.737E-06	2.166E-05	0.9906	0.3068	5.055E-06	0.2334
1.000	1.663E-05	2.184E-05	0.9985	0.2518	4.701E-06	0.2153
2.000	3.857E-05	2.189E-05	1.0010	0.2225	4.376E-06	0.1999
5.000	1.038E-04	2.169E-05	0.9917	0.2076	4.308E-06	0.1986
10.000	2.118E-04	2.156E-05	0.9860	0.2029	4.269E-06	0.1980
20.000	4.267E-04			0.2000		

$$\frac{dP_g}{dx} = \frac{dP_c}{dx} \tag{79}$$

because

$$\frac{dP_b}{dx} = 0 \tag{80}$$

Integration of Equation 79 from the inlet to the outlet end yields

$$P_{cL} - P_{c0} = P_{gL} - P_{g0} \tag{81}$$

It is generally assumed that the capillary pressure at the outlet, P_{cL}, is zero. As a result,

$$P_{c0} = P_{g0} - P_{gL} \tag{82}$$

That is, the capillary pressure at the inlet face is equal to the difference between the pressure in the gas phase at the inlet and the pressure in the gas phase at the outlet.

INLET BRINE RELATIVE PERMEABILITY

Combining Equation 79 with Darcy's law for gas flow yields

$$v_g = -\frac{k\, k_{rg}}{\mu_g}\left(\frac{dP_g}{dx}\right) = -\frac{k\, k_{rg}}{\mu_g}\left(\frac{dP_c}{dx}\right) \tag{83}$$

Here x is distance from the injection face of the sample. Relative permeability to gas, k_{rg}, is a function of brine saturation. Because capillary pressure is also a function of brine saturation, k_{rg} can be written as a function of capillary pressure. Integration of Equation 83 along the length x of the linear sample results in Equation 84.

$$\int_0^L v_g \, dx = -\int_{P_{cL}}^{P_{c0}} \frac{k \, k_{rg}}{\mu_g} \, dP_c = \int_{P_{cL}}^{P_{c0}} \frac{k \, k_{rg}}{\mu_g} \, dP_c = \int_0^{P_{c0}} \frac{k \, k_{rg}}{\mu_g} \, dP_c \tag{84}$$

In Equation 84, capillary pressure at the outlet face is assumed to be zero. Because v_g is constant, Equation 84 becomes

$$v_g \, L = \int_0^{P_{c0}} \frac{k \, k_{rg}}{\mu_g} \, dP_c \tag{85}$$

Differentiating Equation 85 with respect to P_{c0} results in Equation 86.

$$\frac{dv_g}{dP_{c0}} = \frac{k \, k_{rg0}}{\mu_g \, L} \tag{86}$$

Recognizing that P_{c0} equals the pressure drop from the inlet to the outlet face, the relative permeability to gas at the inlet face can be obtained from the slope of v_g plotted against P_{c0}:

$$k_{rg0} = \left(\frac{\mu_g \, L}{k} \right) \left(\frac{dv_g}{dP_{c0}} \right) \tag{87}$$

INLET BRINE SATURATION

To derive Equation 76, an expression for saturation at the inlet face of the porous medium must be obtained. Ramakrishnan and Cappiello (1991) did this by first writing an expression for the average saturation in the medium:

$$\overline{S_b} = \frac{1}{L} \int_0^L S_b \, dx \tag{88}$$

The variable of integration can be changed to capillary pressure using Equation 83:

$$v_g \overline{S_b} = \frac{1}{L} \int_0^{P_{c0}} S_b \frac{k\, k_{rg}}{\mu_g} dP_c \tag{89}$$

By differentiating Equation 89 with respect to P_{c0}, the desired relationship for brine saturation at the inlet face is obtained:

$$S_{b0} = \left[\frac{\mu_g L}{k\, k_{rg}}\right]\left[\frac{d\left(v_g \overline{S_b}\right)}{dP_{c0}}\right] \tag{90}$$

Equation 90 is as given by Ramakrishnan and Cappiello (1991). An alternative form can be obtained by differentiating the product in Equation 90 and using Equation 87 to simplify the result:

$$S_{b0} = \frac{\mu_g L}{k\, k_{rg}}\left[\overline{S_b}\left(\frac{dv_g}{dP_{c0}}\right) + \left(v_g \frac{d\overline{S_b}}{dP_{c0}}\right)\right]$$

$$= \frac{\mu_g L}{k\, k_{rg}}\left[\overline{S_b}\left(\frac{dv_g}{dP_{c0}}\right) + v_g\left(\frac{d\overline{S_b}\, dv_g}{dv_g\, dP_{c0}}\right)\right]$$

$$= \frac{\mu_g L\, dv_g}{k\, k_{rg}\, dP_{c0}}\left[\overline{S_b} + v_g\left(\frac{d\overline{S_b}}{dv_g}\right)\right]$$

$$= \overline{S_b} + \frac{v_g\, dS_b}{dv_g} \tag{91}$$

Equation 91 has a form similar to that of the Welge equation (19). By applying Equations 82, 87, and 90 (or 91) to data for a series of experiments, relationships for relative permeability of the gas and capillary pressure can be obtained.

3.3 Centrifuge Experiments

3.3.1 Hagoort Method

The data processing method proposed by Hagoort (1980) provides a means for obtaining brine relative permeabilities from centrifuge experiments. To develop the theoretical basis for the method, Hagoort assumed that the mobility of the gas phase was infinite and that capillary retention in the rock sample could be ignored. As a result, the method cannot be used to determine gas relative permeabilities.

3.3.1.1 Summary of the Method

The method proposed by Hagoort (1980) requires two steps. First, the brine relative permeability at the outlet of the rock sample, mounted in a centrifuge as shown in Figure 20, is calculated by differentiating the brine production data:

$$k_{rbL} = \left(\frac{\mu_b \phi L}{k \Delta \rho_{bg} \alpha} \right) \left(\frac{dQ_{bp}}{dt} \right) \tag{92}$$

In Equation 92, L is the length of the rock sample and α is the average centrifugal acceleration in the sample; using the terminology of Figure 20, $\alpha = \omega^2 (R_t + R_o) / 2$. Because centrifugal acceleration varies throughout the sample, using an average value leads to some error in the estimate of relative permeability. However, Hagoort (1980) showed the error to be negligible when $(R_t + R_o) / 2L$ exceeds 2.5. The units of angular speed, ω, are radians per second. [To convert from revolutions per minute (rpm) to radians per second, the rpm value is multiplied by $2\pi/60$.] Next the brine saturation at the outlet is obtained:

$$S_{bL} = 1 - Q_{bp} + t \left(\frac{dQ_{bp}}{dt} \right) \tag{93}$$

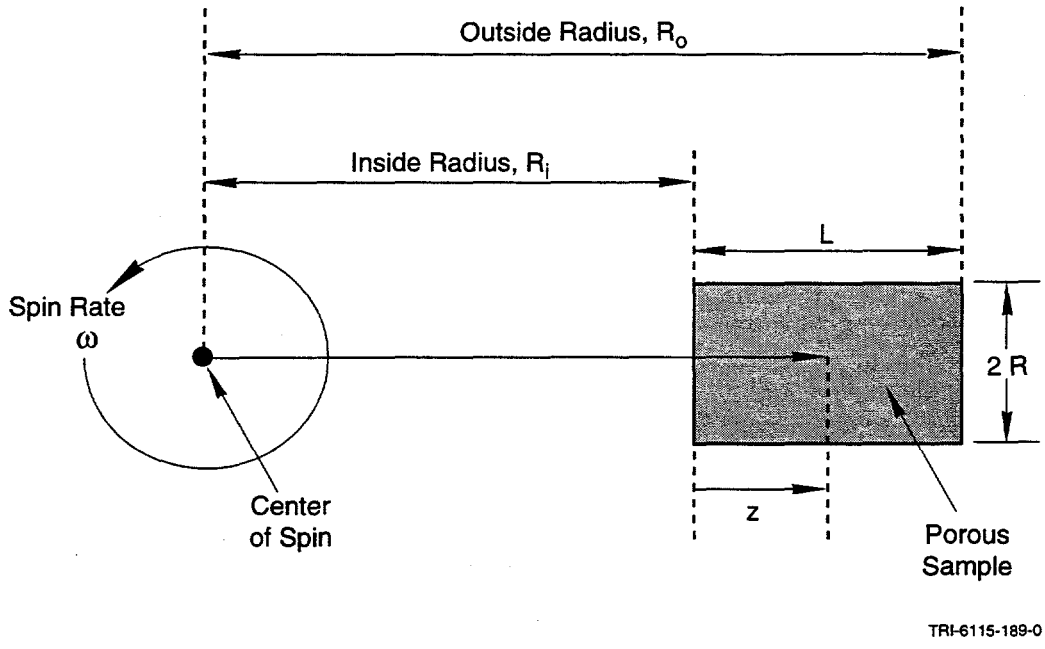

Figure 20. Schematic of centrifuge experiment for derivation of Hagoort method.

Equations 92 and 93 are equivalent to Equations 11 and 16 of Hagoort (1980).

As indicated in the example below, a modified version of the Hagoort method provides more accurate relative permeabilities than the original Hagoort method. At present, no theoretical explanation exists for the success of the modified method. In the modified method, the following two equations are used in place of Equations 92 and 93:

$$k_{rbL} = \frac{\mu_b \, \phi \, L}{k \, \Delta\rho_{bg} \, \alpha} \left(\frac{1 - S_{br}}{1 - S^*_{br}} \right) \frac{dQ_{bp}}{dt} \tag{94}$$

$$S_{bL} = 1 - \left(\frac{1 - S_{br}}{1 - S^*_{br}} \right) Q_{bp} + \left(\frac{1 - S_{br}}{1 - S^*_{br}} \right) t \left(\frac{dQ_{bp}}{dt} \right) \tag{95}$$

In Equations 94 and 95, S^*_{br} is the average brine saturation that remains in the rock sample after infinite drainage time for any centrifuge spin rate. The magnitude of S^*_{br} will

decrease as spin rate increases. In contrast, the residual brine saturation S_{br} is independent of spin rate. The magnitude of S_{br} can be measured by capillary pressure experiments or by high flow-rate displacements. Van Spronsen (1982) proposed an extension of the Hagoort method to measurement of three-phase relative permeability.

3.3.1.2 Example

To clarify use of the Hagoort method, Equations 92 and 93 are applied to production information from simulated gas-brine centrifuge experiments. An example of simulated centrifuge production data is shown in Figure 21a.

A portion of the production data from the Hagoort method of Figure 21a is listed in Table 7 along with the rock and fluid properties that are needed for application of Equations 92 and 93. The production information in Table 7 is differentiated with respect to time using a three-point finite-difference expression. To apply the modified Hagoort method, which is summarized in Equations 94 and 95, S_{br}^{*} and S_{br} must be determined. In Figure 21b, the production data of Figure 21a are plotted against inverse time. This plot facilitates accurate determination of S_{br}^{*} at each centrifuge spin rate. A portion of the data from Figure 20a is processed by the modified Hagoort method in Table 8.

The results of applying Equations 92 and 93 to simulated centrifuge data are compared to the input relative permeability data in Figures 22a and 22b. Figure 22a shows that the accuracy of the Hagoort method increases as the capillary pressure parameters P_{th} and P_{sp} decrease. Figure 22b shows increasing accuracy with increasing spin rate.

The results of the modified Hagoort method are compared with the input brine relative permeabilities in Figure 23. The agreement between the modified Hagoort method and input relative permeabilities is within the bounds of experimental error.

3.3.1.3 Derivation

The derivation presented here follows Appendix B in Hagoort (1980). First an expression is derived for the Darcy velocity of brine in terms of the gas-brine density difference and the capillary pressure. Second a partial differential equation that describes the evolution of saturation profiles is obtained, starting with a material balance for the brine phase. Finally, expressions for calculating the relative permeability relationship are obtained by solving the partial differential equation for the simplified case of negligible capillary effects.

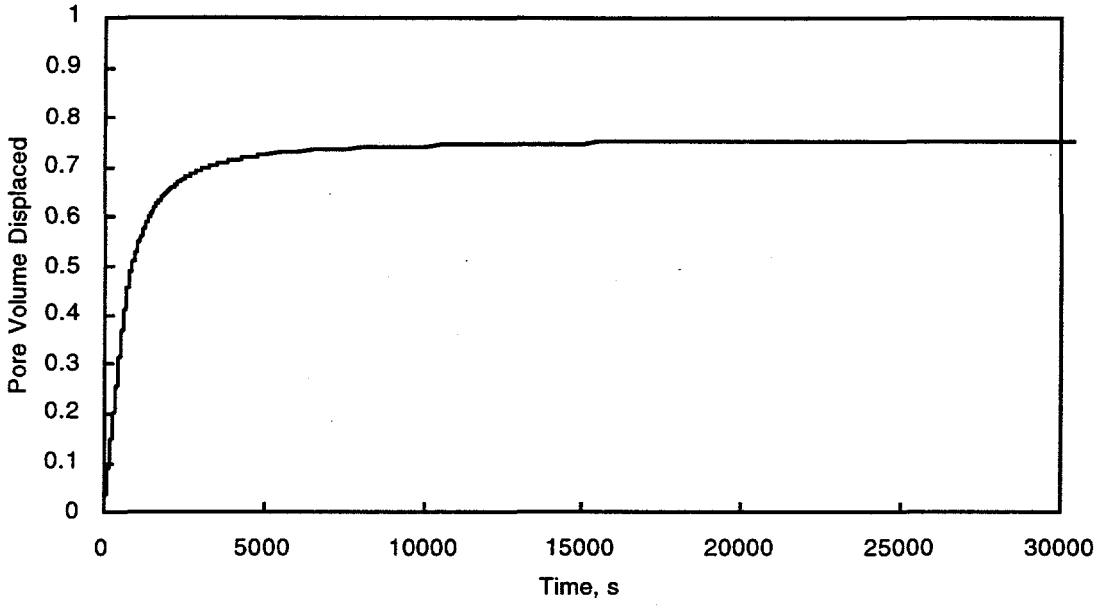

Figure 21a. Time dependence of brine production. Simulation of centrifuge displacement with constant spin rate of 2000 rpm. Rock properties: $k = 0.1$ md, $k_{rb,\max} = k_{rg,\max} = 1$, $nb = ng = 1.75$, $S_{br} = 0.2$, $S_{gc} = 0.1$, and $P_{th} = P_{sp} = 0.2$ atm.

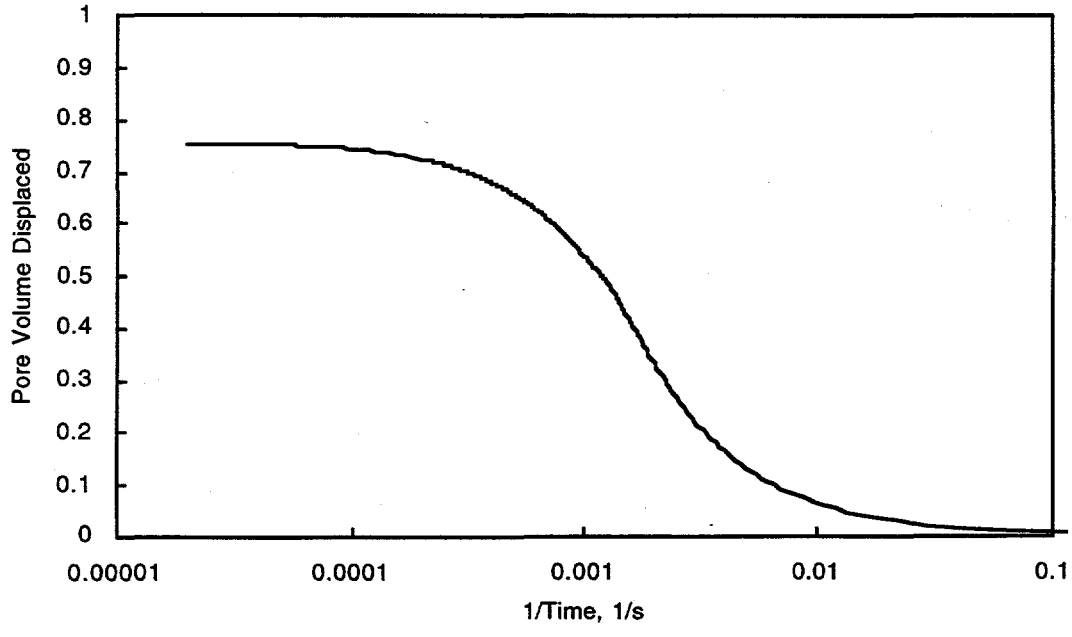

Figure 21b. Inverse time dependence of brine production. Simulation of centrifuge displacement with constant spin rate of 2000 rpm. Rock properties: $k = 0.1$ md, $k_{rb,\max} = k_{rg,\max} = 1$, $nb = ng = 1.75$, $S_{br} = 0.2$, $S_{gc} = 0.1$, and $P_{th} = P_{sp} = 0.2$ atm.

Table 7. Example of Hagoort Data Reduction Method

Simulator Input Data

Spin Rate: 2000 rpm

Radius to Inlet: 10.16 cm

Rock Dimensions

L = 10.16 cm

R = 5.08 cm

Rock Properties

k = 0.1 md

ϕ = 0.01

$nb = ng = 1.75$

$S_{br} = 0.2$, $S_{gc} = 0.1$

$P_{th} = P_{sp} = 0.2$ atm

Fluid Properties

$\rho_b = 1.0$ g/cm^3

$\rho_g = 0.001$ g/cm^3

$\mu_b = 1.0$ cp

$\mu_g = 0.010$ cp

Definitions of Table Headings

V_b = Volume of produced brine

Q_{bp} = Pore volume of produced brine

k_{rgL} = Relative permeability of brine at outlet

S_{gL} = Saturation of gas at outlet

Time (s)	V_b (cm^3)	Q_{bp}	k_{rbL}	S_{bL}
489.00	2.6693	0.3241		
496.50	2.7093	0.3289	0.9956	0.9918
504.00	2.7491	0.3337	0.9931	0.9910
511.50	2.7889	0.3386	0.9881	0.9893
519.00	2.8283	0.3434	0.9794	0.9864
526.50	2.8674	0.3481	0.9757	0.9851
534.00	2.9065	0.3529	0.9719	0.9838
541.50	2.9453	0.3576	0.9619	0.9803
549.00	2.9836	0.3622	0.9544	0.9777
556.50	3.0218	0.3669	0.9507	0.9764
564.00	3.0598	0.3715	0.9432	0.9736
571.50	3.0974	0.3760		

Table 8. Example of Modified Hagoort Data Reduction Method

Simulator Input Data

Spin Rate: 2000 rpm	**Rock Properties**	**Fluid Properties**
Radius to Outlet: 10.16 cm	k = 0.1 md	ρ_b = 1.0 g/cm^3
	ϕ = 0.01	ρ_g = 0.001 g/cm^3
Rock Dimensions	$nb = ng$ = 1.75	μ_b = 1.0 cp
L = 10.16 cm	S_{br} = 0.2, S_{gc} = 0.1	μ_g = 0.010 cp
R = 5.08 cm	$P_{th} = P_{sp}$ = 0.2 atm	

Definitions of Table Headings

V_b = Volume of produced brine

Q_{bp} = Pore volume of produced brine

k_{rbL} = Relative permeability of brine at outlet

S_{bL} = Saturation of brine at outlet

S^*_{br} = Remaining brine saturation from extrapolation to long time = 0.384

Time (s)	V_b (cm^3)	Q_{bp}	k_{rbL}	S_{bL}
360.50	1.5712	0.1907		
380.50	1.6529	0.2007	0.9862	0.9828
400.50	1.7335	0.2105	0.9728	0.9794
420.50	1.8130	0.2201	0.9600	0.9760
440.50	1.8915	0.2296	0.9455	0.9719
460.50	1.9686	0.2390	0.9284	0.9670
480.50	2.0443	0.2482	0.9126	0.9622
500.50	2.1188	0.2572	0.8956	0.9567
520.50	2.1917	0.2661	0.8780	0.9509
540.50	2.2633	0.2748	0.8592	0.9444
560.50	2.3331	0.2832		

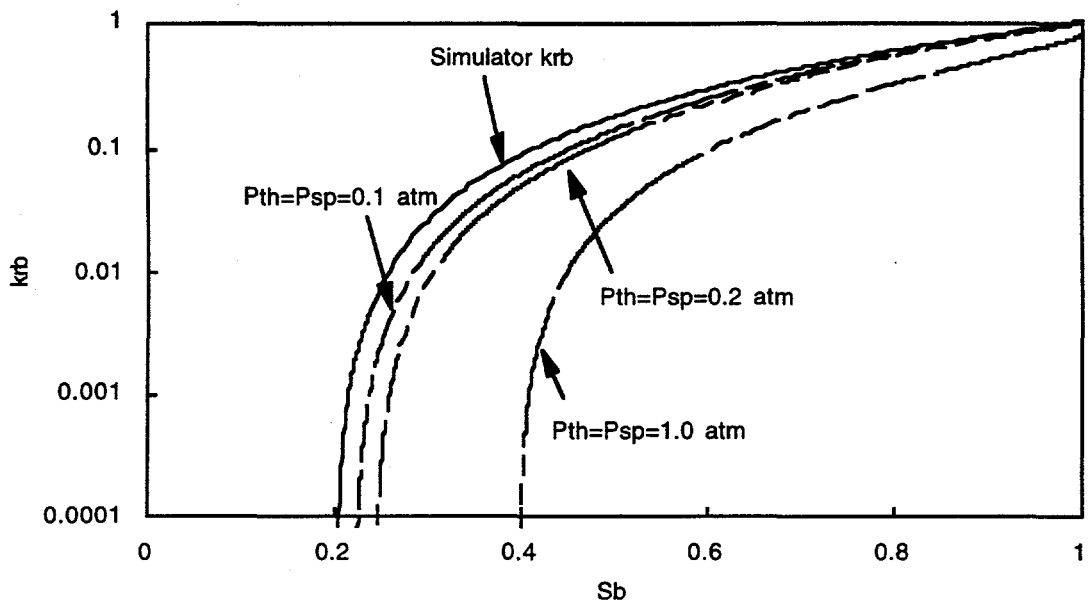

Figure 22a. Comparison of relative permeabilities from the Hagoort method with input to numerical model for different P_{th} and P_{sp} values. Rock properties: $k = 0.1$ md, $k_{rb,\max} = k_{rg,\max} = 1$, $nb = ng = 1.75$, $S_{br} = 0.2$, $S_{gc} = 0.1$.

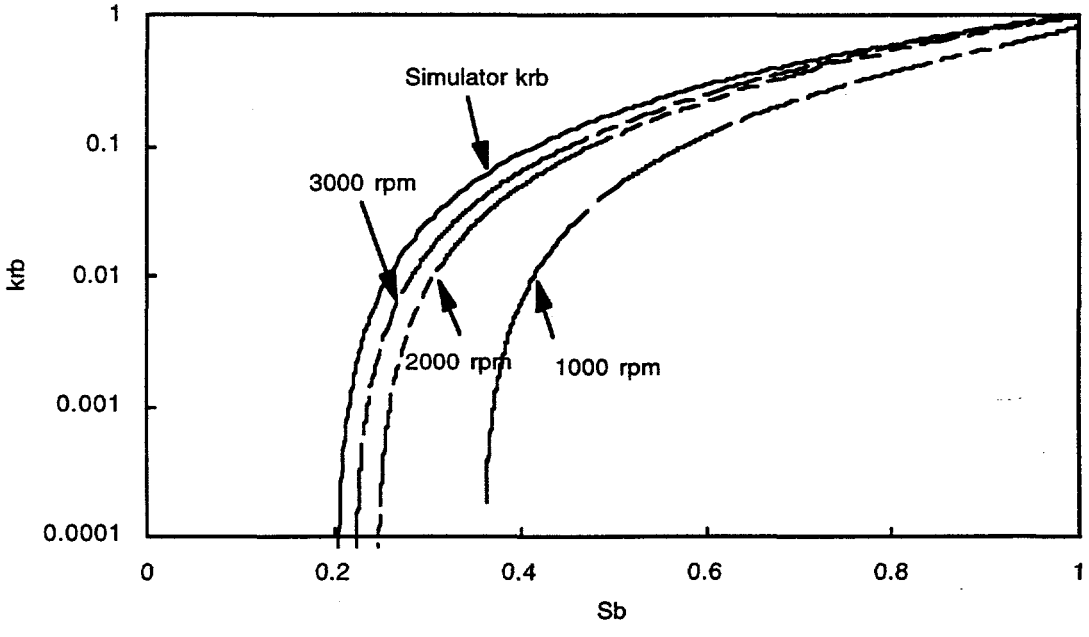

Figure 22b. Comparison of relative permeabilities from the Hagoort method with input to numerical model for different spin rate values. Rock properties: $k = 0.1$ md, $k_{rb,\max} = k_{rg,\max} = 1$, $nb = ng = 1.75$, $S_{br} = 0.2$, $S_{gc} = 0.1$.

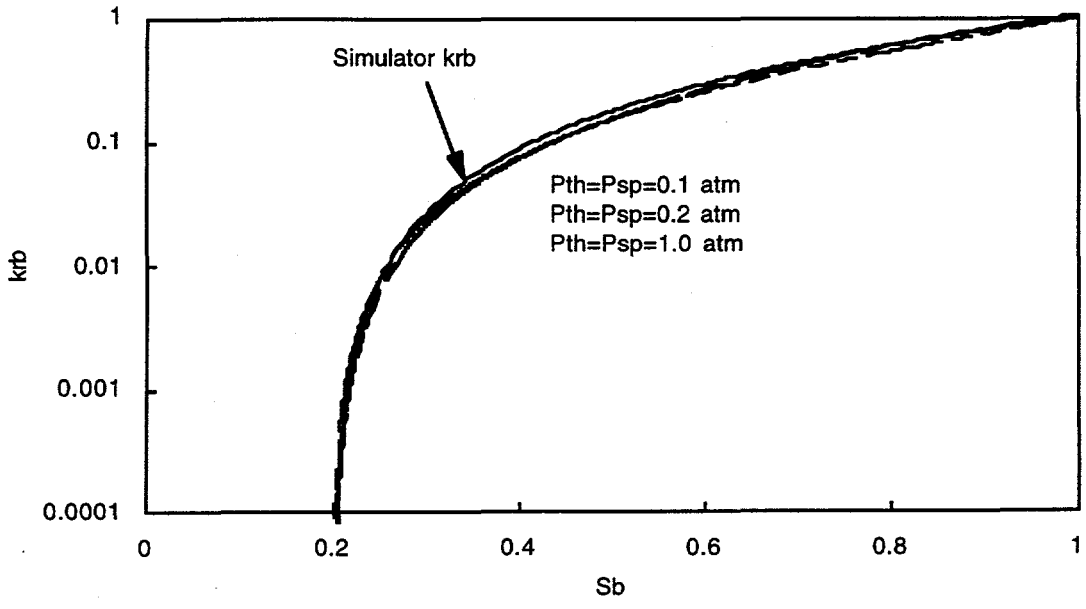

Figure 23. Comparison of relative permeability for the modified Hagoort method with input to numerical method for different P_{th} and P_{sp}. Rock properties: $k = 0.1$ md, $k_{rb,\max} = k_{rg,\max} = 1$, $nb = ng = 1.75$, $S_{br} = 0.2$, $S_{gc} = 0.1$.

DARCY VELOCITY OF BRINE

The Darcy velocity of the flowing brine is given by Darcy's law:

$$v_b = - \left(\frac{k\, k_{rb}}{\mu_b} \right) \left(\frac{\partial \Phi_b}{\partial x} \right) \tag{96}$$

An expression for flow potential in the brine phase, Φ_b, is obtained below by combining the brine flow potential with the gas flow potential and the capillary pressure relationship. It is assumed that the resistance to flow in the gas phase is negligible. Hence the potential for gas flow is constant. The flow potentials for gas and brine, and the Leverett function, $J(S_b)$, are defined as follows:

Brine potential:

$$\Phi_b \equiv P_b - \rho_b \, \alpha \, z \tag{97}$$

Gas potential:

$$\Phi_g \equiv P_g - \rho_g \alpha z = \text{constant} \tag{98}$$

Capillary pressure relationship:

$$P_g - P_b = P_c \equiv \sigma \sqrt{\phi / k}\, J(S_b) \tag{99}$$

These definitions for potential for brine and gas conform to measuring z as shown in Figure 20 in the direction parallel to the average centrifugal acceleration α, which is defined as $\alpha = \omega^2 (R_t + R_o) / 2$. Solving the capillary pressure relationship (Equation 99) for P_b, and substituting for P_g from the gas potential expression (Equation 98), yields

$$P_b = P_g - \sigma \sqrt{\phi / k}\, J(S_b) = \text{constant} + \rho_g \alpha z - \sigma \sqrt{\phi / k}\, J(S_b) \tag{100}$$

With this expression for P_b, the brine potential becomes

$$\Phi_b = \text{constant} - \Delta\rho_{bg} \alpha z - \sigma \sqrt{\phi / k}\, J(S_b) \tag{101}$$

Finally, Equation 96 for brine velocity can be revised with the above expression for brine potential:

$$v_b = \frac{k\, k_{rb}}{\mu_b} \left[\Delta\rho_{bg} \alpha + \sigma \sqrt{\phi / k}\, J' \left(\frac{\partial S_b}{\partial z} \right) \right] \tag{102}$$

in which $J' \equiv \dfrac{\partial J(S_b)}{\partial S_b}$.

Thus the flow of brine results from two effects: one that originates in the relative body forces on the brine and gas and another that originates in the capillary forces. If one examines the result of differentiation with respect to z, it can be seen that these two forces act in opposite directions because J' is negative. The body forces pull brine in the positive z direction, and the capillary forces pull brine in the opposite direction.

PARTIAL DIFFERENTIAL EQUATION FOR EVOLUTION OF SATURATION PROFILES

The material balance on brine flowing parallel to the z-axis is

$$\phi \frac{\partial S_b}{\partial t} + \frac{\partial v_b}{\partial z} = 0 \tag{103}$$

Introducing Equation 102 for v_b, then

$$\phi \frac{\partial S_b}{\partial t} + \frac{k \Delta\rho_{bg} \alpha}{\mu_b} \left(k_{rb}' \frac{\partial S_b}{\partial z} \right) + \frac{k \sigma \sqrt{\phi/k}}{\mu_b} \left(\frac{\partial}{\partial z} \right) \left[k_{rb} J' \left(\frac{\partial S_b}{\partial z} \right) \right] = 0 \tag{104}$$

In preparation for introducing dimensionless quantities, Equation 104 is multiplied by the inverse of $\frac{k \Delta\rho_{bg} \alpha}{\mu_b}$, so

$$\frac{\mu_b \phi}{k \Delta\rho_{bg} \alpha} \frac{\partial S_b}{\partial t} + k_{rb}' \frac{\partial S_b}{\partial z} + \frac{\sigma \sqrt{\phi/k}}{\Delta\rho_{bg} \alpha} \left(\frac{\partial}{\partial z} \right) \left[k_{rb} J' \left(\frac{\partial S_b}{\partial z} \right) \right] = 0 \tag{105}$$

Dimensionless distance, dimensionless time, and the dimensionless capillary/gravity number are defined as follows: $z^* = \frac{z}{L}$, $t^* = \frac{k \Delta\rho_{bg} \alpha t}{\mu_b \phi L}$, $N_{cg} = \frac{\sigma \sqrt{\phi/k}}{\Delta\rho_{bg} \alpha L}$.

With these definitions, Equation 105 becomes

$$\frac{\partial S_b}{\partial t^*} + k_{rb}' \left(\frac{\partial S_b}{\partial z^*} \right) + N_{cg} \left(\frac{\partial}{\partial z^*} \right) \left[k_{rb} J' \left(\frac{\partial S_b}{\partial z^*} \right) \right] = 0 \tag{106}$$

Equation 106 describes saturation history and profile development for finite values of the capillary/gravity number N_{cg}. As elapsed time increases, the saturation profile prescribed by Equation 106 will approach a final profile. The final saturation profile is given by the capillary pressure relationship:

$$\Delta\rho_{bg} \alpha (L - z) = P_c \equiv \sigma \sqrt{\phi/k} \, J(S_b) \tag{107}$$

SIMPLIFICATION FOR NEGLIGIBLE CAPILLARY EFFECTS

If capillary effects are negligible, then the capillary/gravity number N_{cg} equals zero and Equation 106 becomes

$$\frac{\partial S_b}{\partial t^*} + k'_{rb}\left(\frac{\partial S_b}{\partial z^*}\right) = 0 \tag{108}$$

Following the procedure described for deriving Equation 25 of the Welge method, the Buckley-Leverett solution for Equation 108 is

$$z^*_{Sb} = k'_{rb}\, t* \tag{109}$$

Equation 109 describes the saturation profile at any time, t^*. In Equation 109, z^*_{Sb} is the distance that a saturation, S_b, propagates in time t^* from the start of the displacement. The velocity at which a saturation propagates is constant, given by k'_{rb}. If capillary effects were not negligible, the velocity at which a saturation propagates would not be constant, but would decrease toward zero with increasing time.

Using Equation 109 for the saturation profile, the volume of produced brine can be calculated by integrating the saturation profile. The fractional pore volume of produced brine Q_{bp} equals one minus the fractional pore volume of brine remaining in the medium:

$$Q_{bp} = 1 - \int_{z^*=0}^{z^*=1} S_b(z^*)\, dz^* \tag{110}$$

If integrated by parts, Equation 110 becomes

$$Q_{bp} = 1 - \left[S_b(z^*)\, z^*\right]_{z^*=0}^{z^*=1} + \int_{z^*=0}^{z^*=1} z^*(S_b)\, dS_b \tag{111}$$

or

$$Q_{bp} = 1 - S_{bL} + \int_{z^*=0}^{z^*=1} z^*(S_b)\, dS_b \tag{112}$$

Equation 112 can be integrated substituting for z^* from Equation 109:

$$Q_{bp} = 1 - S_{bL} + \int_{z^*=0}^{z^*=1} k'_{rb}\, t^*\, dS_b$$

$$= 1 - S_{bL} + t^* \int_{z^*=0}^{z^*=1} k'_{rb}\, dS_b$$

$$= 1 - S_{bL} + t^* \int_{z^*=0}^{z^*=1} dk_{rb} \tag{113}$$

Because $S_b = S_{br}$ at $z^* = 0$, then k_{rb} must also equal zero at $z^* = 0$; therefore

$$Q_{bp} = 1 - S_{bL} + t^*\, k_{rbL} \tag{114}$$

Differentiating Equation 114 with respect to dimensionless time, and using Equation 109 to rearrange the result, then

$$k_{rbL} = \frac{dQ_{bp}}{dt^*} \tag{115}$$

After the relative permeability is obtained by Equation 115, the saturation at the outlet of the rock sample can be obtained from Equation 116:

$$S_{bL} = 1 - Q_{bp} + t^*\, k_{rbL} \tag{116}$$

Recalling the definition of dimensionless time, Equations 114 and 115 can be arranged in their final forms:

$$k_{rbL} = \left(\frac{\mu_b \, \phi \, L}{k \, \Delta\rho_{bg} \, g} \right) \left(\frac{dQ_{bp}}{dt} \right) \tag{117}$$

$$S_{bL} = 1 - Q_{bp} + t \left(\frac{dQ_{bp}}{dt} \right) \tag{118}$$

Equations 117 and 118 are the desired results of this derivation. These two equations are equivalent to Equations 11 and 16 in Hagoort (1980).

4.0 CONCLUSIONS AND RECOMMENDATIONS

4.1 Conclusions

4.1.1 Pressure Drop, Flow Rate, and Capillary End Effects

Whether at constant pressure drop or at constant flow rate, simulated unsteady-state displacements of brine by gas at normal gravitational acceleration demonstrate that significant amounts of brine can be retained by capillary end effects. The amount of retained brine decreases with increasing pressure drop or flow rate (Section 2.2.1).

With increasing pressure drop or flow rate, the impact of capillary effects on the displacement diminishes. From an experimental point of view, the impact of capillary effects, particularly the capillary end effect, can be judged by comparing tests operated at different pressure drops or flow rates (Section 2.2.1).

The quantitative meaning of "high-rate" and "low-rate" experimental methods must be determined for each sample of rock. The pressure drop or flow rate for which brine retention is not influenced by capillary end effects can be determined from a sequence of experiments at increasing pressure drop or flow rate (Section 2.2.1).

4.1.2 Duration of Experiments

Operating at large pressure drops is essential for completing displacements in an acceptable length of time for low permeability rock samples (Section 2.2.1). For low permeability rock, the amount of time needed to complete an experiment is an important factor in selecting an appropriate method for measuring relative permeability. Simulated unsteady-state high-rate displacements lasted 10 to 20 days for 0.01 md rock (Section 2.2.1). (Steady-state high-rate experiments typically take an order of magnitude more time.)

The time needed to complete a centrifuge displacement decreases as the applied centrifugal acceleration increases. From 1 to 2 days may be required to drain brine from a 0.01-md rock in a centrifuge. Such an experiment would yield brine relative permeability, but not the gas relative permeability (Section 2.2.2).

4.1.3 Data Reduction for Unsteady-State Experiments

Of the unsteady-state methods, the high-rate method is most commonly practiced. The data reduction procedures for this method include the Welge method, the Johnson-Bossler-Naumann (JBN) method, and the Jones-Roszelle method. With the Welge method, the ratio of relative permeabilities k_{rb}/k_{rg} can be accurately calculated from high-rate unsteady-state data for a gas-brine displacement. With the JBN and Jones-Roszelle methods, k_{rb} and k_{rg} can be calculated. The accuracy of the three methods depends on the quality of the experimental data (Sections 3.1.1.2, 3.1.2.2, and 3.1.3.2).

The needed displacement rates for the Ramakrishnan-Cappiello data reduction method transcend the range from "low" to "high" rate. For gas displacing brine, this data reduction procedure can produce the gas relative permeability and the gas-brine capillary pressure relationships (Section 3.2.1.2).

The method of Ramakrishnan and Cappiello demonstrates that relative permeability and capillary pressure information can be obtained from low-rate experiments. History matching of low-rate data can provide more complete information than can be obtained by the Ramakrishnan-Cappiello method.

For displacements of brine by gas in centrifuge experiments, the data can be processed by the Hagoort method or the modified Hagoort method as proposed in Section 3 to obtain relative permeability of the brine phase. To obtain accurate relative permeability relationships with the Hagoort method, "high" centrifuge speeds are required. The modified Hagoort method can accommodate data for a wide variety of centrifuge spin rates (Section 3.3.1.2).

4.2 Recommendations

4.2.1 Data Reduction and Experiments for Salado Formation

4.2.1.1 Steady-State Methods

Data reduction for all steady-state methods is simple. However, the drawback of these methods is the long time required to achieve steady state. Typically, steady-state high-rate experiments take more than ten times longer than unsteady-state high-rate experiments.

Of the various steady-state methods, the stationary-liquid method may be most applicable to anhydrite from the Salado formation. From pressure drop and flow rate data, the gas relative permeability is calculated. Although this method cannot yield brine relative permeabilities, it could be used to complement unsteady-state experiments.

4.2.1.2 Unsteady-State High-Rate Method

Data reduction for unsteady-state high-rate experiments is complex, requiring differentiation of data. However, these methods are perhaps most suited for obtaining relative permeabilities of Salado anhydrite. Depending on the properties of a rock sample, an experiment may last 10 to 20 days. The method is well documented in the literature and well accepted in the industry. The steady-state stationary-liquid method could be used to check the results obtained for gas relative permeability.

4.2.1.3 Unsteady-State Low-Rate Method

Data reduction for the unsteady-state low-rate experimental method requires history matching. Although data reduction is quite complex, low-rate experiments are appealing because their low flow rates resemble the rates that could actually arise in the formations surrounding WIPP. Proponents of the method maintain that gas and brine relative permeabilities and capillary pressure relationships can be obtained from the same experiments. After further research, the low-rate methods may become a viable option for anhydrite from the Salado Formation.

4.2.1.4 Unsteady-State Centrifuge Method

By differentiation of production data from a centrifuge, brine relative permeability can be obtained. According to simulations of this method, the time needed for completing an experiment decreases with increasing permeability of the rock sample and with increasing centrifuge spin rate. The simulations show that experiments with 0.01 md rock can be completed within 1 day.

4.2.2 Application for Salado Anyhdrite Testing

The unsteady-state high-rate method offers the most promise for successful application to measuring relative permeability of Salado anhydrite. In addition, supplemental techniques such as the steady-state method or the unsteady-state stationary-liquid method to measure relative permeability of gas combined with the unsteady-state centrifuge method to measure the relative permeability of brine are recommended. These supplemental techniques should be performed to confirm the accuracy, and quantify the uncertainty, of the data.

5.0 REFERENCES

Arçher, J.S., and S.W. Wong. 1973. "Use of a Reservoir Simulator to Interpret Laboratory Water Flood Data," *Society of Petroleum Engineers Journal*. SPE 3551. Vol. 13, no. 6, 343-347. (Copy on file in the Sandia WIPP Central Files, Sandia National Laboratories, Albuquerque, NM as WPO#20319.)

Batycky, J.P., F.G. McCaffery, P.K. Hodgins, and D.B. Fisher. 1981. "Interpreting Relative Permeability and Wettability from Unsteady-State Displacement Measurements," *Society of Petroleum Engineers Journal*. Vol. 21, no. 3, 296-308.

Brooks, R.H., and A.T. Corey. 1966. "Properties of Porous Media Affecting Fluid Flow," *Journal of the Irrigation and Drainage Division, Proceedings of the American Society of Civil Engineers*. Vol. 92, no. IR2, 61-88. (Copy on file in the Sandia WIPP Central Files, Sandia National Laboratories, Albuquerque, NM as WPO#42326.)

Chapra, S.C., and R.P. Canale. 1988. *Numerical Methods for Engineers*. 2nd ed. New York, NY: McGraw-Hill.

Christiansen, R.L., and S.M. Howarth. 1995. *Literature Review and Recommendation of Methods for Measuring Relative Permeability of Anhydrite from the Salado Formation at the Waste Isolation Pilot Plant (WIPP)*. SAND93-7074. Albuquerque, NM: Sandia National Laboratories. (Copy on file in the Sandia WIPP Central Files, Sandia National Laboratories, Albuquerque, NM as WPO#22658.)

Civan, F., and E.C. Donaldson. 1989. "Relative Permeability From Unsteady-State Displacements With Capillary Pressure Included," *SPE Formation Evaluation*. Vol. 4, no. 2, 189-193.

Coats, K.H. 1987. "Reservoir Simulation," *Petroleum Engineering Handbook*. Ed. H.B. Bradley. Richardson, TX: Society of Petroleum Engineers. Chapter 48.

Collins, R.E. 1961. *Flow of Fluids Through Porous Materials*. New York, NY: Reinhold Publishing Corporation. 145-151.

Dake, L.P. 1978. *Fundamentals of Reservoir Engineering*. New York, NY: Elsevier. 356-365.

Fassihi, M.R. 1989. "Estimation of Relative Permeability from Low Rate, Unsteady-State Tests - A Simulation Approach," *Journal of Canadian Petroleum Technology*. Vol. 28, no. 3, 29-38.

Firoozabadi, A., and K. Aziz. 1991. "Relative Permeabilities from Centrifuge Data," *Journal of Canadian Petroleum Technology*. Vol. 30, no. 5, 33-42.

Hagoort, J. 1980. "Oil Recovery by Gravity Drainage," *Society of Petroleum Engineers Journal*. Vol. 20, no. 3, 139-150.

Hirasaki, G.J., J.A. Rohan, and J.W. Dudley. 1992. *Modification of Centrifuge and Software for Determination of Relative Permeability Curves*. SPE 25290. Richardson, TX: Society of Petroleum Engineers.

Hyman, L.A., M. Brugler, D. Daneshjou, and H.A. Ohen. 1991a. *Improved Evaluation of Coal Reservoirs through Specialized Core Analysis. Annual Report, January 1990-December 1990*. GRI-91/0201. Carrollton, TX: Core Laboratories; Chicago, IL: Gas Research Institute.

Hyman, L.A., H.A. Ohen, J.O. Amaefule, and D. Daneshjou. 1991b. "Simultaneous Determination of Capillary Pressure and Relative Permeability in Coalbed Methane Reservoirs," *1991 Coalbed Methane Symposium Proceedings, The University of Alabama/Tuscaloosa, May 13-17, 1991*. Paper 9118. Tuscaloosa, AL: University of Alabama. 85-96.

Hyman, L.A., M.L. Brugler, D. Daneshjou, and H.A. Ohen. 1992. "Advances in Laboratory Measurement Techniques of Relative Permeability and Capillary Pressure for Coal Seams," *Quarterly Review of Methane from Coal Seams Technology*. Vol. 9, no. 2, 9-13.

Jennings, J.W., D.S. McGregor, and R.A. Morse. 1988. "Simultaneous Determination of Capillary Pressure and Relative Permeability by Automatic History Matching," *SPE Formation Evaluation*. Vol. 3, no. 2, 322-328.

Johnson, E.F., D.P. Bossler, and V.O. Naumann. 1959. "Calculation of Relative Permeability from Displacement Experiments," *Transactions of the American Institute of Mining, Metallurgical, and Petroleum Engineers*. Vol. 216, 370-372.

Jones, S.C., and W.O Roszelle. 1978. "Graphical Techniques for Determining Relative Permeability from Displacement Experiments," *Journal of Petroleum Technology*. Vol. 30, no. 5, 807-817.

Kerig, P.D., and A.T.Watson. 1986. "Relative-Permeability Estimation from Displacement Experiments: An Error Analysis," *SPE Reservoir Engineering*. Vol. 1, no. 2, 175-182.

Kerig, P.D., and A.T.Watson. 1987. "A New Algorithm for Estimating Relative Permeabilities from Displacement Experiments," *SPE Reservoir Engineering*. SPE 14476. Vol. 2, no. 1, 103-112.

Lai, W., and H. Brandt. 1988. "A Pressure-History-Matching Method for Determination of Relative Permeabilities," *SPE Reservoir Engineering*. Vol. 3, no. 2, 651-661.

MacMillan, D.J. 1987. "Automatic History Matching of Laboratory Corefloods to Obtain Relative Permeability Curves," *SPE Reservoir Engineering*. SPE 12356. Vol. 2, no.1, 85-91. (Copy on file in the Sandia WIPP Central Files, Sandia National Laboratories, Albuquerque, NM as WPO#25207.)

Mattax, C.C., and R.L. Dalton. 1990. *Reservoir Simulation*. Monograph 13. Richardson, TX: Henry L. Doherty Memorial Fund of AIME, Society of Petroleum Engineers.

Nordtvedt, J.E., G. Mejia, P-H. Yang, and A.T. Watson. 1993. "Estimation of Capillary Pressure and Relative Permeability Functions from Centrifuge Experiments," *SPE Reservoir Engineering*. Vol. 8, no. 4, 292-298.

Odeh, A.S., and B.J. Dotson. 1985. "A Method for Reducing the Rate Effect on Oil and Water Relative Permeabilities Calculated from Dynamic Displacement Data," *Journal of Petroleum Technology*. Vol. 37, no. 12, 2051-2058.

Ohen, H.A., J.O. Amaefule, L.A. Hyman, D. Daneshjou, and R.A. Schraufnagel. 1991. "A Systems Response Model for Simultaneous Determination of Capillary Pressure and Relative Permeability Characteristics of Coalbed Methane," *Reservoir Engineering Proceedings, SPE Annual Technical Conference and Exhibition, Dallas, TX, October 6-9, 1991*. SPE 22912. Richardson, TX: Society of Petroleum Engineers. 247-261.

O'Meara, D.J., Jr., and J.G. Crump. 1985. "Measuring Capillary Pressure and Relative Permeability in a Single Centrifuge Experiment," *Proceedings of the 60th Annual Technical Conference and Exhibition of the Society of Petroleum Engineers, Las Vegas, NV, September 22-25, 1985*. SPE 14419. Richardson, TX: Society of Petroleum Engineers of AIME.

Peaceman, D.W. 1977. *Fundamentals of Numerical Reservoir Simulation*. New York, NY: Elsevier.

Qadeer, S., K. Dehghani, D.O. Ogbe, and R.D. Ostermann. 1988. "Correcting Oil/Water Relative Permeability Data for Capillary End Effect in Displacement Experiments," *1988 California Regional Meeting of the Society of Petroleum Engineers, Long Beach, CA, March 23-25, 1988*. SPE 17412. Richardson, TX: Society of Petroleum Engineers. 247-258.

Ramakrishnan, T.S., and A. Cappiello. 1991. "A New Technique to Measure Static and Dynamic Properties of a Partially Saturated Porous Medium," *Chemical Engineering Science*. Vol. 46, no. 4, 1157-1163.

Sigmund, P.M., and F.G. McCaffery. 1979. "An Improved Unsteady-State Procedure for Determining the Relative-Permeability Characteristics of Heterogeneous Porous Media," *Society of Petroleum Engineers Journal*. Vol. 19, no. 1, 15-28.

Spillette, A.G., J.G. Hillestad, and H.L .Stone. 1986. "A High-Stability Sequential Solution Approach to Reservoir Simulation," *Numerical Simulation II.* SPE Reprint Series No. 20. Richardson, TX: Society of Petroleum Engineers. 55-68.

Tao, T.M., and A.T. Watson. 1984a. "Accuracy of JBN Estimates of Relative Permeability: Part 1 - Error Analysis," *Society of Petroleum Engineers Journal.* Vol. 24, no. 2, 209-214.

Tao, T.M., and A.T. Watson. 1984b. "Accuracy of JBN Estimates of Relative Permeability: Part 2 - Algorithms," *Society of Petroleum Engineers Journal.* Vol. 24, no. 2, 215-223.

Udegbunam, E.O. 1991. "A Fortran Program for Interpretation of Relative Permeability from Unsteady-State Displacements with Capillary Pressure Included," *Computers & Geosciences.* Vol. 17, no. 10, 1351-1357.

Van Spronsen, E. 1982. "Three-Phase Relative Permeability Measurements Using the Centrifuge Method," *Proceedings, 3rd Joint SPE/DOE Symposium of Enhanced Oil Recovery, Tulsa, OK, April 4-7, 1982.* SPE/DOE 10688. Dallas, TX: Society of Petroleum Engineers of AIME. 217-240.

Watson, A.T., P.C. Richmond, P.D. Kerig, and T.M. Tao. 1988. "A Regression-Based Method for Estimating Relative Permeabilities from Displacement Experiments," *SPE Reservoir Engineering.* August 1988, 953-958. (Copy on file in the Sandia WIPP Central Files, Sandia National Laboratories, Albuquerque, NM as WPO#25206.)

Welge, H.J. 1952. "A Simplified Method for Computing Oil Recovery by Gas or Water Drive," *Transactions of the American Institute of Mining and Metallurgical Engineers.* Vol. 195, 91-98.

Willhite, G.P. 1986. *Waterflooding.* Society of Petroleum Engineers Text Book Series Volume 3. Richardson, TX, Society of Petroleum Engineers. 60-66.

Wylie, C.R. 1975. *Advanced Engineering Mathematics.* 4th ed. New York, NY: McGraw-Hill.

WIPP
UC721 - DISTRIBUTION LIST
SAND94-1346

Federal Agencies

US Department of Energy (4)
Office of Civilian Radioactive Waste Mgmt.
Attn: Deputy Director, RW-2
Associate Director, RW-10
Office of Human Resources & Admin.
Associate Director, RW-30
Office of Program Mgmt. & Integ.
Associate Director, RW-40
Office of Waste Accept., Stor., & Tran.
Forrestal Building
Washington, DC 20585

US Department of Energy
Albuquerque Operations Office
Attn: National Atomic Museum Library
P.O. Box 5400
Albuquerque, NM 87185-5400

US Department of Energy
Research & Waste Management Division
Attn: Director
P.O. Box E
Oak Ridge, TN 37831

US Department of Energy (5)
Carlsbad Area Office
Attn: G. Dials
D. Galbraith
M. McFadden
R. Lark
J. A. Mewhinney
P.O. Box 3090
Carlsbad, NM 88221-3090

US Department of Energy
Office of Environmental Restoration and
Waste Management
Attn: M. Frei, EM-30
Forrestal Building
Washington, DC 20585-0002

US Department of Energy (3)
Office of Environmental Restoration and
Waste Management
AttnJ. Juri, EM-34, Trevion II
Washington, DC 20585-0002

US Department of Energy
Office of Environmental Restoration and
Waste Management
Attn: S. Schneider, EM-342, Trevion II
Washington, DC 20585-0002

US Department of Energy (2)
Office of Environment, Safety & Health
Attn: C. Borgstrom, EH-25
R. Pelletier, EH-231
Washington, DC 20585

US Department of Energy (2)
Idaho Operations Office
Fuel Processing & Waste Mgmt. Division
785 DOE Place
Idaho Falls, ID 83402

US Environmental Protection Agency (2)
Radiation Protection Programs
Attn: M. Oge
ANR-460
Washington, DC 20460

Attn: Project Director
Yucca Mountain Site Characterization Office
Director, RW-3
Office of Quality Assurance
P.O. Box 30307
Las Vegas, NV 89036-0307

Boards

Defense Nuclear Facilities Safety Board
Attn: D. Winters
625 Indiana Ave. NW, Suite 700
Washington, DC 20004

Nuclear Waste Technical Review Board (2)
Attn: Chairman
J. L. Cohon
1100 Wilson Blvd., Suite 910
Arlington, VA 22209-2297

State Agencies

Attorney General of New Mexico
P.O. Drawer 1508
Santa Fe, NM 87504-1508

Environmental Evaluation Group (3)
Attn: Library
7007 Wyoming NE
Suite F-2
Albuquerque, NM 87109

NM Energy, Minerals, and Natural
Resources Department
Attn: Library
2040 S. Pacheco
Santa Fe, NM 87505

NM Environment Department (3)
Secretary of the Environment
Attn: Mark Weidler
1190 St. Francis Drive
Santa Fe, NM 87503-0968

NM Bureau of Mines & Mineral Resources
Socorro, NM 87801

Laboratories/Corporations

Battelle Pacific Northwest Laboratories
Battelle Blvd.
Richland, WA 99352

Los Alamos National Laboratory
Attn: B. Erdal, INC-12
P.O. Box 1663
Los Alamos, NM 87544

Tech Reps, Inc. (3)
Attn: J. Chapman (1)
Loretta Robledo (2)
5000 Marble NE, Suite 222
Albuquerque, NM 87110

Westinghouse Electric Corporation (5)
Attn: Library
J. Epstein
J. Lee
B. A. Howard
R. Kehrman
P.O. Box 2078
Carlsbad, NM 88221

S. Cohen & Associates
Attn: Bill Thurber
1355 Beverly Road
McLean, VA 22101

**National Academy of Sciences,
WIPP Panel**

Howard Adler
Oxyrase, Incorporated
7327 Oak Ridge Highway
Knoxville, TN 37931

Tom Kiess
Board of Radioactive Waste Management
GF456
2101 Constitution Ave.
Washington, DC 20418

Rodney C. Ewing
Department of Geology
University of New Mexico
Albuquerque, NM 87131

Charles Fairhurst
Department of Civil and Mineral Engineering
University of Minnesota
500 Pillsbury Dr. SE
Minneapolis, MN 55455-0220

B. John Garrick
PLG Incorporated
4590 MacArthur Blvd., Suite 400
Newport Beach, CA 92660-2027

Leonard F. Konikow
US Geological Survey
431 National Center
Reston, VA 22092

Carl A. Anderson, Director
Board of Radioactive Waste Management
National Research Council
HA 456
2101 Constitution Ave. NW
Washington, DC 20418

Christopher G. Whipple
ICF Kaiser Engineers
1800 Harrison St., 7th Floor
Oakland, CA 94612-3430

John O. Blomeke
720 Clubhouse Way
Knoxville, TN 37909

Sue B. Clark
University of Georgia
Savannah River Ecology Lab
P.O. Drawer E
Aiken, SC 29802

Konrad B. Krauskopf
Department of Geology
Stanford University
Stanford, CA 94305-2115

Della Roy
Pennsylvania State University
217 Materials Research Lab
Hastings Road
University Park, PA 16802

David A. Waite
CH_2 M Hill
P.O. Box 91500
Bellevue, WA 98009-2050

Thomas A. Zordon
Zordan Associates, Inc.
3807 Edinburg Drive
Murrysville, PA 15668

Universities

University of New Mexico
Geology Department
Attn: Library
141 Northrop Hall
Albuquerque, NM 87131

University of Washington
College of Ocean & Fishery Sciences
Attn: G. R. Heath
583 Henderson Hall, HN-15
Seattle, WA 98195

Colorado School of Mines (20)
Department of Petroleum Engineering
Attn: R. L. Christiansen
Golden, CO 80401

Libraries

Thomas Brannigan Library
Attn: D. Dresp
106 W. Hadley St.
Las Cruces, NM 88001

Government Publications Department
Zimmerman Library
University of New Mexico
Albuquerque, NM 87131

New Mexico Junior College
Pannell Library
Attn: R. Hill
Lovington Highway
Hobbs, NM 88240

New Mexico State Library
Attn: N. McCallan
325 Don Gaspar
Santa Fe, NM 87503

New Mexico Tech
Martin Speere Memorial Library
Campus Street
Socorro, NM 87810

WIPP Public Reading Room
Carlsbad Public Library
101 S. Halagueno St.
Carlsbad, NM 88220

Foreign Addresses

Atomic Energy of Canada, Ltd.
Whiteshell Laboratories
Attn: B. Goodwin
Pinawa, Manitoba, CANADA R0E 1L0

Francois Chenevier (2)
ANDRA
Route de Panorama Robert Schumann
B. P. 38
92266 Fontenay-aux-Roses, Cedex
FRANCE

Claude Sombret
Centre d'Etudes Nucleaires de la Vallee Rhone
CEN/VALRHO
S.D.H.A. B.P. 171
30205 Bagnols-Sur-Ceze, FRANCE

Commissariat a L'Energie Atomique
Attn: D. Alexandre
Centre d'Etudes de Cadarache
13108 Saint Paul Lez Durance Cedex
FRANCE

Bundesanstalt fur Geowissenschaften und
Rohstoffe
Attn: M. Langer
Postfach 510 153
D-30631 Hannover, GERMANY

Bundesministerium fur Forschung und
Technologie
Postfach 200 706
5300 Bonn 2, GERMANY

Institut fur Tieflagerung
Attn: K. Kuhn
Theodor-Heuss-Strasse 4
D-3300 Braunschweig, GERMANY

Gesellschaft fur Anlagen und Reaktorsicherheit
(GRS)
Attn: B. Baltes
Schwertnergasse 1
D-50667 Cologne, GERMANY

Shingo Tashiro
Japan Atomic Energy Research Institute
Tokai-Mura, Ibaraki-Ken, 319-11
JAPAN

Netherlands Energy Research Foundation ECN
Attn: J. Prij
3 Westerduinweg
P.O. Box 1
1755 ZG Petten
THE NETHERLANDS

Svensk Karnbransleforsorjning AB
Attn: F. Karlsson
Project KBS (Karnbranslesakerhet)
Box 5864
S-102 48 Stockholm
SWEDEN

Nationale Genossenschaft fur die Lagerung
Radioaktiver Abfalle (2)
Attn: S. Vomvoris
P. Zuidema
Hardstrasse 73
CH-5430 Wettingen
SWITZERLAND

AEA Technology
Attn: J. H. Rees
D5W/29 Culham Laboratory
Abington, Oxfordshire OX14 3DB
UNITED KINGDOM

AEA Technology
Attn: W. R. Rodwell
044/A31 Winfrith Technical Centre
Dorchester, Dorset DT2 8DH
UNITED KINGDOM

AEA Technology
Attn: J. E. Tinson
B4244 Harwell Laboratory
Didcot, Oxfordshire OX11 ORA
UNITED KINGDOM

Internal

MS	Org.	
1320	6719	E. J. Nowak
1322	6121	J. R. Tillerson
1324	6115	P. B. Davies
1324	6801	S. M. Howarth (10)
1328	6749	D. R. Anderson
1328	6741	H. N. Jow
1335	6705	M. Chu
1341	6748	J. T. Holmes
1395	6800	L. Shephard
1395	6707	M. Marietta
1395	6841	V. H. Slaboszewicz
1324	6115	T. L. Christian-Frear (2)
1324	6115	C. Boney
1324	6115	S. W. Webb
1330	6811	K. Hart (2)
1330	4415	NWM Library (20)
9018	8940-2	Central Technical Files
0899	4414	Technical Library (5)
0619	12690	Review and Approval Desk (2) For DOE/OSTI